Summer 8-2020

Understanding Oxidative Aging of Asphalt Binder and it's Effects on Cracking Susceptibility of Asphalt Mix

Md Shams Arafat

UNDERSTANDING OXIDATIVE AGING OF ASPHALT BINDER AND ITS EFFECTS ON CRACKING SUSCEPTIBILITY OF ASPHALT MIX

by

Md Shams Arafat, B.S., M.S.

A Dissertation Presented in Partial Fulfillment
of the Requirements for the Degree
Doctor of Philosophy

COLLEGE OF ENGINEERING AND SCIENCE
LOUISIANA TECH UNIVERSITY

August 2020

ABSTRACT

Every year around 400 million tons of asphalt mix is being laid in the United States and a significant portion of it is required for pavement rehabilitation. Cracking is one of the most common pavement distresses that is still not fully understood by the researchers. Very few states mandate tests for cracking resistance during the mix design phase; in addition, the test methods vary a lot from state to state. In the presence of oxygen, the asphalt binder over time undergoes chemical changes and becomes stiff which is known as oxidative aging that makes asphalt pavement more susceptible to cracking. Therefore, proper characterization of asphalt aging is a prerequisite to study the cracking mechanism of asphalt mix. In this dissertation, efforts are given for characterization of oxidative aging, investigation of the effect of aged binder on cracking susceptibility, and development of an antioxidant to reduce the aging-induced cracking.

In this study, rheological characterization of laboratory aged binder and extracted binder from asphalt mix was performed using dynamic shear modulus of the binder to understand oxidative aging. Then the correlation between laboratory binder aging and binder aging in asphalt mix was established and a Rolling Thin Film Oven (RTFO) aging test protocol for warm mix asphalt (WMA) was developed. Another factor for cracking susceptibility of asphalt pavement is the excessive content of reclaimed asphalt pavement (RAP). RAP is added to the hot mix asphalt (HMA) for economic and environmental interest but the highly aged binder in RAP makes the mix stiffer and escalates the

cracking. Because it is quick and simple, the viability of using a handheld Fourier Transformed Infrared (FT-IR) spectrometer was investigated to detect and quantify the aging of binder by measuring the absorbance intensity of carbonyl groups. An in-situ test method was developed to determine the reclaimed asphalt pavement (RAP) content in the plant mix using a handheld FT-IRS.

The use of rejuvenators is the most suitable strategy to accommodate a higher amount of RAP in HMA and bio-based rejuvenators are of high interest. In this study, four types of cracking tests were performed on asphalt mix made with two different categories of rejuvenators: petroleum-based and bio-based oil. It was concluded that petroleum-based aromatic oil performed better to restore the cracking potential of the mix with high RAP content. Sound understanding of the cracking mechanism is necessary to find the right cracking susceptibility test for asphalt mix and design a cracking resistant mix. A finite element model of semi-circular bend (SCB) test of asphalt mix incorporating the cohesive zone material (CZM) model was performed using ANSYS to simulate and predict the fracture potential of asphalt mix as conducted in the laboratory according to ASTM D 8044 test method. The CZM properties of fine aggregate mastic (FAM) needed for ANSYS model of SCB test was determined by a laboratory double cantilever beam test and corresponding finite element model of double cantilever beam test., It was concluded that critical energy release rate (*Jc*) of asphalt mixture predicted from ANSYS model of SCB test was precise when compared with the laboratory SCB test of asphalt mix.

Finally, locally sourced Lignin was used as an asphalt performance enhancer as well as an antioxidant. It was observed that lignin could improve the high-temperature

performance grade of the binder and reduce the aging index. Mix made of lignin modified binder showed better cracking resistance by improving the flexibility index.

Through this study, understanding oxidative aging helped with developing a revised short-term aging protocol for warm mix asphalt. One of the immediately implementable outcomes of this research is the in-situ application of handheld FT-IR spectrometer for quality control during the mix production at the plant through determining the reclaimed asphalt pavement content. This research will contribute to choosing suitable rejuvenators by understanding the cracking mechanism of asphalt mix through different tests. The finite element cohesive zone material model developed in this study can precisely predict fracture resistance of the mix in semicircular bending test by performing a double cantilever beam test of fine aggregate mastic. Viability of using bio-based rejuvenator for RAP mixes and also the suitability of utilizing locally sourced lignin as an oxidant in asphalt binder were addressed in this research and the findings will help implement these environmentally friendly alternatives in resolving cracking related problems in asphalt pavements.

APPROVAL FOR SCHOLARLY DISSEMINATION

DEDICATION

To

My wife

TABLE OF CONTENTS

LIST OF TABLES

LIST OF FIGURES

ACKNOWLEDGMENTS

First and foremost, I wish to thank the Almighty God for all the blessings and privileges that I have been given in my life. I would like to express my profound gratitude to my advisor Dr. Nazimuddin M. Wasiuddin for his invaluable direction, encouragement, constant support, and considerable patience throughout this journey. Without his scholarly guidance and suggestions in every aspect of this dissertation, it would not have been possible. Special thanks are extended to the committee members Dr. Henry Cardenas, Dr. Tom Iseley, Dr. Shawn Sun, and Dr. Jay Wang for their time, suggestions, and interactions.

I am grateful to Dr. Delmar Salomon and Dr. Sven Eklund for their guidance in FT-IR spectroscopy related work. I appreciate the contribution of the coauthors Dr. Lynam, Narendra Kumar, and Ekugbere Owhe for the syntheses of the Lignin in their laboratory. I thank my research lab colleagues Mohammad Readul Islam and Lamiya Noor (coauthors), Daniel Stagg, Waleed Omer, Roksana Hossain, and other students who helped me in laboratory work.

Finally, I would like to thank my parents, who sacrificed their dreams but did not get the chance to watch this accomplishment. I would also like to thank my sister and in-laws for their mental support all these years. Last, this acknowledgment will be incomplete without mentioning my wife, Nahid Farzana. You have been a constant source of love and motivation in my life.

CHAPTER 1

INTRODUCTION

The United States has 2.7 million miles of paved roads and highways which makes the largest road network in the world. 94% of all those roads are paved with asphalt, making a total of almost 18 billion tons of hot mix asphalt laid in the road and an additional 400 million tons of asphalt being laid every year [1.1]. Each year, 231 billion dollars are required to keep the existing roads in fair condition. This is a huge amount of taxpayer's money and states cannot afford this much for maintenance of the roads and highways. As a result, the road infrastructures are not in the best condition. For example, Louisiana received a D+ rating which is not the standard people expect [1.2]. Among different kinds of distresses of the pavement, cracking is one of the most common problems that is still not fully understood by the researchers. A significant portion of road maintenance is associated with rehabilitation due to cracking.

Although cracking is a critical issue for asphalt pavement and asphalt mix design is becoming more complex with the use of modifiers and reclaimed asphalt pavements, very few states mandate a cracking susceptibility test in the mix design phase [1.3]. Currently, different types of cracking test methods are being performed by different agencies: semi-circular bend test (at low and intermediate temperature), disk-shaped compact tension, Texas overlay test, indirect tension test, bending beam fatigue test, etc. Among the states that implemented the cracking test, the performed test methods vary

from state to state. Consequently, the results are not consistent and the same mix can be ranked differently in different test methods. Four major types of cracking are commonly observed in asphalt pavement, namely, thermal/low-temperature cracking, reflection cracking, bottom-up fatigue cracking, and top-down cracking, and these are affected by numerous factors and interactions [1.4]. The primary cause behind the cracking of asphalt mix is that with time the asphalt loses its flexibility and becomes less strain tolerant. In the presence of oxygen, the asphalt binder undergoes chemical changes and becomes stiff which is known as oxidative aging that leads to flexibility loss.

To build a sustainable, longer lasting, and cracking resistant pavement, a sound understanding of the cracking mechanism is important. Therefore, this study has been initiated to understand the aging of asphalt binder and its effect on the cracking susceptibility of asphalt mixes.

1.1 Research Objectives

Three main aspects of this dissertation are characterization of oxidative aging, investigation of the effect of aging on cracking susceptibility of the asphalt mix, and finally development of an antioxidant and application of a rejuvenating agent on the pavement. Figure 1.1 shows the broader aspects and individual chapters under each category. The detailed research objectives of each chapter in this study are summarized as follows:

- To investigate the aging time and temperature of rolling thin film oven (RTFO) and short-term oven aging (STOA) on stiffness ($G^*/\sin\delta$) of a binder for developing an RTFO aging model by correlating the rheological properties of STOA mixes to predict the STOA effect by testing the binder in RTFO.

- To implement the handheld FT-IR spectrometer in the field as a tool for quality control of plant mix containing RAP. Selection of a suitable index derived from FT-IR spectral analysis and utilization of those indices for understanding and quantifying the laboratory aging of the binder and mix using ATR (Attenuated Total Reflectance)-FTIR.
- To evaluate the bio-based and petroleum-based rejuvenators based on the cracking susceptibility of hot mix asphalt made of a high amount of RAP. Rejuvenators are used to accommodate a higher amount of RAP in the mix.
- To determine the optimum content of rejuvenators.
- To determine the cohesive zone material (CZM) properties of fine aggregate mastic (FAM) and explain by finite element modeling the fracture behavior of asphalt mix in the semicircular bend (SCB) test according to ASTM D 8044.
- To study the effectiveness of lignin as an antioxidant to enhance the asphalt binder's rheological properties and to improve the cracking resistance of asphalt mix by reducing the aging by the use of an antioxidant.
- To quantify the sealing potential of an emulsified rejuvenating agent by measuring the hydraulic conductivity of the field core specimens before and after the fog seal application, and to assess the effect of a fog seal on surface friction characteristics over a prolonged period by evaluating international friction index parameter as an indicator.

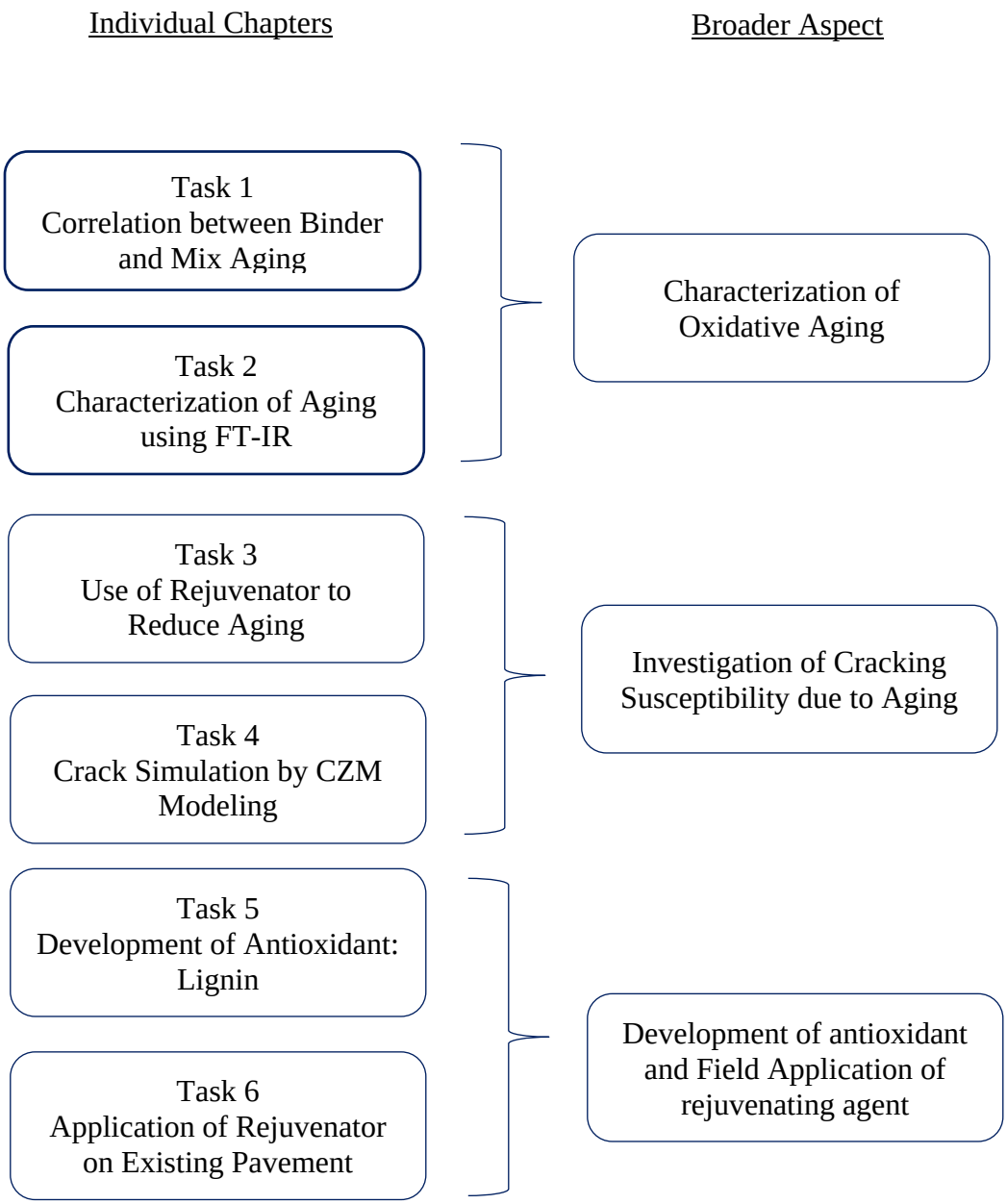

Figure 1-1 Research objective and outline.

1.2 Background and Research Need

1.2.1 Characterization of Oxidative Aging (Tasks 1 & 2)

Oxidative aging is the chemical and rheological changes that occur throughout the service life of the asphalt binder and consequently stiffens the binder. The aging mechanism can be investigated in the laboratory by various test methods: rheological tests of binder-penetration, ductility, and loss of mass test, viscosity, complex modulus, and phase angles; chemical tests of binder-SARA (Saturate, Aromatic, Resin and Asphaltene) fraction, FT-IR (Fourier transform Infrared) spectroscopy, GPC (gel permeation chromatography); and mechanical test of the mix-dynamic modulus, resilient modulus; etc. Since each test has its specific feature to define aging, processing time and convenience to perform the test are also important factors for aging determination in the laboratory as well as in the field. FT-IR spectroscopy requires less time compared to other tests and can also provide reliable results. The principle of FT-IR spectroscopy is to detect the molecular structures of a sample based on their vibrational and rotational frequency at a specific wavenumber. Previous studies showed that both carbonyl (CO) sulfoxide (SO) functional groups are affected by the oxidative aging in asphalt binder. FT-IR has the potential to quantify the intensity of these two groups. It is important to determine if both groups can successfully quantify the oxidative aging.

Addition of Reclaimed Asphalt Pavement (RAP) in asphalt mixture supports economic and environmental interests; however, the highly aged RAP is one of the potential sources of inferior cracking resistance of the pavement. So, continuous quality control during the production phase is crucial. It has been a challenging task to quickly detect the amount of RAP in the hot mix asphalt (HMA) by examining the fresh mix in

the plant. Very few studies have been conducted to quantify the amount of RAP in the mix as a part of quality control purposes. Most importantly, chemical changes in the RAP were not addressed properly in previous studies. Determination of mix aging during the production phase involves the separation of binder from the mix. So, a quick extraction process is needed that can be conveniently implemented in the field. As RAP contains a highly aged binder, it should be possible to detect the presence of RAP by investigating the aging state of the fresh mix using FT-IRS and a portable one is very convenient to use in the field. A test protocol is needed to be developed before successful implementation of the handheld FT-IR spectroscopy in the field.

1.2.2 Investigation of Cracking Susceptibility due to Aging (Tasks 3 & 4)

Every year almost 70 million tons of asphalt pavement is reclaimed in the US. 10% use of RAP can save up to 8% of overall material cost. But, aged binder in RAP makes the mixture stiffer and escalates the cracking susceptibility of the mixture at intermediate and low temperature which is the cause to restrict the maximization of RAP use in hot mix asphalt. The several modes of asphalt pavement cracking—thermal, reflection, fatigue, and top-down—are all affected by the high use of RAP if proper considerations are not made during the mix design. The use of rejuvenators is a suitable way to incorporate more RAP by offsetting the stiffness of the aged binder. Before field application of rejuvenated mix in the field, the designed mix must be studied for cracking susceptibility. A wide variety of laboratory tests and models to assess the cracking potential of asphalt mixtures are in practice and quite a few are recommended for routine use. For example, the Louisiana DOTD requires for a minimum value of *Jc* parameter from intermediate temperature SCB test, the Texas DOT puts the overlay test in their

standard specifications, and the Illinois DOT implements a balanced mix design method where flexibility index parameter from intermediate temperature SCB test is utilized. In this study, these three types of tests along with SCB at low temperature is performed on unaged and long-term laboratory aged specimens. Because of variations in RAP binder grades and a wide variety of rejuvenators, it is necessary to develop a procedure of mix design and selection of the optimum doses. This study is intended to address this mix design issue and to evaluate the performance of a traditional (Aromatic Oil) and recently become popular (Bio-based oil) rejuvenators through different cracking tests.

Sound understanding of the cracking mechanism can help to design a mix with higher cracking resistance. Failure in the asphalt mix occurs in the form of fracture that initiates between the aggregate and thin layer of asphalt binder as well as fine aggregate mastic (FAM). Laboratory tests in combination with numerical modeling can provide a better understanding to characterize the cracking behavior of asphalt mix. Being a viscoelastic material, the fracture of asphalt concrete shows both the brittle and quasi-brittle manner. At a higher loading rate or low temperature, the linear elastic fracture mechanics (LEFM) can a reasonable approach to predict the crack growth. But, at intermediate temperature and slow loading rate, the fracture process zone ahead of the crack tip is no longer an elastic region and requires different considerations than the LEFM. Cohesive Zone Material (CZM) model is an efficient and powerful approach to model crack initiation and propagation which considers the inelastic fracture process zone. The success of numerical modeling in the CZM model is directly related to proper identification of the cohesive properties of the media of fracture propagation. If the relation of the mix test geometry on the cohesive properties of FAM can be established,

the mix fracture behavior can be predicted without performing the mix test. Louisiana DOTD requires for a minimum value of *Jc* parameter from intermediate temperature SCB test (ASTM D 8044) which is a measure to quantify the cracking resistance of a mix. A mix must pass this test before the application in the field. This test is performed at an intermediate temperature and at a 0.5 mm/min loading rate. At this temperature and loading rate, the mixture is subjected to quasi-brittle failure. Crack in the mix propagates through the fine aggregate mastic (FAM) and the crack path avoids any large particle on its propagation. So, it can be considered that the critical fracture energy release rate (*Jc*) should be a function of the FAM. It should be possible to model the fracture behavior of asphalt mix in the SCB test by knowing the properties of the FAM. If the model is properly calibrated, an idea regarding the fracture resistance of the mix can be obtained by varying the FAM properties before performing the SCB test in the laboratory.

1.2.3 Development and Field Application (Task 5 & 6)

As a pavement ages, the oxidation process increases the stiffness of the pavement and makes it more susceptible to failure from load and thermal stresses. Slowing down a pavement's oxidative aging can maintain its flexibility and delay the aging-related issues. Lignin is the second most abundant biomass (plant) material available on our planet. Lignin has gained considerable attention as a modifier for asphalt because of its antioxidant properties and its potential to enhance the rheological properties of the binder. Lignin derived from locally sourced rice hull can be used as a modifier in asphalt and lignin modified binder should be more cracking resistance. This work investigates the incorporation of three kinds of lignin from biomass into asphalt binder to determine its effect on the binder's properties. Lignin precipitated from black liquor, Kraft lignin

that is commercially available, and lignin that is produced from rice hulls using deep eutectic solvent (DES) in the laboratory were added into asphalt binder. Extensive rheological testing of these binders was performed to reveal the enhancements possible with lignin addition. Asphalt mix prepared with a binder having lignin was tested for rutting, cracking, and moisture-induced damage susceptibility.

Rejuvenating agents can be sprayed on the pavement surface in liquid emulsion form which is known as a fog seal. Fog seal reduces the stiffness of the existing oxidized binder in the pavement and consequently lowers the cracking susceptibility of the pavement. Apart from its rejuvenating effect there arises two important issues due to the application of fog seal: reduction of hydraulic conductivity and comptonization with frictional resistance. However, reported research efforts until now are not sufficient enough to decisively prove either of these concepts. Very few studies were conducted to measure the effectiveness of the fog seal based on its capability to improve the permeability. To accurately quantify the field permeability using existing field permeameters on different pavement surfaces is a challenging task itself, let alone finding the improvement of permeability due to fog seals. Perhaps the most important trade-off that fog seal exhibits is the loss surface friction. Immediate loss of friction after application and friction recovery time varies by the product and application rate. Friction recovery time also depends on weathering and traffic. Over time, the constant rubbing action between the tire and the aggregate surface allows the thin layer of fog seal on top of the aggregate surface to be worn out, which helps the surface to regain its micro-texture. But, for low volume roads, the rate of recovery of the friction may be very slow. Very few studies addressed this particular issue of fog sealing on low volume roads.

Therefore, considering fog seals as a low-cost maintenance option for low volume roads, the friction characteristics of this surface after the treatment should be assessed thoroughly.

1.3 Organization of the Dissertation

The findings of the study are presented in this dissertation in the format of six standalone articles (four of them are already published in peer-reviewed journal papers). Each chapter from two to seven contains one article and chapter eight is the overall conclusion and recommendations for future studies.

In chapter 2, the correlation of binder aging in rolling thin film oven (RTFO) and asphalt mix aging in the oven is established. Because of the wide range of mixing temperatures and the variations in storage and paving times, field short-term aging differs significantly. To simulate the aging of binder and mix in the laboratory, a series of RTFO tests and short-term oven aging (STOA) were conducted. Rheological tests were performed on aged binder and extracted binder form aged mix to determine the aging index. A correlation between the binder and mix aging is established based on the aging index obtained through two different aging methods. Chapter 2 is a published paper in the International Journal of Pavement Research and Technology.

A test method is developed to determine the quantity of reclaimed asphalt pavement (RAP) in asphalt mix using a handheld Fourier transformed infrared (FT-IR) spectrometer in chapter 3. The effect of binder and mix aging was quantified in terms of carbonyl index (I_{CO}). A quick extraction procedure is developed that can be performed in the field in 15 minutes to collect enough binder for spectral data collection. At the end, the RAP mixes from ten selected projects were investigated during the production phase

using a handheld FT-IRS to determine the RAP content in the fresh mix. This chapter is a combination of one journal paper published in the ASCE Journal of Material in Civil Engineering and one conference proceeding published in the RILEM International Symposium on Bituminous Materials.

In chapter 4, bio-based and petroleum-based rejuvenators were evaluated based on cracking susceptibility of the hot mix asphalt prepared with low and high RAP content. Application of rejuvenators is the most effective way to incorporate high amount of RAP in the hot mix asphalt. Because of the high variability in RAP and availability of different kinds of rejuvenator in the market, a well-defined procedure is required to determine the optimum amount of rejuvenator. In this study, the procedure is developed, and the effectiveness of rejuvenators is investigated by the ability to reduce the cracking susceptibility of the rejuvenated mix. Cracking susceptibility of the mix was determined by a semi-circular bend test performed at intermediate and low temperatures as well as by an overlay test. The work of this chapter was presented at the annual conference of transportation research board. More work is done later and is written in a per file format soon to be submitted as a journal paper.

Finite element simulation was conducted in chapter 5, to predict the critical strain energy release rate (*Jc*) of asphalt concrete obtained by semi-circular bend test (SCB) according to ASTM D 8044. The model used the contact debonding feature for fracture analysis in ANSYS by adopting the bilinear cohesive zone material (CZM) method. To determine the *Jc* value of a certain mix, the DCB test was performed at test temperature using fine aggregate mastic (FAM) and the compressive modulus of asphalt concrete was determined. Using the DCM finite element model, the cohesive properties of FAM were

determined. Traction from the DCB test and the adjusted fracture energy based on the asphalt concrete modulus were used as input parameters for SCB finite element model with three different notch length and the *Jc* value was determined.

In chapter 6, the feasibility of using locally sourced lignin as an antioxidant in asphalt mixture is studied. This work investigates the incorporation of three kinds of lignin from biomass into asphalt binder to determine its effect on the binder's properties. Lignin precipitated from black liquor ("B"), Kraft lignin that was commercially available ("C"), and lignin that was produced from rice hulls using deep eutectic solvent (DES) in the laboratory ("L") were added into asphalt binder. Extensive rheological testing of these binders was performed to reveal the enhancements possible with lignin addition. Asphalt mix prepared with binder having lignin was tested for rutting, cracking, and moisture-induced damage susceptibility. This chapter is published in the Journal of Cleaner Production

Chapter 7 investigates the effect of the application of fog seal which is a lightly sprayed application of diluted emulsion on an asphalt pavement surface. Fog seals extends the life span of a pavement by reducing the stiffness of the existing oxidized binder. The application of fog seals comes with an additional advantage of a reduction in hydraulic conductivity of the pavement. But, the most important trade-off that fog seal is the loss of friction resistance of the surface. Quantification of these two parameters has been a challenge. In this study, four low volume parish roads in Caddo Parish, LA have been selected and two emulsions, namely CSS-1H and E-fog, were used to evaluate the reduction in hydraulic conductivity and to assess the characteristics of friction over time. This chapter is already published in the Transportation Research Record journal.

Chapter 8 summarizes the important conclusions from the previous chapters. It also includes recommendations for future studies.

CHAPTER 2

UNDERSTANDING THE SHORT-TERM AGING OF WARM MIX ASPHALT USING ROLLING THIN FILM OVEN[†]

2.1 Introduction

Though Warm Mix Asphalt (WMA) possesses several benefits over Hot Mix Asphalt (HMA): lower fuel consumption, extended paving season, increased hauling distance, and the possibility to incorporate more Reclaimed Asphalt Pavement (RAP), the use of WMA is still not indisputable. Rut resistance is one of the most important performance measures for newly compacted asphalt mix. Both the WMA and HMA are used in the field but sometimes they do not perform equally, especially when rutting is the main concern. Inferior rut resistance is one of the potential sources of questionable performance of WMA [2.1, 2.2]. Irrespective of WMA technologies used, and the binder or aggregate types, laboratory tests provide enough evidence to conclude that WMA is more susceptible to rutting than the HMA [2.3-2.6]. But the scenario of rutting susceptibility in roadways does not completely match with the laboratory experience. Sometimes the WMA could perform equally or even better in the field [2.7, 2.8]. Most of the laboratory rutting tests proved that WMA is more susceptible to rutting whereas, field

[†] This chapter or portions thereof has been published previously in the International Journal of Pavement Research and Technology under the title as it is in chapter title. Volume 12 (2019), DOI: 10.1007/s42947-019-0076-2. The current version has been formatted for this dissertation.

performance of WMA is not as poor as it is found by laboratory testing. A number of simulative rutting tests are being performed in different states: Asphalt Pavement Analyzer, Hamburg Wheel-Tracking Device, Laboratory Wheel-Tracking Device at Purdue University, Dry Wheel-Tracker, Rotary Loaded Wheel Tester, and Model Mobile Load Simulator are some of the equipment used for testing [2.9]. Very few of these tests use full-scale loading conditions.

Apart from the existing small-scale testing, rutting susceptibility of WMA in the laboratory was verified by using a full-scale wheel load tester developed at Louisiana Tech University [2.10]. A full-scale wheel load testing will eliminate the need for rigorous field evaluation and is expected to create the similar effect the pavement can experience under vehicular loading. A whole test was set up and the results are described briefly in figure 2-1. This full-scale wheel load tester was hand-built at Louisiana Tech University by welding together a frame that could support a load of up to 6000 pounds. The tester primarily used a piston powered by a 23-horsepower hydraulic pump to move a single wheel back and forth which was supported by the steel frame. To hold the brick shape test specimens during the test, a mold was prepared from quarter-inch thick steel plate. It could hold five specimens for both the dry and submerged rutting tests. The temperature of the test specimens was controlled by two 1500-watts infrared heaters during the dry test and during the submerged test the water was heated by an immersion heater.

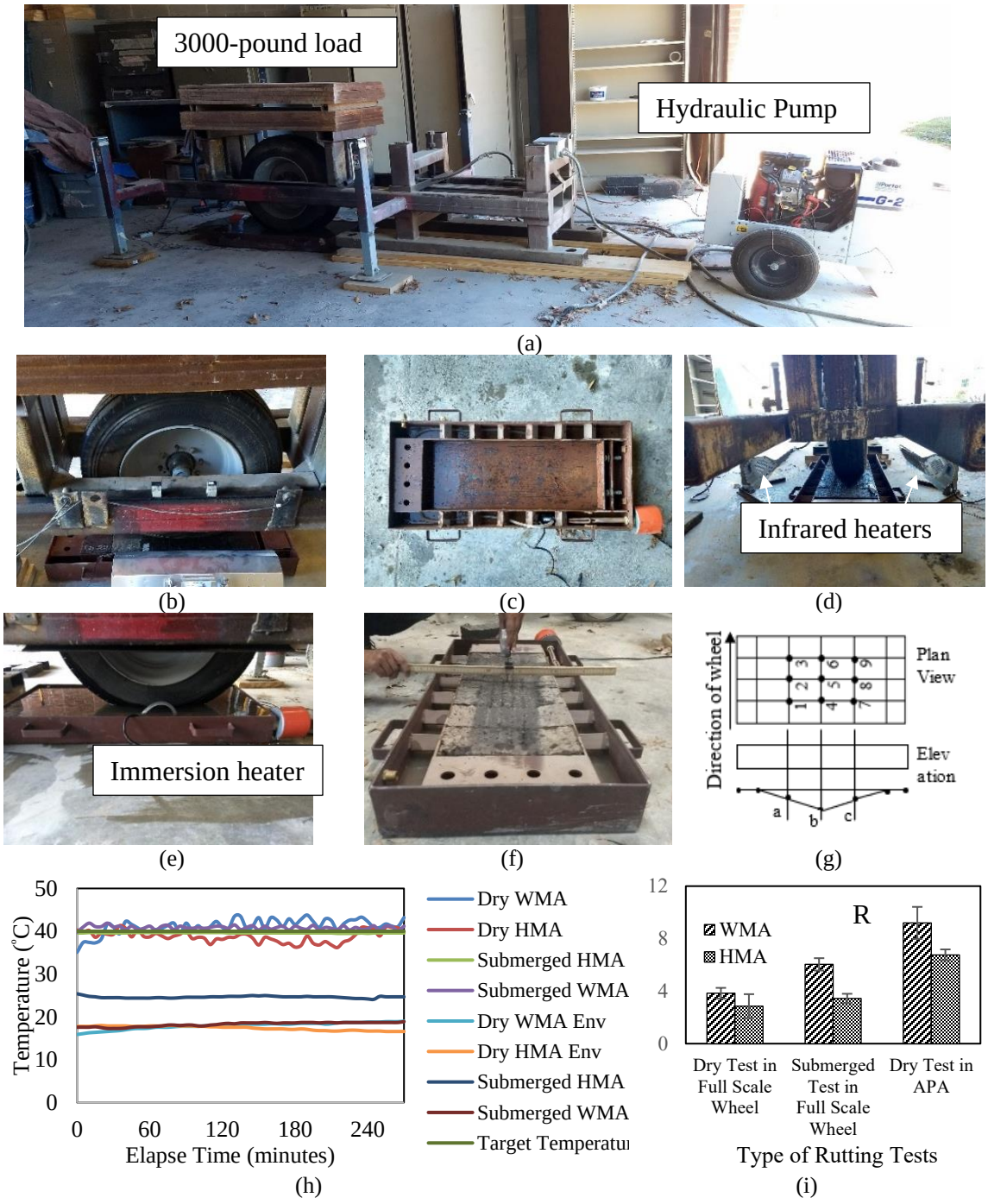

Figure 2-1 Details of Full-scale wheel load testing: (a) full view of full-scale wheel load tester, (b) sensors and magnets to control the span of wheel, (c) specimen mold made of steel for testing, (d) testing in dry conditions is going on, (e) testing in submerge conditions is going on, (f) afterword the testing rut depth is measured manually for individual specimen, (g) 9 different points on the brick specimen where rut depth was measured and qualitative representation of rut depth, (h) variation of temperature with time during the test, (i) average rut depth obtained in different tests [2.10].

The test was performed at 40 ºC though the binder was PG 64. Because of the slower speed of the wheel, it might cause severe damage at 64 ºC. The specimens were placed in the middle of the mold with two supporting specimens at ends, and the side was tightened properly. In the case of submerged testing, the specimens were saturated at testing temperature for 12 hours. The machine was loaded with 3000 pounds of load using thick steel plates before the test started. The speed of the wheel pass was selected as 13 seconds per cycle and it took four and a half hours for the machine to complete the whole test. After 1200 cycle wheel passes, the final rut depths were measured manually at 9 different points on each specimen.

It was clear that WMA specimens experienced more rut than the HMA specimens in both the dry and submerged conditions. The average increase in rut depth for the WMA specimen was 34% than the HMA specimens. This increase in rut might not be statistically significant as the sample size was small, but this trend was similar for all the specimens. Physical observation of specimens after the submerged testing exhibited that moisture caused significant damage to both the HMA and the WMA. The increase in rut depth for HMA after submerged testing is 20%, whereas for WMA this change was 57%. This is a clear indication of moisture-induced damage of the asphalt mix and WMA is more susceptible to this damage than that of HMA.

The hardening of the binders in the mix happens over time because of the volatilization of light asphalt component and oxidation during service life. This process is referred to as aging [2.11]. During the mixing and compaction process, binders undergo aging at higher temperatures, and, consequently, a higher oxidation rate occurs which is known as short term aging. As WMA is produced at a lower temperature than HMA,

there is a probability for WMA that the binder in the mix does not attain enough stiffness [2.3, 2.4]. Full-scale wheel load testing performed by the authors corroborates with the assumption that lower short-term aging of WMA may lead the compacted mix subjected to more rutting in comparison with traditional HMA. Complex modulus of unaged binder and recovered binder from WMA and HMA used for rutting tests were determined using a DSR. The result was calculated in terms of the aging index (AI), which is the ratio $G^*/\sin\delta$ value of aged and unaged binder. AI for unaged, WMA, and HMA binders were found 1.00, 1.50, and 3.78 respectively. Lower mixing and aging temperature of WMA caused the lower AI of recovered WMA binder than the binder recovered from HMA. It was observed that higher rut depth is associated with the binder having lower $G^*/\sin\delta$ value and vice versa. The specimens were made of the same mix, compacted at the same air void, and tested under similar conditions. The only difference is that one in WMA and the other is HMA. So, the difference in rutting depth was solely the result of lower aging and consequently the lower stiffness of the binder.

Rolling thin film oven (RTFO) test (AASHTO T 240) was adopted by the Strategic Highway Research Program (SHRP) for simulating the short-term aging of the binder in the laboratory [2.12]. The duration of the RTFO test was chosen as 85 minutes and it was expected that 85 minutes of aging at 163ºC would create the oxidative aging effect of average field conditions irrespective of binder type or mixing technology. In reality, because of wide mixing temperature range, variation in the duration of storage and paving times, field aging differs significantly from that of RTFO aging for HMA let alone for the WMA as there does not exist any established method to predict the binder aging in the laboratory [2.13]. Standard RTFO test might be an approach to characterize

the binder but it is not capable of representing the short-term aging of the binder in the field as well as in laboratory [2.4]. Although few studies were conducted to modify the RTFO aging procedure for modified binders [2.15, 2.16], still, no established protocol is available for RTFO aging to simulate WMA aging.

For asphalt mixture, the recommended laboratory procedure for short-term aging is to heat the loose mix in a forced draft oven, which is known as short term oven aging (STOA). AASHTO R 30 recommends conditioning the loose HMA for 2 hours at compaction temperature for volumetric design, and 4 hours at 135ºC for preparing specimens for performance testing. In a recent study conducted by Epps Martin et al., 2 hours of STOA at 135ºC for HMA and 116ºC for WMA was recommended to simulate the short-term aging [2.17]. There should exist a correlation between STOA and RTFO aging as both are performed in a controlled environment. Lee et al. predicted the required RTFO aging time to get the same effect of STOA based on the increased large molecular size (LMS) ratio obtained by the Gel Permeation Chromatography (GPC) method for HMA [2.18] but that study did not deal with WMA. There is a need to develop an RTFO aging model which can correlate the STOA for a WMA as well as for a wide range of aging time and temperature combination.

2.1.1 Objective

The primary objective of this study is to develop an RTFO aging model by correlating the rheological properties of STOA mixes to predict the STOA effect by testing the binder in RTFO. Some goals considered while accomplishing these objectives are:

- Investigate the effect of RTFO aging time and aging temperature on the rutting parameter (G*/sinδ) of binder.
- Investigate the effect of short-term oven aging (STOA) time and temperature on the rutting parameter (G*/sinδ) of binder extracted from oven aged mix.
- To clearly explain in detail how plant produced mix is subjected to the short-term aging in the field

2.2 Materials and Experimental Plan

HMA and WMA used for this study were produced in the laboratory as well as in the plant. Laboratory mix was a ½ inch NMS mix with 4.6% asphalt content. Advera was used as a WMA additive. Two types of binders were used: PG 64 and PG 58, and the aggregate was crushed granite and manufactured sand. These mixes were subjected to short term aging in the oven at three different temperatures, and the binder was extracted and recovered from the mix for stiffness testing.

HMA and foamed WMA plant mix were collected from Madden Contracting Co Inc. The nominal maximum size of the mix was ½ inch and aggregate was limestone. PG 64-22 asphalt binder was used for the mix with 5.0% asphalt content. Loose HMA and WMA specimen were collected immediately after mixing and stored in a cardboard box. After 2, 4, and 8 hours, a small portion of the mix was separated for further extraction. In the case of HMA, a specimen was collected from the construction site which had a 55 minutes hauling distance. Another HMA loose mix was collected from the silo after 14 hours of storage at 163 ºC. Recovered binder from the loose mixes was tested in DSR for determining the complex modulus.

A series of RTFO tests were conducted on two binder types at three different temperatures and for four aging periods. STOA was performed for the same time duration on laboratory mix produced at the same three RTFO aging temperatures. Table 1 describes the detailed experimental plan for this study.

Table 2-1 Experimental plan.

Short Term Aging of Binder in RTFO					
Conditioning	**Binder**	**Temperature**	**Duration**	**Rheology**	
RTFO Aging of Binder	PG 64, PG 58	163^{0}C, 148^{0}C, 135^{0}C	0, 60, 120, 240 minutes	Dynamic Shear Modulus at 64^{0}C (for PG 64 binder) and 58^{0}C (PG 58 binder) with 25 mm plate, 12 rad/sec angular frequency, 10% strain rate	
Short Term Aging of Mix					
Conditioning	**Binder**	**Temperature**	**Duration**	**Extraction**	**Rheology**
Oven Aging of Laboratory Mix	PG 64, PG 58	150^{0}C, 135^{0}C, 120^{0}C	0, 60, 120, 240 minutes	One batch from each temperature and duration. Total 24 extractions	Dynamic Shear Modulus at 64^{0}C (for PG 64 binder) and 58^{0}C (PG 58 binder) with 25 mm plate, 12 rad/sec angular frequency, 10% strain rate
Plant Produced Mix (without reheating)	PG 64	171^{0}C, 141^{0}C	Immediately after mixing, From wrapped box at 2, 4, 8 hours duration for HMA and WMA. For HMA additional specimens were collected from Site and from silo after 14 hours of mixing.	6 extractions for HMA and 4 extractions for WMA	

2.3 Methodology

2.3.1 Development of HMA and WMA Mix Design in the Laboratory

To conduct this study an HMA mix design was developed in the laboratory using PG 64-22 binder. Mix was produced at 163ºC and aged 150ºC for 2 hours in an oven. At design gyration of 100, the air void was found 3.89%. Optimum asphalt content was determined according to the table 502-5 of section 502 of the 2006 Louisiana Standard Specifications for Roads and Bridges [2.19]. The same mix design was followed when the mix was prepared with PG 58-22 binder.

To get an optimum WMA mix design, the gradation of aggregate and asphalt content was not altered. Advera was added to the binder as a WMA additive. The challenge was to figure out the optimum amount of Advera that could produce WMA at lower mixing and aging temperature with the same density as that of HMA. After a numbers of trials, two advera contents at two mixing temperatures were selected for preparing WMA in the laboratory for further testing. Advera was added by 0.3% (by weight of the binder) for WMA where mixing and aging temperatures were 148 and 135 ºC respectively, and 0.5% advera was used for WMA where mixing and aging temperature were 135 and 120 ºC respectively. For both the cases, mixes were aged for 2 hours in the oven to simulate the short-term aging. In this asphalt mix design, it was assumed that oven aging temperature would be 13 to 15ºC lower than the mixing temperature.

2.3.2 Investigation of Plant Produced Mix

An asphalt mixing plant in Natchitoches, LA was visited to observe the whole scenario of mixing, storage, and transportation of the mix. The plant, Madden Contracting Co Inc. could produce both HMA and foamed WMA. At every step of mixing, storage, and transportation the temperature, as well as the duration, was monitored. Aggregate at ambient temperature was fed into the mixing drum where they were heated at 175ºC for 10 to 15 minutes. Binder was being heated at 170ºC in a separate tank. Aggregate and liquid binder came into contact at 15 ft from the end of the drum. At this place, the temperature was maintained at 170ºC. The mixing process was continued for 2 to 4 minutes and the mix was then sent to the silo through the conveyer. At the end of the drum, the temperature was observed 170ºC for HMA. The mix was then

stored in a silo at 163ºC. The silo was kept heated by the circulated hot oil by the periphery of the silo wall. The mix could be stored in a silo for 30 minutes to 16 hours depending on the requirement from the site. When the truck was ready the mix was discharged from the silo to the truck. For this study, the mix was collected in a cardboard box from the truck. At the time of loading to the truck, the temperature of the mix was observed from 144 to 155ºC. a specimen was also collected from the construction site after 55 minutes since the mix was loaded in the truck. The temperature at the site was found 130 ºC, which can be considered as compaction temperature.

In the case of WMA, the aggregate was heated at 140 ºC, but the temperature of the binder tank was kept constant at 170 ºC. Foaming water is added as 2% by weight of the binder. The duration of mixing time and other processes is like that of the HMA mixing process. When the mix is being transferred to the silo, the temperature was found to be 140 ºC. The temperature of the silo where WMA was stored was 153ºC which is higher than the mixing temperature. When the WMA sample was collected from the truck the temperature was found between 121 and 126ºC. Figure 2-2. (a-h) describes the different stages of plant mix production and observed temperatures are reported in the figure.

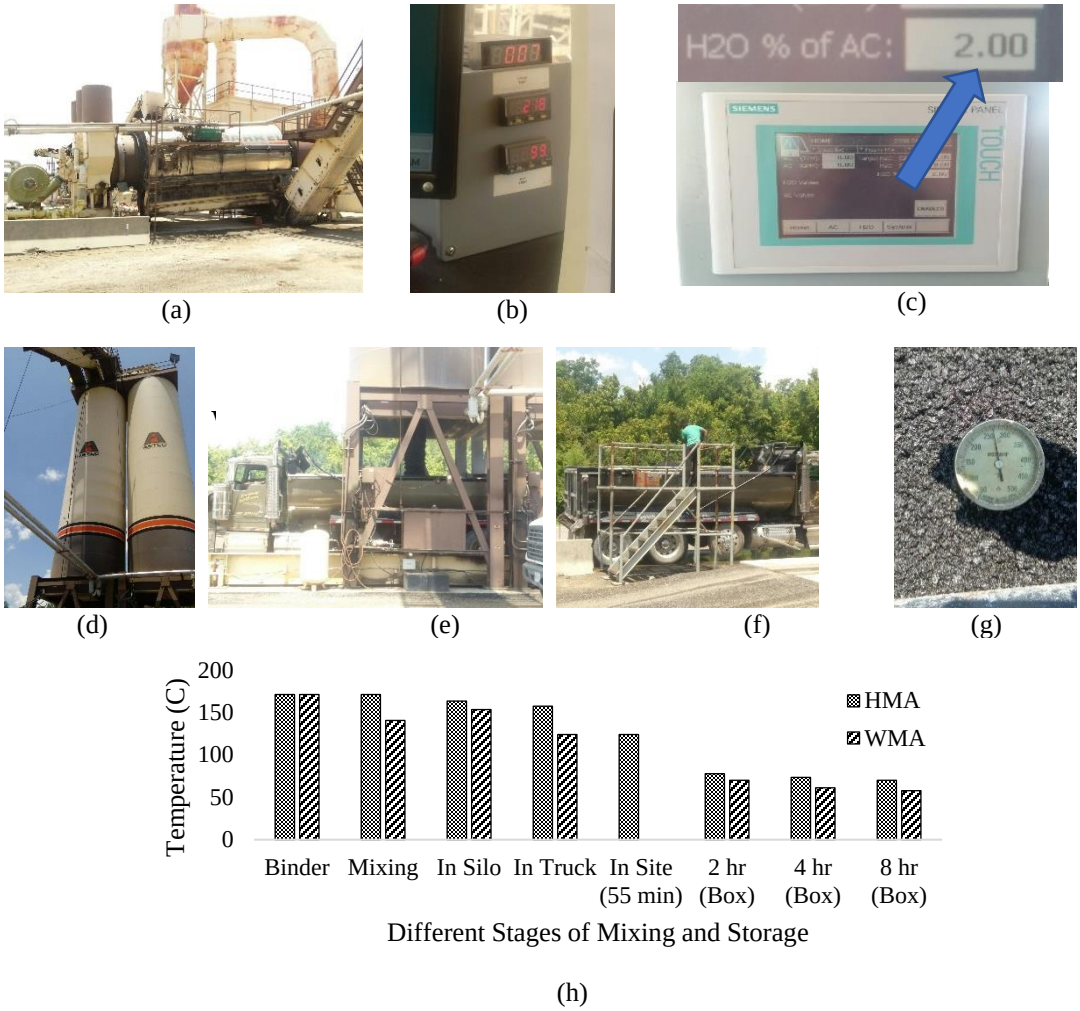

Figure 2-2 Collection of mix from the plant: (a) mixing drum in the plant, (b) temperature is monitored from the plant control room, (c) foaming water content regulator, (d) mix is stored in a silo at elevated temperature, (e) mix is being delivered into the truck, (f) loose mix is being collected in a cardboard box for later extraction, (g) temperature of the mix in the truck is monitored using thermometers, (h) temperature at different stages of mixing and storage for HMA and WMA.

2.3.3 Testing of Rheological Properties of STOA and RTFO Aged Binder

To simulate the short-term binder aging in the laboratory, the RTFO test was done following AASHTO T 240 standard but at three different temperatures: 163, 148, and 135ºC. The temperatures were selected in such a way that they would match with the

mixing temperature of the HMA and WMA. The duration of short-term aging in RTFO was selected as 1 hour, 2 hours, and 4 hours. The specimen was collected after a specified time duration and tested in DSR to find the stiffness.

Short-term oven aging (STOA) of the mix was performed according to AASHTO R 30 at three different conditioning temperatures: 150, 135, and 120 ºC. The duration of the STOA was set as, 1 hour, 2 hours, and 4 hours to match with the duration of RTFO aging.

The binder from short term aged mix was extracted using a centrifuge following the ASTM D 2172 using n-Propyl Bromide as an extraction solvent and then was recovered using rotary evaporator following the ASTM D 5404. The recovered binder was then tested to determine the stiffness using DSR (AASHTO T 315).

2.4 Results and Discussions

2.4.1 Investigation of the Aging Index of Plant-Produced Mix

After the mixing process, the mix is stored in a silo at an elevated temperature. The shortest time the mix was stored in the silo was around 30 minutes. The mix was then delivered to the truck and transported to the construction site. Mix was collected in a cardboard box for extraction and recovery in the future. The longest time the mix was kept in the silo was overnight, to be precise it was 14 hours. One box of mix was collected from the hauling truck. Figure 2-3. shows the aging index (AI) of HMA and WMA at a different duration of time after mixing. The AI is calculated based on the $G^*/\sin\delta$ value of unaged binder: 1.408 kPa. It is observed that the aging index of HMA when the first truck is being loaded was 1.989. The mix collected from the construction site, 55 minutes after being loaded the truck exhibits the aging index of 2.115. It indicates

that carrying the mix to the construction site has very little influence on increasing the stiffness of the binder. Mix was stored in the cardboard box and was wrapped thoroughly. Those boxes were kept under the sunlight and were fully wrapped by tape so that the mix does not come into direct contact of outside air. It was expected that the mix would be sufficiently aged inside the cardboard box, but because of quick heat dissipation, the mix was not aged as expected. The specimen was taken out after 2, 4, and 8 hours from separate boxes to check the change in aging. Figure 2-3. shows a change in the aging index with time. The maximum change in the aging index is observed as 6.833 in the mix which was stored in the silo for 14 hours. It is expected that though mixes are stored at an elevated temperature in a silo, it might not get aged because it does not come into contact with air. This assumption is not completely true. A significant part of the short-term aging is happening in the silo. A WMA mix was also collected from the boxes at 2, 4, and 8 hours time intervals, and the aging indices are plotted in Figure 2-3. In the case of WMA, a specimen was not available to collect from the the silo after 14 hours. From two to eight hours of storage in the cardboard box, HMA showed an 87% increase in AI while WMA showed only a 20% increase.

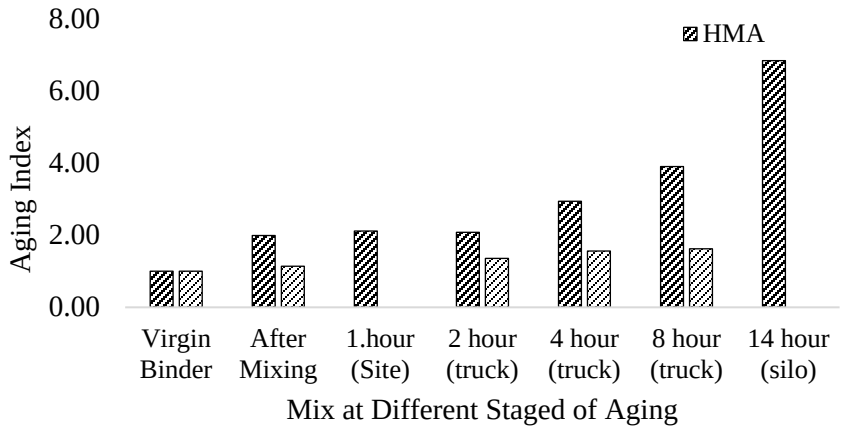

Figure 2-3 Aging Index of plant produced mix at different stages.

2.4.2 Effect of Mixing Temperature on Short-Term Aging

How mixing temperature affects the aging of the binder in the mix was investigated in this study. HMA and WMA specimens were collected right after the mixing process where mixes were not allowed for further aging in the oven. HMA was mixed at 163ºC and WMA was mixed at 135ºC. Binder was extracted and recovered from the mix and the rutting parameter (G*/sinδ) was determined in DSR. The result is reported in Figure 2- 4 as the aging index (AI), which is the ratio of the G*/sinδ of binder after and before aging. From the figure, it is observed that AI of the PG 64 binder changes 5.7% for HMA and 9.7% for WMA. In the case of PG 58 binder, the values are 16.9% and 33.6%. On the other hand, WMA and HMA are collected from the plant mix as soon as possible after the mixing. HMA was collected after 40 minutes of mixing while WMA was collected after 30 minutes of mixing from the silo. The aging index between them is noticeable. The aging index for HMA increases 50.6% and for WMA this increase is 25.9%.

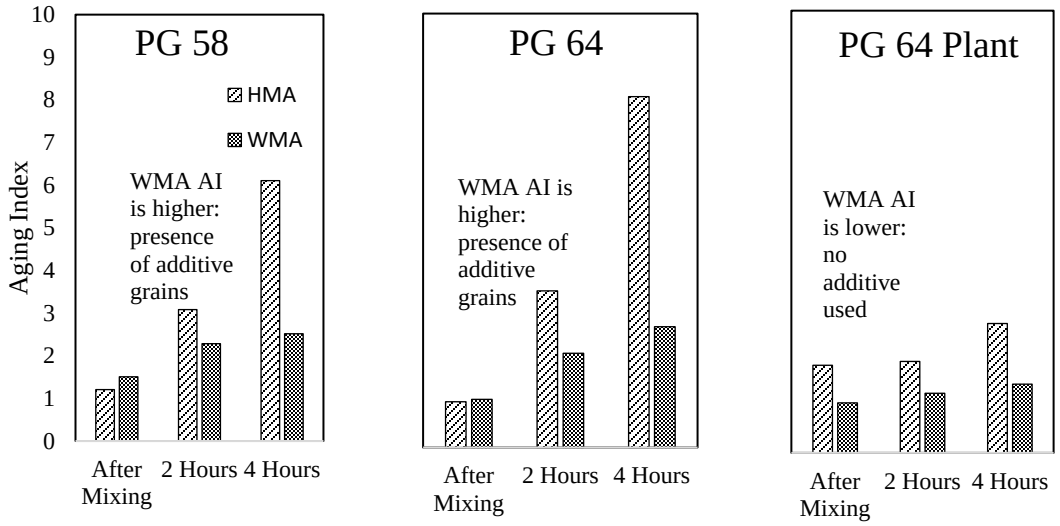

Figure 2-4 Effect of mixing temperature on binder aging during the mixing process.

The results imply that a portion of the short-term aging of the binder occurs during the mixing process. During the heating and mixing process, binder loses its volatile parts and some oxidative reactions may take place. This aging process is more pronounced in cases of plant mixing because the mixing process is done in the drum at a higher ambient temperature of 170 ºC. Laboratory mix is produced at a lower ambient temperature than that of the plant mix.

Though laboratory WMA is mixed at lower temperatures, it shows an increase of AI higher than the HMA, but the plant mix WMA exhibits a lower increase in AI than HMA. In the laboratory, Advera was used as a WMA additive and the fine particles of the additive can act as a filler material which results in an increase in the complex modulus [2-20]. With aging time, the effect of granular particles of the additive was superseded by the aging effect of binder, which is clear from Figure 2-4. In the plant mix, as water was used as a foaming agent, the percent increase in AI of WMA was lower than that of HMA. There is also a possibility that during the storage period, some parts of

aging occurred at different temperatures for WMA and HMA which eventually distinguished the two mixes in terms of AI. So, it can be concluded that the laboratory mixing process cannot completely simulate aging during the mixing process that is happening in the plant.

2.4.3 Development of an Aging Model

2.4.3.1 *Effect of time and temperature on the aging index of RTFO aged binder*

The Aging index of RTFO aged binders are plotted in Figure 2-5(a) and 2-5(b) against time. As binders got exposed for a longer time in heat and airflow, they got more aged. It is observed that the change in the aging index with time follows a linear relationship for both the PG 64 and PG 58 binders irrespective of the aging temperature. The coefficient of determination varies from 0.91 to 0.99 which is an indication of a good linear relationship. If the aging temperature is raised, it follows the linear relationship but with a higher rate because a higher RTFO aging temperature expedites the short-term aging mechanism of the binder. The change in slope with temperature was used later to develop an aging model which is discussed later in section 4.3.5. In this study short-term aging of the binder is investigated where the binder as well as the mix was aged up to four hours. The linear relationship observed here is true for a short-term aging scenario where binder is aged at high temperature but for a shorter period.

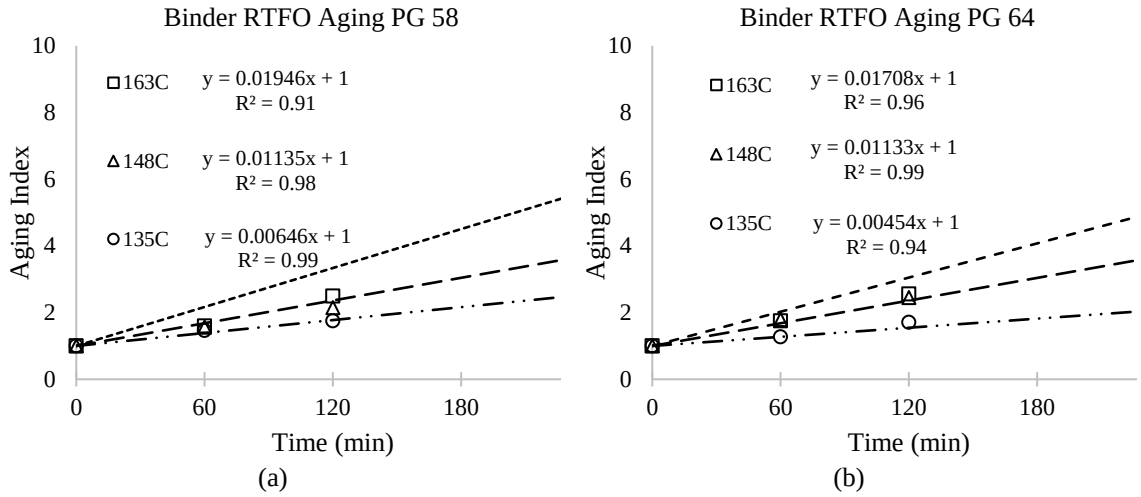

Figure 2-5 Effect of RTFO aging on binder.

2.4.3.2 *Effect of time and temperature on the aging index of oven aged mix*

Mix was taken out of the oven after STOA for a stipulated time at a predefined temperature. It was then cooled at room temperature. Binder was extracted and recovered the next day for testing the rheological properties in DSR. The aging index of recovered binder from the oven aged mix is plotted in Figure 2-6 (a) and (b). Aging index is observed to change linearly with duration of oven aging like RTFO aging and the rate of change is higher at high aging temperature.

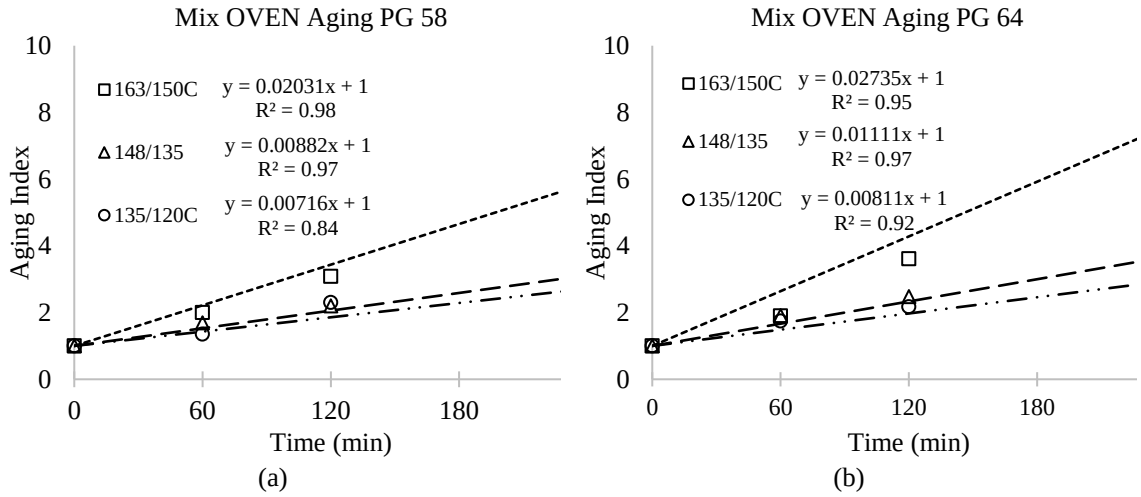

Figure 2-6 Effect of short-term oven aging of mix.

2.4.3.3 *Effect of binder grade on aging index*

Aging Index was determined in two different methods using two types of binders, at three aging temperatures and for three different aging duration. A multi-factor ANOVA was performed to determine the factors affecting the aging index. The result is tabulated in Table 2. A P-value smaller than 0.05 indicates that the factor significantly affects the experiment. From Table 2, it is understandable that both the aging duration (time) and the aging temperature havesignificant effects on the aging index. Binder grade does not have any statistically significant effect on the aging index as the p-value is larger than 0.05.

Table 2-2 ANOVA to determine the variables that affect the Aging Index.

Source	RTFO Aging				OVEN Aging			
	DF	F-Value	P-Value	Remark	DF	F-Value	P-Value	Remark
Time	3	19.26	0.000	Significant	3	12.74	0.000	Significant
Temperature	2	5.32	0.016	Significant	2	5.30	0.016	Significant
Binder Grade	1	0.09	0.767	Not significant	1	0.69	0.419	Not significant

2.4.3.4 *Rate of change of aging index with temperature*

From figure. 2-5(a), 2-5(b), 2-6(a), and 2-6(b) it is evident that at higher aging temperature, for both the RTFO and oven aging, the rate of change in the aging index is higher. It is expected that there might exist a relationship between the rate of change in the aging index and the aging temperature. Figures 2-7(a) and 2-7(b) are the plots of the slope of the AI-time line obtained from figure 2-5 and figure 2-6. As binder grade does not have a statistically significant effect on AI of the binders, one linear relationship is considered including two different grade binders for each aging method. It is noticeable that oven aging accelerates the aging process faster than that of RTFO aging as the rate of change in AI is higher for the oven aged mix (figure 2-7(a)) in comparison to RTFO aged binder (figure 2-7(b)). The reason behind the higher AI of the mix can be attributed to the larger surface area and lower film thickness of the binder in the mix in comparison to the binder film when being aged in RTFO.

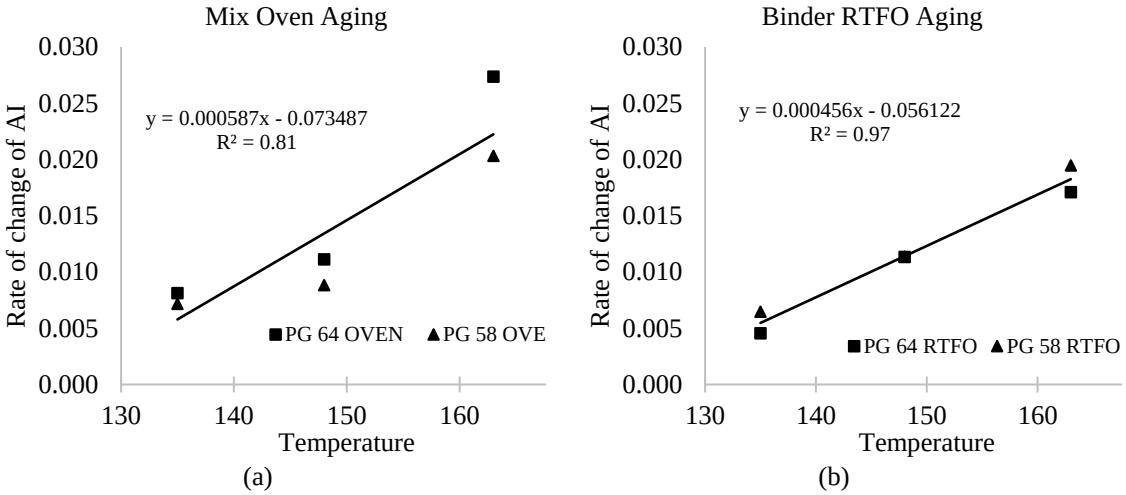

Figure 2-7 Rate of change of AI with temperature.

2.4.3.5 *Proposed RTFO aging equations*

Figure 2-5(a), 2-5(b) and 2-7(b) can be utilized to develop an aging model for RTFO aged binder and Figure 2-6(a), 2-6 (b) and 2-7(a) can be utilized to develop the model for oven aged mix. Short-term aging of binder or the mix is dependent on both the aging temperature and the aging time as discussed in section 4.3.3. So, the model should consider two input parameters: temperature and time. Figures 2-5 and 6 provide the relationship between the aging index and time at three different temperatures. When the slope of the AI-time line for oven aged mix (Figure 2-6(a) and Figure 2-6(b)) are plotted against aging temperature in Figure 2-7(a) they show a linear relation with the regression equation $y = 0.000587x - 0.073487$, where y is the slope of AI-Time line at given temperature x. This equation can be used to predict the slope of the AI-Time line when the aging temperature is given. Whenever the slope at any temperature is obtained, the aging index with time can be calculated as they follow a linear relationship.

A linear equation in the form given in Eq. (2.1), where *Sr* is the temperature-dependent calculated slope of AI-Time plot, can predict the AI of aged binder. As the AI of unaged binder is 1, when the aging duration is zero minutes, the equation should return the AI value of 1.

$$AI = S_r * Time + 1 \qquad \text{(Eq. 2.1)}$$

Further manipulation of the Eq. (2.1) reduces it to Eq. (2.2) where *m* is the slope of Rate of change of AI-Temperature plot and *C* is the intercept obtained from the regression equation shown in Figure 2-7. The Eq. (2.2) is valid for both the RTFO aging of binder and STOA of mix.

$$\begin{aligned} AI &= S_r * Time + 1 \\ &= (m * Temp + C) * Time + 1 \\ &= m * Temp * Time + C * Time + 1 \\ &= mx_1 * x_2 + C * x_2 + 1 \end{aligned} \quad \text{(Eq. 2.2)}$$

Following this approach, two aging equations are developed shown as Eq. (2.3) and Eq. (2.4). where x_1 is the aging temperature and x_2 is the aging duration for oven aged mix. In the case of RTFO aged binder, x_1 and x_2 are substituted by y_1 and y_2 respectively.

Oven Aging: $AI = 0.000587x_1 * x_2 - 0.073487 * x_2 + 1$ (Eq. 2.3)

RTFO Aging: $AI = 0.000456y_1 * y_2 - 0.056122 * y_2 + 1$ (Eq. 2.4)

Eq. (2.3) and Eq. (2.4) were used to predict the AI of oven aged mix and RTFO aged binder respectively. Aging temperature and duration used in those equations are the independent variables. Observed AI values are plotted against Predicted values in Figure 2-8(a) for RTFO aging and in Figure 2-9(a) for oven aging. The 95% confidence interval band is also provided in the plot. The residuals are plotted in Figure 2-8(b) and Figure. 9(b) for the corresponding models. From Figure 2-8(a) and 2-9(a) it can be noted that the observed AI value changes linearly with the predicted value obtained by the proposed equations Eq. (2.3) and Eq. (2.4) respectively. Considering a linear relationship, between observed and predicted values the regression equation can be rewritten as:

$$Observed\ AI = \beta_1 * Predicted\ AI + \beta_0$$

β_1 and β_0 are the slope and the intercept of the Observer-Predicted plot (Figure 2-8(a) and Figure 2-9(a)).

If the proposed model can accurately predict the AI of the tested specimen, the observed and predicted values will be the same, which indicates that the slope will be equal to 1 and the intercept will be 0. The equation becomes:

$$Observed\ AI = Predicted\ AI$$

Equation of AI for mix oven aging with R^2 value of 0.89 is obtained as

$$Observed\ AI = 1.01 * Predicted\ AI - 0.03$$

Similarly, the equation for RTFO aging with an R^2 value of 0.85 is obtained as

$$Observed\ AI = 1.00 * Predicted\ AI - 0.12$$

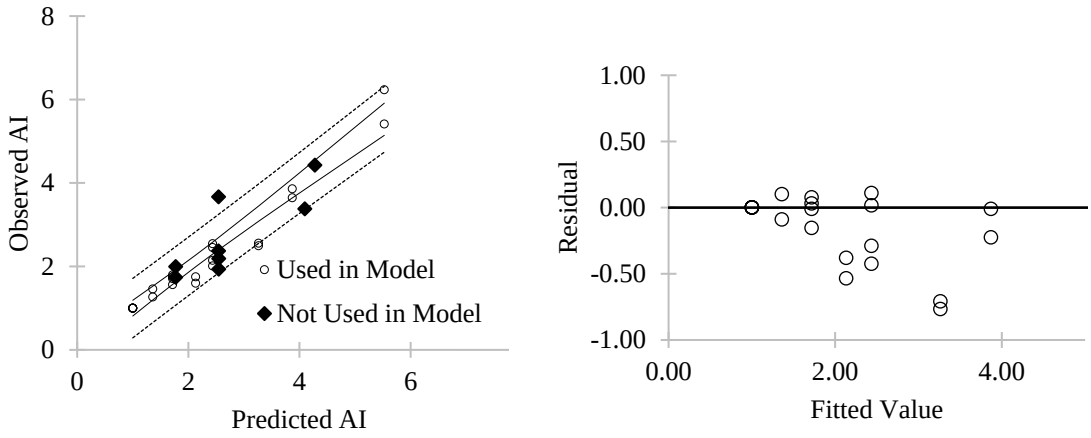

(a) (b)

Figure 2-8 Proposed aging index (AI) model for RTFO aging of binder.

A hypothesis testing was performed on the slope and the intercept of the Observed AI-Predicted AI line. The results of hypothesis testing is given in Table 2-3. For both the parameters, there are strong evidence that the null hypothesis cannot be

rejected. That means with a 95% confidence interval it can be concluded that the slope of the Observed AI-Predicted AI line is 1 and the intercept of the line is 0. So, it can be concluded that the proposed model can successfully predict the AI when aging time and temperature are provided. The residuals plotted in Figure. 8(b) and 9(b) also supports the conclusion as there is no obviously visible trend is observed.

Table 2-3 Hypothesis testing to check the validity of the proposed model.

Hypothesis		**RTFO Aging**			**OVEN Aging**		
		t stat.	**P-Value**	**Remark**	**t stat.**	**P-Value**	**Remark**
Slope	H_0: slope = 1 H_1: slope ≠ 1	1.770	0.092	Cannot Reject	1.813	0.083	Cannot Reject
Intercept	H_0: intercept = 0 H_1: intercept ≠ 0	0.895	0.380	Cannot Reject	0.165	0.870	Cannot Reject

In Figure 2-8(a) and Figure 2-9(a), along with the 95% confidence interval, a 95% prediction interval band is also provided. The points presented in dark solid legends were not used to develop the Eq. (2.3) and Eq. (2.4) but were used to validate the model. Except for one point in each plot, the predicted AI of both the oven aged mix and RTFO aged binder fall inside the prediction interval which supports the validity of the proposed aging equations.

To develop this prediction model, the binder was aged in RTFO from 135 to 163 ºC. Mixing temperatures of the mix were between 135 and 163 ºC. Figure 2-8 and Figure 2-9 show that at a higher temperature, the uncertainty of the data point to follow a linear regression is higher. So, beyond this temperature range, which was used to develop the model, it may not predict the actual aging of the RTFO aged binder as well as the oven aged mix.

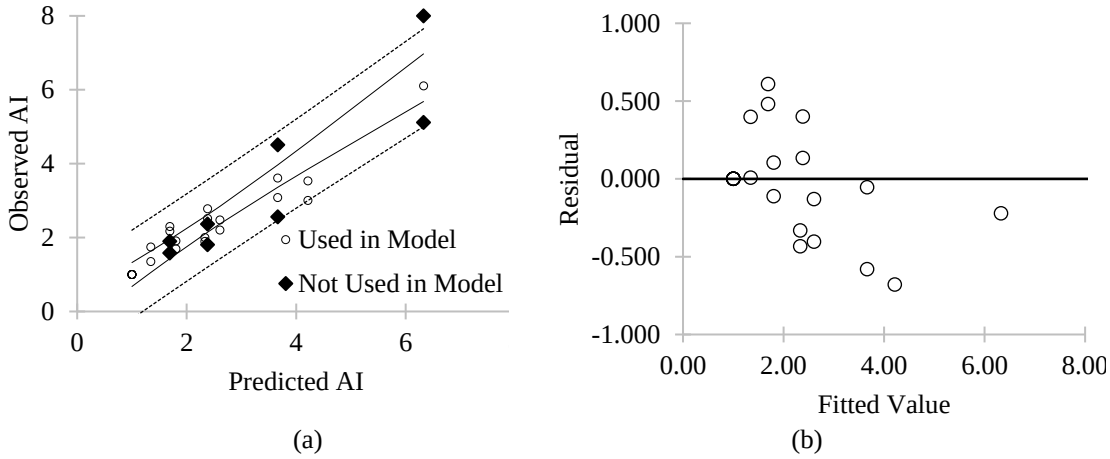

Figure 2-9 Proposed aging index (AI) model for short-term oven aging of mix.

2.4.3.6 *Application of the model to determine RTFO test temperature and time to simulate oven aging*

This model can be utilized to select the suitable RTFO aging temperature and time so that it can successfully predict the effect of mix aging. The Eq. (2.3) for oven aging can be rearranged as follows:

$$\begin{aligned} AI\ (OVEN) &= 0.000587(x_1) * (x_2) - 0.073487 * (x_2) + 1 \\ &= 0.000587(x_1) * (x_2) - 0.056122 * (1.31x_2) + 1 \\ &= 0.000456(0.98x_1) * (1.31x_2) - 0.056122 * (1.31x_2) + 1 \\ &= 0.000456(y_1) * (y_2) - 0.056122 * (y_2) + 1 \\ &= AI\ (RTFO) \end{aligned} \quad \text{(Eq. 2.5)}$$

In the above equation coefficient of x_2 is divided into two parts so that one-part matches with the coefficient of y_2. A similar idea is applied for the coefficient of x_1 too. AI (OVEN) equation implies that RTFO aging should be conducted at the temperature of $0.98*x_1$ and the duration should be $1.31*x_2$ to get the same aging effect on the binder when the mix is aged in the oven for x_2 minutes and the mixing temperature was x_1ºC. For example, if a mix is produced at 140ºC and it is aged in the oven for 2 hours, to get

the same aging effect in RTFO, the test should be conducted at *0.98*140* or 137 ºC and duration should be selected as *1.31*120* or 157 minutes.

2.4.3.7 *RTFO aging model for plant mix*

In this study, a good correlation was found between binders RTFO aging and mix oven aging. RTFO causes less aging effect than that caused by the oven aging. In the field, it is difficult to predict the short-term aging because numbers of variables are involved. So, it is not possible to develop a model that can predict the short-term mix aging in the field with the data collected from one site. Mixing time, temperature, storage time, hauling distance, and time factors can be considered while predicting the short-term plant aging, but it will be site-specific. So, the RTFO aging time and temperature can be selected following the method developed in this study to match the aging effect in RTFO with the specific field condition.

2.5 Conclusions

- Change in stiffness for RTFO aged binder and oven aged mix follows a linear relationship with aging time. The rate of change of AI also changes linearly with temperature. STOA exhibits more sensitivity to temperature than that of RTFO aged binder.
- There exists a correlation between RTFO aged binder and oven aged mix. Following the aging model developed in this study aging temperature and duration can be selected for RTFO testing to simulate the aging effect that a binder experiences in oven aging of the mix. To get the similar binder stiffness of

oven aged mix prepared at x_1ºC and being aged in the oven for x_2 minutes the binder should be aged in RTFO for $1.31*x_2$ minutes at $0 .98* x_1$ ºC.

- The main portion of short-term aging in the field occurs during the storage of the mix in the silo. A very small portion of aging occurs during the mixing phase.
- Because of a wide variety of factors, RTFO aging cannot be directly correlated with plant aging. The RTFO aging test protocol needs to be adjusted depending on the actual field condition.

CHAPTER 3

DEVELOPMENT OF A TEST METHOD TO MEASURE RAP PERCENTAGE IN ASPHALT MIXES IN THE FIELD USING A HANDHELD FT-IR SPECTROMETER[†]

3.1 Introduction

Addition of Reclaimed Asphalt Pavement (RAP) in asphalt mixture supports economic and environmental interest, however, quantification of aging state of these RAP aggregates for quality control purposes can help to predict their performance [3.1]. Besides, evaluation of asphalt binder and mixture aging can provide an over-all understanding of pavement performance, deterioration, and quality assurance. Aging is not only a physical phenomenon by stiffening the asphalt binder, but also the chemical and rheological changes that occurred during this process. In response to that, studies showed that carbonyl compound in asphalt binder increases with the increased amount of oxygen due to reaction between them at high temperature and pressure. It signifies the oxidation chemistry of asphalt binder [3.2]. This oxidation process reduces the fatigue life of asphalt pavement as well as initiates embrittlement and subsequent cracking [3.3].

The aging mechanism can be investigated in the laboratory by various test methods considering their contribution in assessing certain properties of the aged binder.

[†] This chapter or portions thereof has been published previously in the Journal of Materials in Civil Engineering under the title as it is in chapter title. (2020), DOI: 10.1061/(ASCE)MT.1943-533.0003442 The current version has been formatted for this dissertation.

Among these tests, physical changes in aged binders can be evaluated by penetration, ductility, and loss of mass test, and chemical changes can be evaluated by SARA fraction (saturate, aromatic, resin and asphaltene) analysis and FT-IR (Fourier transform Infrared) absorbance or transmittance spectroscopy. Also, mechanical and rheological changes can be evaluated by dynamic modulus, resilient modulus, fatigue resistance, rutting potential, cracking susceptibility, viscosity, and complex modulus and phase angles [3.4]. Since each test has its specific feature to define aging, processing time is also an important factor for accelerating aging determination in the laboratory as well as in the field. Based on this factor, FT-IR spectroscopy requires less time compared to other tests and can also provide reliable results. The principle of FT-IR spectroscopy is to detect the molecular structures of a sample based on their vibrational and rotational frequency at a specific wavenumber in the range of 600 cm^{-1}-4000 cm^{-1} when an infrared beam passes through the sample and absorbed by it. This absorbance displays in the form of an absorbance intensity versus wavenumber in cm^{-1}. According to Beer's law, this absorbance intensity is proportional to the concentration of the molecule. From this relationship, the amount of a particular functional group can be determined [3.5].

Previous studies with FT-IR spectrometer in aging determination showed that the C=O (carbonyl) compound in asphalt binder increased with the increase in temperature and aging duration [3.6]. Besides, oxidation reaction occurring in service life is significantly higher compared to RTFO (rolling thin film oven) and PAV (pressure aging vessel) aging of asphalt binder with respect to C=O oxidation [3.7]. Researchers also showed that total absorbance in C=O and S=O (sulfoxide) of FT-IR spectra correlated with rheological parameters for different aging conditions [3.8]. Liang et al. showed that

the C=O absorbance area in FT-IR spectra had a linear relationship with aging duration at PAV condition [3.9]. The aging rate in PAV for different durations is also higher compared to field aging due to escalated exposure temperature. It was also found that high PG (performance grade) binder aged slower in field aging. Also, S=O oxidation was observed in the early stage of aging and the increasing pattern in oxidation was inadequate in later stages. Hofko et al. (2017) conducted an extensive study on FT-IR to visualize its capability in different analysis methods for quantifying C=O and S=O aging indices and recommended the importance of analysis method selection for FT-IR measurement [3.10]. Inter-laboratory studies suggested that C=O aging index in unaged and RTFO aged binders are significantly different compared to PAV aged binder [3.11]. Jing et al. also showed the effect of temperature, pressure, and ageing duration on C=O and S=O indices of FT-IR spectra and their correlation with rheological properties [3.12].

From the previous studies, it was evident that the FT-IR spectrometer has the potential to quantify aging in terms of C=O and S=O oxidation measurement. However, in most of the studies, FT-IR spectrometer has been used as a supporting tool to show the chemical changes due to oxidation. Also, the effect of binder performance grade (PG) and binder sources in the chemical oxidation process was not addressed significantly. Most importantly, chemical changes during the oxidation process in the asphalt mixture and oxidation stage of the RAP aggregate were not addressed properly in previous studies. Addressing these issues as a knowledge gap in evaluating FT-IR spectrometer performance to quantify aging in asphalt binder and mixture, in this study FT-IR spectrometer has been used as a primary technique to evaluate aging of four different PG grade asphalt binder obtained from four different sources. Both binder aging and mixture

aging were conducted to observe their changes in different aging conditions as a background study to comprehend the extent of aging in terms of carbonyl index. The chemical aging stage of RAP aggregates obtained from ten different sources was then envisaged. The RAP aggregate and asphalt mixtures were extracted using a quick extraction procedure using DCM (Dichloromethane) as well as a standard test method for bitumen extraction and asphalt recovery using the rotary evaporator to evaluate the efficacy of quick extraction for in-situ oxidation measurement of asphalt mixture [3.13]. Finally, a handheld FT-IR spectrometer was used to conduct field measurement of plant mix samples extracted by a quick extraction method. Results obtained from laboratory measurements were used to identify the aging state of plant mix samples for quality assurance.

3.1.1 Objective

The objective of this study is to implement the handheld FT-IR spectrometer in the field as a tool for quality control of plant mix containing RAP. To achieve this goal following specific objectives were accomplished:

- Understanding and quantifying the laboratory aging of the binder and mix using ATR (Attenuated Total Reflectance)-FTIR.
- Selection of a suitable index derived from FT-IR spectral analysis that can quantify both the binder and mix aging.
- Development of a quick extraction process that can be easily implemented in the plant/ field.
- Characterization of the RAP aging based on the existing aging condition.

- Determine the RAP content in the hot mix asphalt in the plant by a handheld FT-IRS as a measure of quality control

3.2 Materials and Experimental Plan

3.2.1 Materials

In this study, eight neat/ unmodified binders of four different performance grades obtained from four regional sources were used to visualize if their aging indices are different or not in unaged condition. These binders are- PG52-34(LA), PG58-28(MS, TX), PG64-22(LA, MS, and NC), and PG67-22(MS and TX). Hot mix asphalt having ½ inch nominal maximum size of granite aggregate with 4.6% asphalt content was used to investigate the mix aging. Reclaimed asphalt pavement (RAP) from ten different sources were collected from RAP piles in mixing plants and from milling sites. The age of those RAP aggregate varies from roughly 3 to 20 years. Plant visits were made to two different places in Louisiana to collect data with a vision to implement the quality control procedure using the handheld FT-IRS. All visited plants were producing hot mix asphalt containing 15% RAP using a PG 67-22 binder. Dichloromethane (DCM) was used to perform the quick extraction procedure in the field to collect binder residue from RAP as well as from the fresh mix. DCM was purchased from Sigma-Aldrich in anhydrous form and over 99.8% pure. It contains 40-150 ppm amylene as a stabilizer. The molecular weight of the DCM was 84.93 m/mol. For the verification study, mix as well as from ten different plants were collected. Detail information of those mixes is provided later in section 3.6.

3.2.2 Experimental Plan

ATR-FTIR spectra of binder and extracted mix were recorded in the laboratory and in the Plant/ field. Different binders were subjected to standard and extended RTFO aging and PAV aging and absorbance spectra were collected for analysis. Similar spectra were obtained for laboratory aged mix also. RAPs from ten different sources were analyzed to investigate the extent of aging. Finally, FT-IR spectra were collected in the plant during the production phase. Unaged binder from the tank, RAP from the pile before mixing, and fresh mix were collected to record the spectra to predict the RAP present in the mix as measures of quality control. Besides the FT-IR testing plan, DSR tests were also performed on unaged and PAV aged PG58-28(TX), PG64-22(NC), and PG67-22(TX) binders to determine the stiffness/high-temperature grade. RAPs from five different sources were extracted and recovered to find the high-temperature grade which was then compared with PAV aged binder. Figure 3-1 is the ATR-FT-IR spectra collection plan for the study.

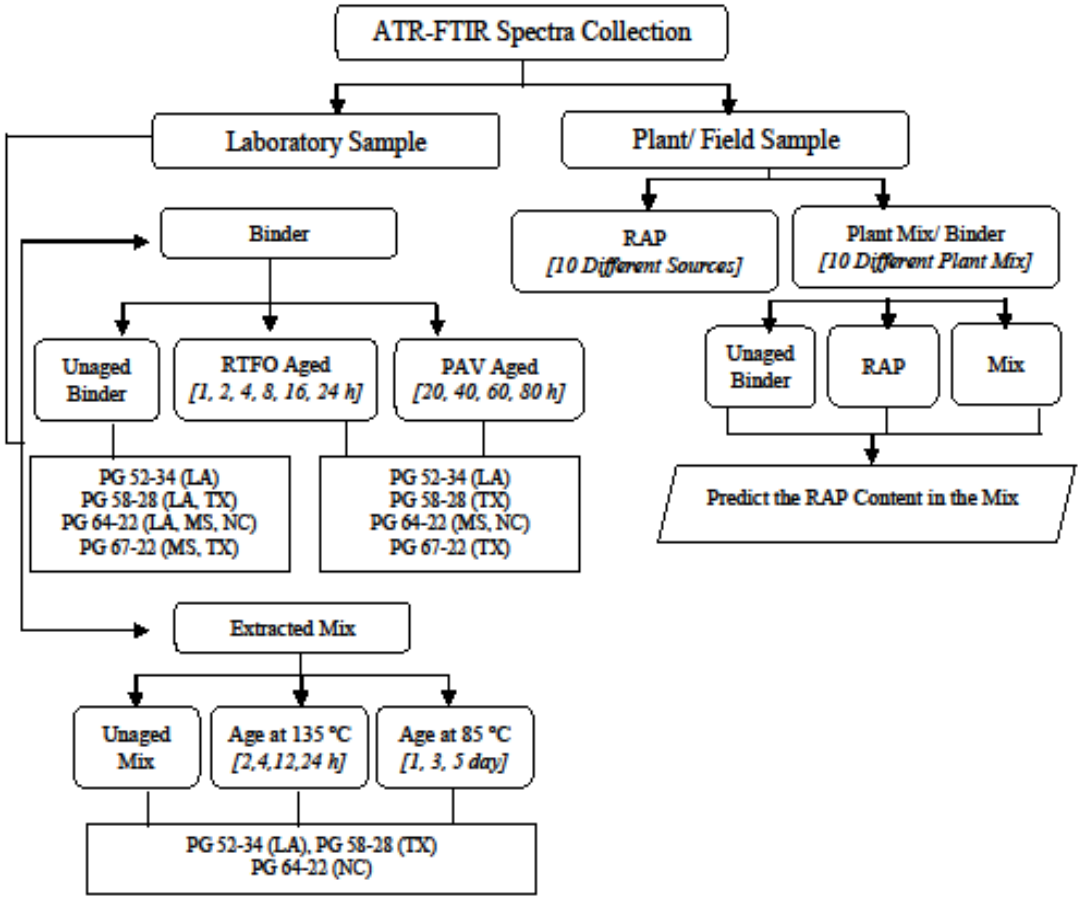

Figure 3-1 Detailed experimental plan for the study.

3.3 Methodology

3.3.1 Binder Aging

Laboratory aging of binder was conducted by using two accelerated aging methods: RTFO (AASHTO T 240) and PAV (AASHTO R 28). For the RTFO aging procedure, samples were kept at 163ºC for 1 hour to 24 hours, and samples were collected at different intervals. For PAV aging procedure, unaged binder samples were kept at 100 ºC under 2.1 MPa pressure for 20, 40, 60, and 80 hours which is referred to as 1-PAV, 2-PAV, 3-PAV, and 4-PAV respectively in further discussion in this paper.

3.3.2 Mix Aging

Loose mix was aged in a forced draft oven in the lab at two different temperatures. According to NCAT recommendation, one aging temperature was selected as 135 ºC which is also recommended by AASHTO R30 for short-term aging [3.14]. Mix was aged up to 24 hours at 135ºC and samples were collected after 2, 4, 12, and 24 hours. Another set of the mix was aged at 85ºC up to five days and samples were collected after 1, 3, and 5 days. Oven aged mix was then extracted using a quick extraction method developed in this study and the binder residue was used for data collection in FT-IR.

3.3.3 Dynamic Shear Rheometer Test on Extracted Binder

PAV aged and extracted binders from RAP were tested in DSR following the AASHTO T 315 to determine the complex modulus. Binder from RAP was extracted and recovered following the ASTM D 2172 and ASTM D 5404 respectively. 'Ensolv-ex' (n-Propyl Bromide) was used as the extraction solvent in this part of the study. DSR tests were performed using 25 mm parallel plate geometry at 10 rad/sec angular frequency and 12% strain rate. Those parameters were selected because the target of the test was to determine the temperature at which the G*/sinδ value equals 1.0 kPa. Each sample was tested at least at three different temperatures at 6 ºC temperature intervals. The test temperature was chosen in such a way that the temperature corresponding to the G*/sinδ value of 1.00 kPa could be determined directly from the plot.

3.3.4 Quick Extraction Process of Asphalt Mixture in the Field

A quick extraction method is developed in this study which can be implemented in the field in less than 15 minutes with minimal supplies and effort. An asphalt mix

sample was collected and kept in the open air for 10 to 15 minutes to cool down (figure 3-2a). Approximately 100 grams of loose asphalt mix was taken in a 16-oz mason jar (figure 3-2b). Then around 100 milliliters of DCM were poured into the jar (figure 3-2c). Proper care should be taken to make sure that the mix is air-cooled so that the DCM does not get evaporated as soon as it comes with contact with the mix. The jar was then shaken moderately and left for 5 minutes with closed lid. The solvent with dissolved asphalt was then filtered through an 80-micron nylon mesh filter and the liquid was collected in a metal pan with a large surface area (figure 3-2d). In this case, a standard PAV pan with a 5-inch diameter was used. It is not necessary to drain the whole liquid as a very small amount of binder residue is required for FT-IR analysis. The pan with few millimeters depth of liquid was left in an open place for 10 minutes while all the DCM got evaporated (figure 3-2e). The binder residue was then collected using a metal spatula and placed on the FT-IR crystal for spectra collection (figure 3-2f). Figure 3-2 shows the step by step procedure that was followed in the field for quick extraction of plant mix. RAP was also extracted by following the same procedure. The extracted mix should be visually inspected carefully to ensure that no asphalt residue remains in the extracted mix, especially when heavily oxidized RAP is extracted.

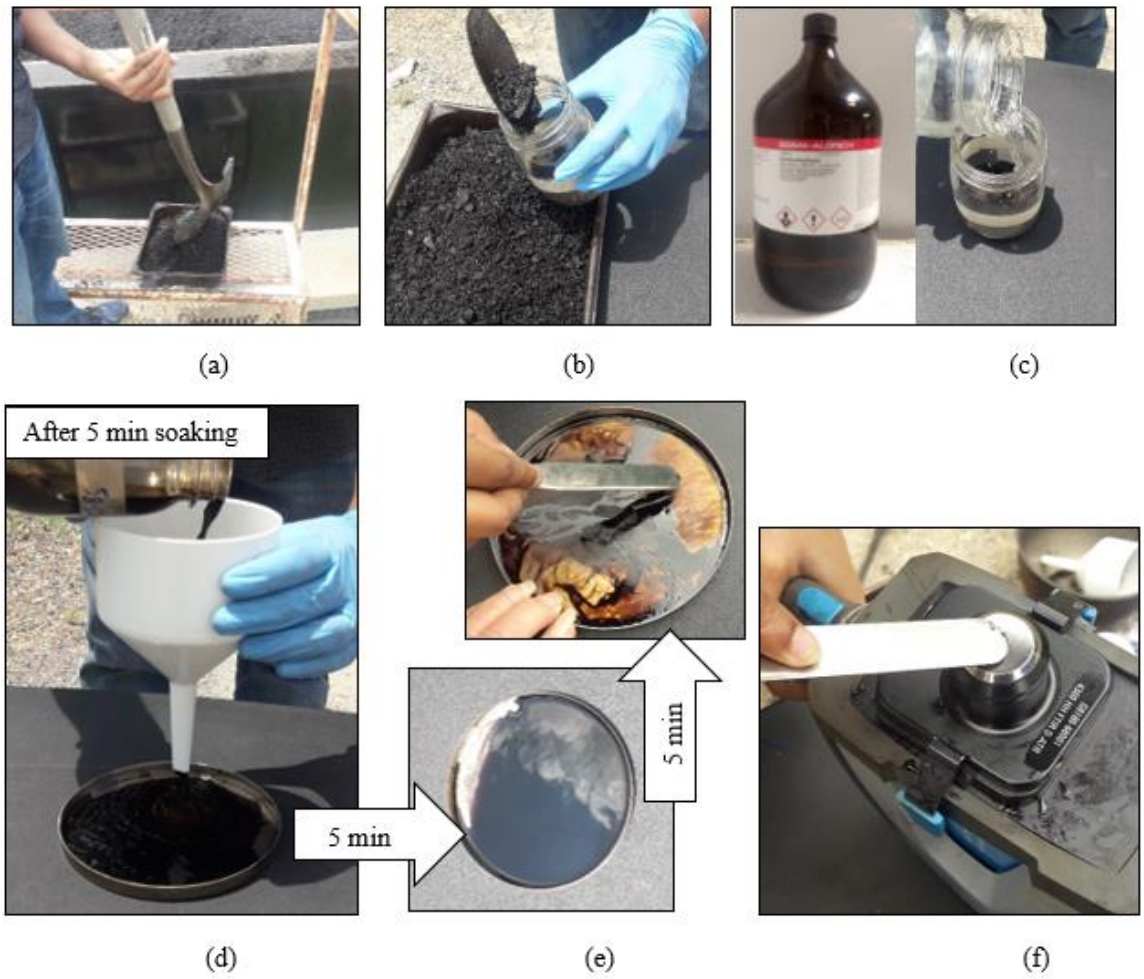

Figure 3-2 Quick extraction process of asphalt mixture implemented in the field: (a) HMA collection from the truck, (b) Pouring loose HMA in the mason jar, (c) Use of DCM to extract the binder form mix, (d) The solvent is being filtered, (e) DCM is being evaporated quickly and the asphalt residue is left on the pan, (f) Asphalt binder is placed on the FT-IR crystal to collect the spectra.

3.3.5 Fourier Transform Infrared Spectroscopy (FT-IR)

Agilent 4300 handheld FT-IR was used for spectroscopy data collection for this study. It is a portable and handheld analyzer which can be used to measure solid and liquid samples in the laboratory as well as in field condition. A single reflection diamond ATR (Attenuated Total Reflectance) sample interface was used for data collection considering its flexibility in measuring high absorbing material in solid, liquid, and

viscoelastic state and having resistivity against corrosion and scratching. The sample was placed on the ATR sensor by a spatula to cover a 200 μm active sensor area. Since it is a surface technology only 2 μ depth of the surface can be analyzed. Due to this small and stable path length, no sample preparation is necessary for ATR-FTIR measurement. Each spectrum was collected in the spectral region of 600 cm^{-1}- 4000 cm^{-1} at 4 cm^{-1} resolution by the default Microlab Mobile software equipped with the instrument and reported as an average of 24 spectra. Before each scan, a background spectrum was also collected to avoid the interference of any impurities on the sensor area which could impede the scanning process of sample spectra. Also, real-time data viewer in the software was used to ensure a proper attachment between the sensor area and the sample.

3.3.6 Method for Data Analysis

In this study, FT-IR spectral interpretation was conducted by both qualitatively and quantitatively. For qualitative analysis, spectra were analyzed in the fingerprint region (650 cm^{-1}- 1800 cm^{-1}) to identify the presence of a new functional group added to the asphalt binder and extracted mix due to different aging conditions. Also, the difference between spectra of neat binder and extracted binder from the mix was also observed. From qualitative analysis, principal functional groups susceptible to aging were identified. After this identification, quantitative analysis was performed to measure the degree of aging. In this study, peak height ratio was used for the quantitative measurement of aging. This measurement was obtained by dividing the peak height of the aging susceptible functional group to the height of the functional group which is unsusceptible to aging [3.15]. The height was measured by drawing a baseline

considering two lowest points (can be named as valley) on each side of the peak and then added the middle point of the baseline to the top point of the peak.

From the qualitative analysis, it was observed that key functional groups in unaged asphalt binder are- asymmetric stretching vibration of CH_2 at 2920 cm^{-1}, symmetric stretching vibration of CH_2 at 2851 cm^{-1}, stretching vibration of C=C at 1600 cm^{-1}, asymmetric bending vibration of CH_2 and CH_3 at 1455 cm^{-1}, symmetric bending vibration of CH_3 at 1375 cm^{-1}, stretching vibration of S=O at 1030 cm^{-1}, out-of-plane deformation of CH at 870 cm^{-1}, 817 cm^{-1}, and 745 cm^{-1}, and aromatic ring vibration of CH at 721 cm^{-1}. After aging, it was observed that the absorbance of the C=O functional group at 1695 cm^{-1} became intense in asphalt binder as well as in asphalt mixture. In addition, an increase in peak intensity of the S=O functional group at 1030 cm^{-1} was also observed in the aged binder and mix samples.

After qualitative analysis, quantitative analysis was performed by measuring the peak heights of C=O and S=O functional group at 1695 cm^{-1} and 1030 cm^{-1} and divided them with the height of asymmetric stretching vibration of CH_2 at 2920 cm^{-1} which was considered unsusceptible to aging. This quantification process for C=O and S=O functional groups were symbolized as carbonyl index (I_{CO}) and sulfoxide index (I_{SO}). For measuring peak height, a baseline was drawn by connecting the valleys on both sides of the peak. It was observed that the location of the valleys remained unchanged irrespective of the binder type or intensity of aging. The baseline for the C=O functional group extended from the wavenumber 1684 to1718 cm^{-1}. For S=O and asymmetric stretching vibration of CH_2, the limits of the baselines were 978 cm^{-1} to 1080 cm^{-1} and 2753 to 2995 cm^{-1}, respectively.

Table 3-1 contains the values as well as the coefficient of variation (CV) of peak height at six different wavenumbers (cm^{-1}). This table is produced using PG64-22(NC) binder of different aging levels using all four aging methods. Except at wavenumber 1695 cm^{-1}, peak height remains unaffected by aging conditions as expected. A similar type of table can be prepared for other binders too. The CV% provides the measure of the repeatability of the data collection procedure. Each data point in the table is the average of ten individual spectra collected from at least three different locations of the specimen container.

Table 3-1 Average peak height at different wavenumbers from absorbance spectra of PG 64-22 (NC) binder after different laboratory aging methods.

Binder (aged & unaged)	**1375**		**1455**		**1600**		**1695**		**2851**		**2920**	
	Avg.	**CV%**	**Avg.**	**CV%**	**Avg.**	**CV%**	**Avg.**	**CV%**	**Avg.**	**CV%**	**Avg.**	**CV%**
Unaged-Binder	0.057	1	0.125	1	0.016	8	0.005	12	0.207	2	0.288	2
2hr-RTFO	0.056	1	0.125	1	0.017	3	0.006	10	0.208	2	0.289	2
16hr-RTFO	0.054	2	0.123	2	0.019	3	0.010	8	0.203	2	0.282	2
1-PAV	0.055	2	0.125	1	0.017	3	0.008	7	0.205	1	0.286	1
4-PAV	0.053	4	0.120	4	0.018	6	0.010	9	0.198	5	0.272	5
Unaged-Mix	0.057	2	0.126	1	0.017	4	0.005	7	0.210	2	0.293	1
2hr-135C	0.057	1	0.126	1	0.016	2	0.005	11	0.207	1	0.289	1
24hr-135C	0.056	1	0.125	1	0.017	2	0.008	7	0.205	1	0.285	1
1day-85C	0.057	0	0.126	0	0.017	2	0.006	8	0.209	0	0.291	0
5day-85C	0.055	1	0.124	1	0.019	3	0.011	6	0.205	1	0.284	1

3.4 Results and Discussion

3.4.1 Aging Indices of Unaged Binders

Two types of aging index parameters were considered to quantify the laboratory aging of both the binder and the mix: Carbonyl Index (I_{CO}) and Sulfoxide Index (I_{SO}). To quantify the change in indices due to aging, the initial unaged I_{CO} needs to be known for

different binders. In this study, a total eight unaged binders were studied to estimate the base value of I_{CO} and I_{SO}. As mentioned earlier, one of the objectives of this study is to characterize the RAP based on their extent of aging. Most of the cases, RAP are the blends from different sources and the life history of RAP is mostly unknown. An estimate of the base value of different indices needs to be made irrespective of binder grade or sources to determine the state of aging of the RAP. Indices for unaged binders are provided in figure 3-3. It can be mentioned that the average value of the indices for each binder is calculated from ten separate spectra and the plot in figure 3-3 for unaged binder contains eight binder samples. So, the box plot is made of total of eighty data points.

From figure 3-3(a) it can be observed that the spread of I_{CO} for the unaged binder is higher than the aged binder. Unaged binders possess very low peak height in the absorbance spectra corresponding to carbonyl group because the concentration of carbonyl group is very low in unaged binder. This value can be affected by the variation of the absorption value of the valley on either side of the peak. But aged binders have significantly higher peak height value which is less likely to be affected by the variation of the absorption value of the valley. In the case of I_{SO}, the variation is much higher for the aged binder than the unaged binder. A higher variation of I_{SO} indicates that the concentration of the sulfoxide produced due to aging is not consistent and might not be considered as a reliable metric to quantify aging. As the carbonyl index possesses less variability for aged binder, this index can be considered as a stronger marker to quantify the aging phenomenon more confidently than the sulfoxide index.

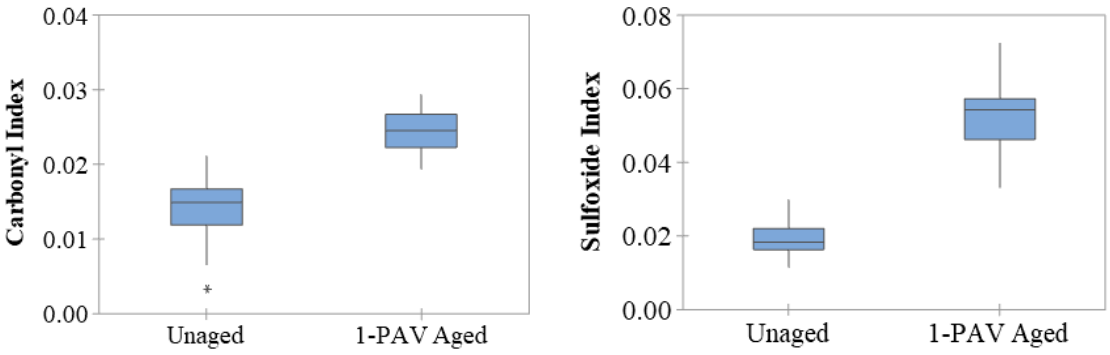

Figure 3-3 (a) Carbonyl and (b) Sulfoxide index of unaged binder and comparison of those indices to the 1-PAV aged binder.

3.4.2 Effect of Quick Extraction Process on Carbonyl and Sulfoxide Indices

A quick extraction process is developed in this study which can be performed in 15 minutes and can produce enough extracted binder for recording FT-IR spectra. For this quick extraction process, Dichloromethane (DCM) was used as a solvent to dissolve the binder from the mix. The rationale behind choosing the solvent is that it has distinct peaks at wavenumber 746 and 1265 cm^{-1} which do not overlap or interfere with the peak at 1695 cm^{-1} corresponding to the carbonyl in aged asphalt binder. Of course, the rate of evaporation is much faster, which is an added advantage to perform the extraction in the field. The influence of the quick extraction process on binder FT-IR spectra is explained with the aid of figure 3-4. Spectra of the neat and residue of dissolved PG 58-28 binder overlap on each other indicating the complete evaporation of the DCM from the binder. So, the presence of DCM in the binder residue should not be a concern.

Two different extractions were performed where afterward the extraction processes the solution was filtered through 80-micron and 25-micron nylon filter separately. Spectra of the residue show that there exist significantly large peaks with

different absorption values at wavenumber 1030 cm^{-1}. In either aged or unaged asphalt binder, sulfoxide shows a peak at 1030 cm^{-1} but for a similar extent of aging, the peak height is supposed to be equal. There is a probability that, fine particles that could pass through the filter added some silica in the residue. Silicon oxide shows a peak at wavenumber 1000 cm^{-1}. Because of the interference of the molecular vibration at this region a peak with a wide area is observed. Residue filtered through a 25-micron filter shows a smaller peak as it contains few fines. But the filtration process requires a much longer time and still cannot remove all the fines. To eliminate the effect of fines in the residue a mix was prepared with aggregate larger than #200 particles and extracted through a 25-micron filter. Still, some fines are present as observed in figure 3-4. For this reason, the aging of extracted binders cannot be quantified by the sulfoxide index. There is no interference at wavenumber 1695 cm^{-1} corresponding to carbonyl either because of the solvent of the fines. So, the extraction method can successfully quantify the aging of the mix using the carbonyl index.

The effectiveness of the quick extraction method can be supported by providing the carbonyl index of unaged binder and extracted binder from the unaged mix. Theoretically, both should have similar indices. The average I_{CO} for unaged and extracted binders were found to be 0.0146 and 0.0140, respectively, which differs by only 4.1%.

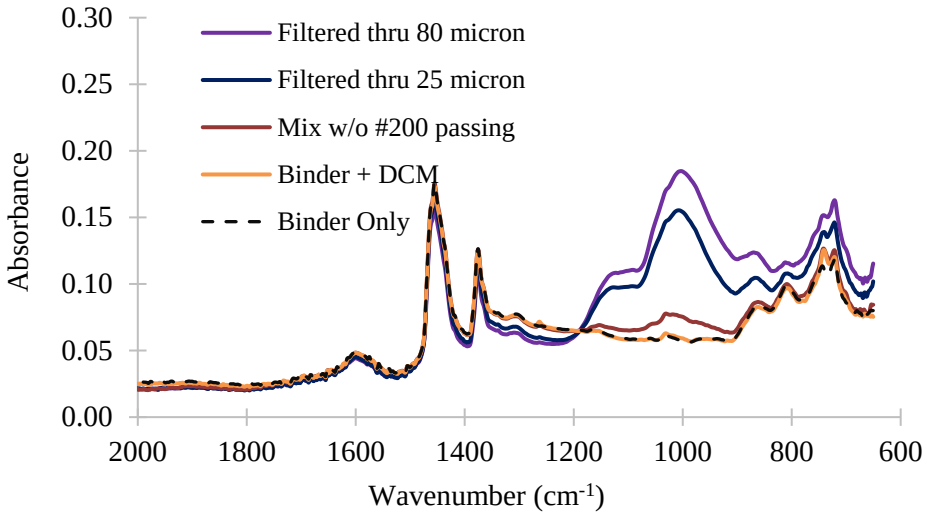

Figure 3-4 Absorption spectra of an extracted binder containing various quantities of fines.

3.4.3 Variation of Sulfoxide Index (I_{SO}) due to Laboratory Aging

3.4.3.1 *Inconsistent increase in Sulfoxide Index with duration of aging*

The concentration of both carbonyl and sulfoxide increased due to aging. An increase in carbonyl index for different hours of PAV aged binders are shown in the box plot (Figure 3-5). I_{CO} for eight unaged binders and five aged binders arebinders are plotted in each box of the plot. A gradual increase in I_{CO} for a PAV aged binder is noticeable from Figure 3-5(a). A similar pattern is observed in the RTFO aged binder which is not shown here. In the case of the sulfoxide index, the increasing trend ceases after a certain level of aging and then starts decreasing as observed from Figure 3-5(b). Extended duration of accelerated aging may cause some sulfoxide to decompose to sulfones and lower the I_{SO} [3.6]. For this reason, a known value of I_{SO} cannot be directly correlated to the extent of the aging of a binder. With the increase in aging duration, unlike the carbonyl index, the variability of sulfoxide index value due to different binder grade increases. As the increasing trend of sulfoxide index is not consistent and varies a

lot because of the binder grade, this index might not be suitable for quantifying the aging of an unknown binder.

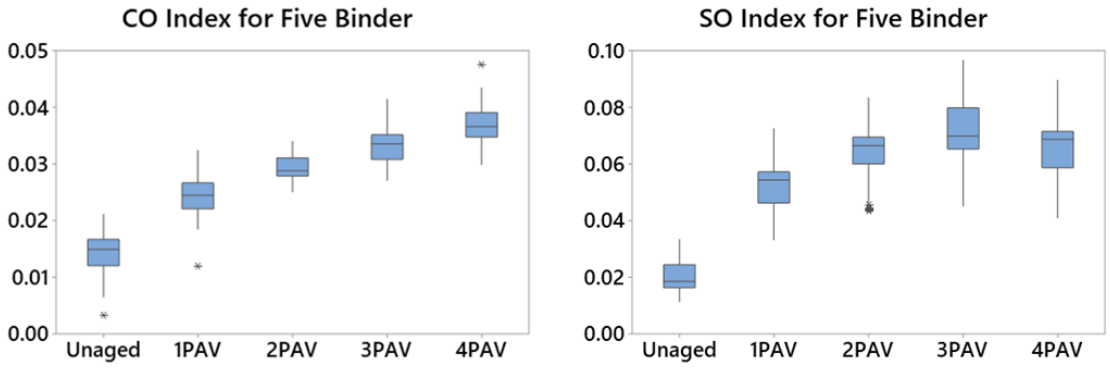

Figure 3-5 (a) Carbonyl (I_{CO}) and (b) Sulfoxide (I_{SO}) index for PAV aged binder.

3.4.3.2 *Different behavior in RTFO and PAV aging*

Sulfoxide index for the PAV and RTFO aged of five binders are provided in Figure 3-6(a) and 3-6(b). It is observed that I_{SO} for PAV aged binders are much higher than the RTFO aged binder. Even the sulfoxide index of 1PAV aged binder is much higher than the 24-hour of RTFO aged binder. Another study performed by the authors verified that 8-hour of RTFO aging created an equivalent effect to 1PAV aging in terms of carbonyl index. But similar types of relationships cannot be established for I_{SO} index. Moreover, I_{SO} depends on the aging method. Aging at a higher pressure and longer duration (in PAV) creates more sulfoxide than the aging at a higher temperature (in RTFO). Since the concentration of sulfoxide is dependent on the aging process, this index may be unreliable to quantify the aging of a mixture in the field or aging of RAP.

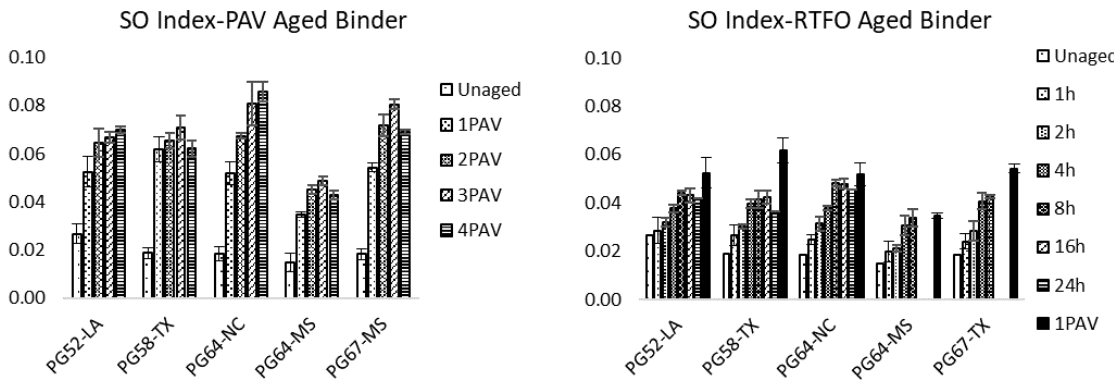

Figure 3-6 Sulfoxide index for (a) RTFO aged binder and (b) Short-term oven aged mixture.

3.4.3.3 *Unusually high Sulfoxide index of an unaged mixture*

In this study, I_{SO} of short-term and long-term aged mixtures were determined using ATR-FTIR. It was observed that the I_{SO} of the unaged mix was much higher than the unaged binder (Figure 3-7(a) and this value varies considerably from mix to mix. Moreover, no noticeable trend is observed in the STOA mixture. A similar observation was made in the LTOA mixture too. It can be noted that a small amount of binder was extracted in the field to determine the I_{SO} of the mix. There might be a chance that the I_{SO} is influenced by the mixing process.

Five different extractions were performed using the same binder and the I_{SO} was calculated. It is observed from Figure 3-7(b) that the solvent does not have any effect on the I_{SO} as both the neat binder and binder residue from the solvent have a similar sulfoxide index. There exists a large increase in I_{SO} when the binder is extracted from the mixture. Usually, the dissolved binder from the mixture is filtered through an 80-micron nylon filter. If it was filtered using a 25-micron filter the I_{SO} decreases. Binder extracted from a mix made without #200 and fine particles reduce the I_{SO} significantly. Still, it was much higher than that of the unaged binder. Some fine particles present in the mix can be

present in the extracted binder which influences the I_{SO}. Interference of the molecular vibration of silicon oxide (at wavenumber 1000 cm^{-1}) from the fines and sulfoxide (at wavenumber 1030 cm^{-1}) creates higher peak value in the spectra and consequently results in a higher sulfoxide index. Determination of the carbonyl index is not influenced by the fines present in the mixture (Figure 3-7(b). That is why the sulfoxide index cannot be considered as a reliable metric to quantify the aging of the mixture.

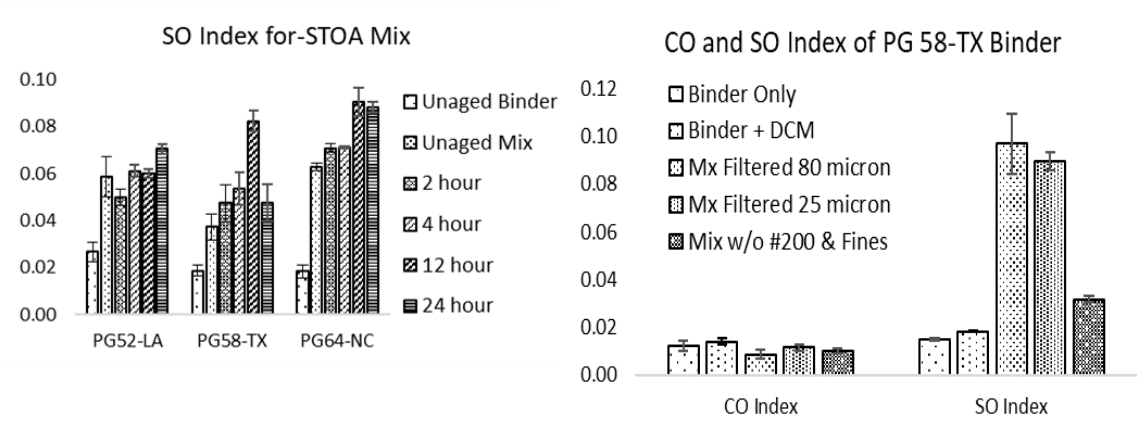

Figure 3-7 (a) Sulfoxide index of short-term oven aged mix, (b) Effect of fines on carbonyl and sulfoxide index.

3.4.4 Increase in Carbonyl Index (I_{CO}) due to Laboratory Aging

The effect of laboratory aging on an increase in carbonyl index was observed through the binder and mix aging. Five different binders were aged up to 80 hours in PAV and the carbonyl indices were recorded at 20 hours interval. It was observed that for some cases there exists a significant difference in carbonyl index due to variation of the binder grade or source. But the maximum deviation of carbonyl content of a binder from the mean value of all the binders at a certain aging level is around 12% for all four aging conditions. So, irrespective of binder grade or sources the carbonyl indices were grouped

based on the aging level. Figure 3-8 is the change in I_{CO} because of the laboratory aging of the binder as well as for the mix.

All four subplots of figure 3-8 exhibit a general trend that the carbonyl index increases with the duration of the aging process. Contrary to the findings from several researchers, the I_{CO} does not linearly increase with the duration of the aging process [3.9]. At the beginning of the aging process, the rate of increase is higher but with time the rate diminishes. RTFO can create a similar aging index (0.0376) in 24 hours which can be attained by PAV in 80 hours (0.0372). Although ,in the end, the indices are equal, but at the beginning, RTFO ages the binder at a faster rate than the PAV which can be qualitatively understood from the figure 3-8(a) and 3-8(b).

Long term mix aging is performed in two different ways. Loose mix was aged in force draft oven at 135 ºC for a maximum of 24 hours at 85 ºC for a maximum of 5 days. Mix was collected at regular intervals and extracted to monitor the aging condition. Aging at 85 ºC temperature creates a slightly less (0.0254) index than that obtained in 12 hours of aging at 135 ºC (0.0296). Careful observation of figure 3-8(a) and 3-8(c) reveals that 4, 12 and 24 hours of mix aging at 135 ºC have the equivalent effect of binder aging of 1-PAV, 2-PAV and 4-PAV respectively.

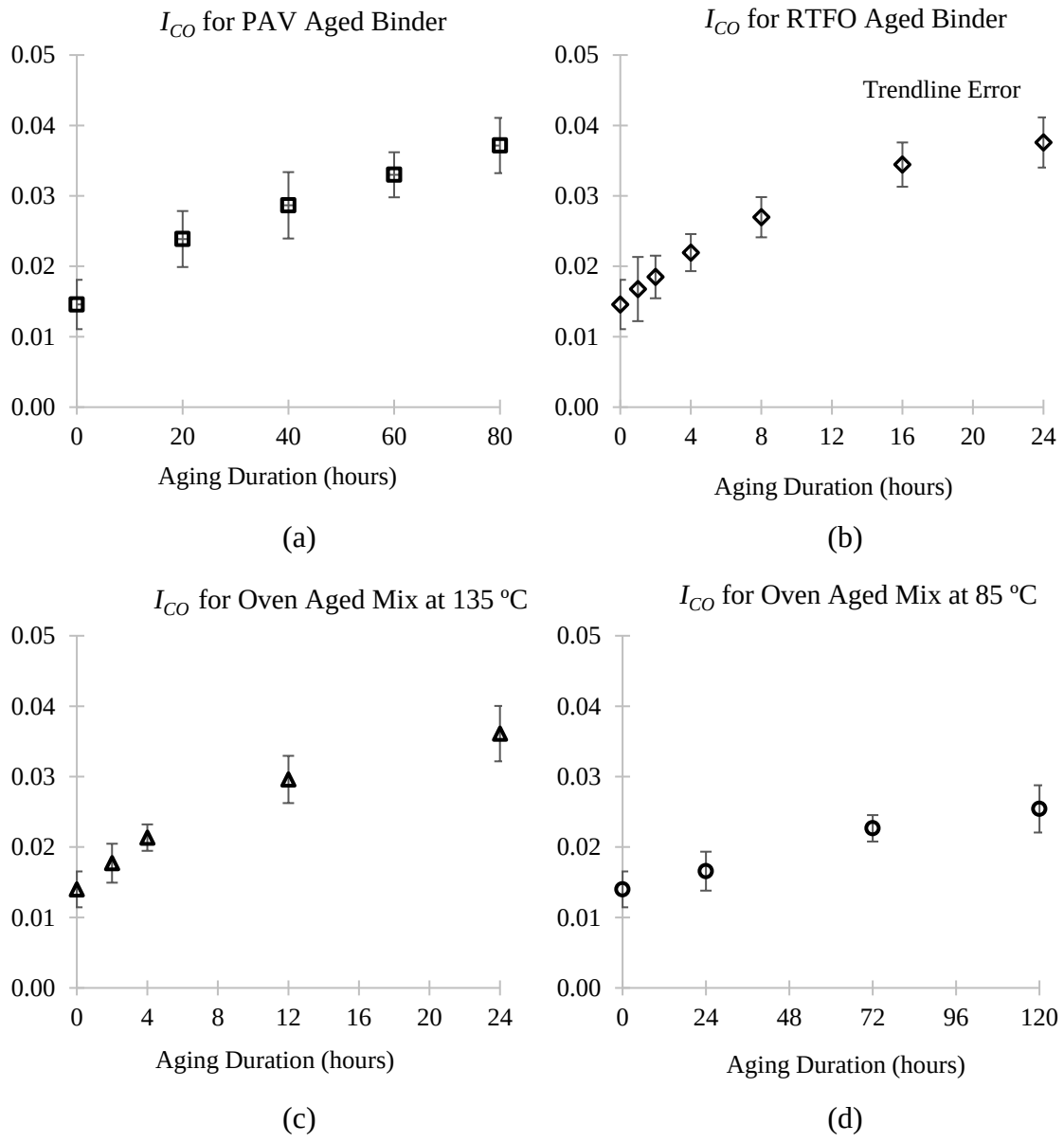

Figure 3-8 Increase in carbonyl index with the duration of different laboratory aging methods: (a) PAV aging, (b) RTFO aging, (c) Oven aging at 135 ºC, and (d) Oven aging at 85 ºC.

3.4.5 Understanding the Aging State of RAP

Because of the variability of sources and inadequate information regarding the history of the reclaimed asphalt pavement it is a challenging task to characterize the RAP based on the severity of aging. Traditional binder extraction from the RAP is not a

convenient option for a quick field study to determine the aging state as it requires time and use of a huge amount of solvent. The extracted binder provides the information regarding the stiffness of the RAP binder but does not provide any insight regarding the chemical change because of oxidative aging. The aging process of course increases the stiffness of the binder but measuring the stiffness alone might not be a true estimate of aging. Figure 3-9(a) shows the carbonyl index of ten different RAPs collected from different plants and sites. They are named based on the carbonyl content arranged in ascending order. The average carbonyl index for each RAP binder is computed from ten individual spectra obtained from two different extractions of each RAP. Carbonyl index of the RAP studied here, varies from 0.0274 to 0.0607 with a maximum coefficient of variation of 12%. So, it observed that the I_{CO} of naturally occurring RAP varies at a wide range. FT-IR can be used to characterize the RAP based on their extent of aging. Instead of fixing the maximum amount of RAP in HMA irrespective of their severity of aging, the quantity can be adjusted. A higher amount of RAP with lower I_{CO} can be recommended whereas, the use of RAP with high I_{CO} can be restricted. Of course, further study on mix properties should be conducted to adjust the amount of RAP use based on the carbonyl index.

Four horizontal dotted lines in the plot indicate the carbonyl index corresponding to different PAV aging levels. The age of the RAP used for this study varies from 3 years to over 20 years. So, it can be expected that a large age distribution of RAP is coved in the study. All the RAP binders are aged above the 1-PAV aging level. Seven out of ten RAPs are aged above the 4-PAV level. PAV aging is showing the limitation to predict the actual aging that a binder undergoes in real life. The results indicate that in service life

aging of binder produces much higher carbonyl content than that of the laboratory mix aging method practiced by different agencies.

To investigate the potential of further aging of RAPs, RAP-1 and RAP-10 are aged in a forced draft oven at 135 ºC for 24 hours. The reason behind the selection of those two RAPs is, they possess the least and most carbonyl index respectively. The increase in carbonyl index for RAP-1 and RAP-10 are 48% and 34% respectively because of oven aging. It can be inferred that even though RAP contains a highly aged binder it possesses the potential to get more aged with time. A hypothesis can be made that the oxidative aging is a never-ending process. Further study must be conducted to prove this hypothesis.

Stiffness of the binder is a parameter that might not truly quantify the chemical changes due to oxidative aging. Figure 3-9(b) is the plot of high-temperature grade (temperature in degree Celsius at which $G^*/\sin\delta = 1$ kPa) for both PAV aged and traditionally extracted RAP binder against the carbonyl index. High-temperature grade follows a linear relationship with the carbonyl index for both cases with satisfactory R^2 values of over 0.80. An intriguing observation from the plot is that PAV aged binder with similar carbonyl index to RAP binder possess higher stiffness than that of the RAP binder. The rate of increase of stiffness of PAV aged binder is much higher than that of the RAP binder. In the field, the aging process increases the carbonyl content without increasing the stiffness at the same rate that happens in PAV aging. Stiffness of a binder is contributed by the concentration of oxidative aging products as well as the dispersion of those molecules. Agglomerated molecules can produce more stiffness although the concentration of the aging product is the same. The accelerated aging method may

facilitate the molecular agglomeration at a faster rate than that happens in the field by the natural aging process in a longer course of time. This might be the reason of the higher stiffness of the laboratory aged binder.

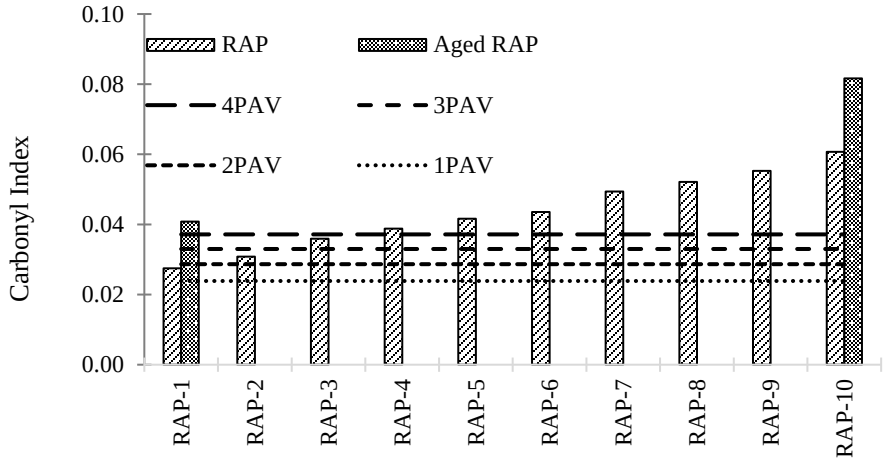

(a)

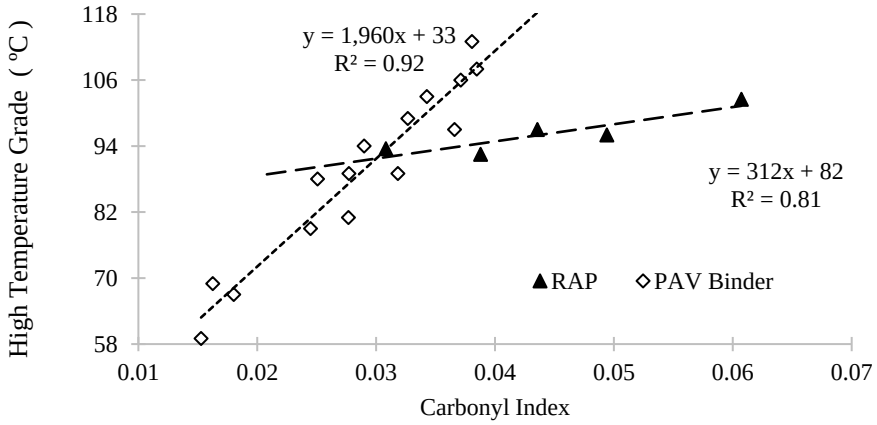

(b)

Figure 3-9 Comparison of PAV aged binder and naturally aged RAP: (a) Carbonyl Index, (b) High-temperature grade.

3.4.6 Quality Control of Plant Mix Using FT-IR Spectrometer

Quality control of RAP contained HMA during the production is a challenge. Quality control involves making sure that the mix contains the specified amount of RAP and the RAP is homogeneously blended. To investigate the potential of handheld FT-IRS in quality control of plant mix the research team visited two different plants in Louisiana. Design RAP content for the mixes was 15% as Louisiana Specification does not allow more than that in surface course. At each plant, the ATR-FTIR spectra of the asphalt binder as well as the quickly extracted RAP binder were recorded before the plant started the operation. The process of quick extraction of RAP and recording ten FTIR spectra of both virgin and extracted binder required less than 30 minutes. Three mix samples were collected at different time intervals and FT-IR spectra were recorded.

For quantifying the RAP content in the mix, it is assumed that the carbonyl index in a binder blend increases linearly with an increased amount of aged binder in a blend. Two extreme ends of the carbonyl index of the binder blend are limited by the carbonyl index of the unaged binder and the highly aged RAP binder respectively. If the carbonyl index of a binder blend can be determined provided that both the upper and lower limits are known, the percentage of aged binder in the blend can be calculated. To establish this assumption of linear change in the carbonyl index, four binder blends were prepared with 10%, 20%, 40%, and 80% of aged binder. Understandably, 0% and 100% represents the unaged and highly aged binder. For this study, a 4-PAV aged binder was used instead of the RAP binder for convenience. Figure 3-10 shows the increase of carbonyl index from 0.0163 (for unaged binder) to 0.0381 (for aged binder) with an increase of the percentage

of aged binder. It is observed from figure 3-10 that all the points lie around the straight line obtained by connecting the lowest and height value with an R^2 value of 0.98.

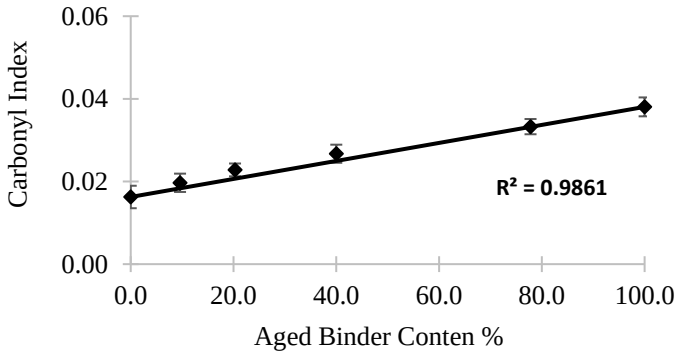

Figure 3-10 Linear increase in Carbonyl Index with an increase of aged binder.

Figure 3-11(a) is the test results for plant mix containing RAP-8. The mix was made of 15% RAP aggregate with a design asphalt content of 5.0%. The contribution of binder from RAP was 0.8% which yielded the RAP binder ratio of 0.16 or 16%. The carbonyl index of unaged binder and RAP binder was found to be 0.0158 and 0.0521 respectively. The predicted carbonyl index of the mix made of 16% of the RAP binder was calculated to be 0.0216 by the following equation:

$$I_{CO-Mix} = I_{CO-Binder} * (1 - RBR) + I_{CO-RAP} * RBR \qquad \text{(Eq. 3.1)}$$

Figure 3-11(a) shows the carbonyl index for three different samples collected from the same plant. There is a difference in the carbonyl index which can be utilized to calculate the corresponding RAP binder percent in the mix. If I_{CO} of the unaged binder corresponds to 0% and I_{CO} of RAP binder corresponds to 100% RAP binder, for a given value of I_{CO} the percentage of RAP binder in the mix can be determined by the following equation:

$$RAP\% = \frac{I_{CO\,(Mix)} - I_{CO\,(Unaged\ binder)}}{I_{CO\,(RAP)} - I_{CO\,(Unaged\ binder)}} * 100 \qquad \text{Eq. 3.2}$$

The percentage of RAP binder in the mix made of RAP-8 with 16% design RAP binder, varies from 16% to 20%. For the other mix made of 15.4% design RAP binder, the amount was found to be between 14% and 22%. There might be a probability of using a higher amount of RAP in the mix or the RAP was not properly blended from where the sample was collected. Whatever the reasons are, the FT-IRS can detect the variation in the carbonyl index and dictates the investigation of the mix production anomaly.

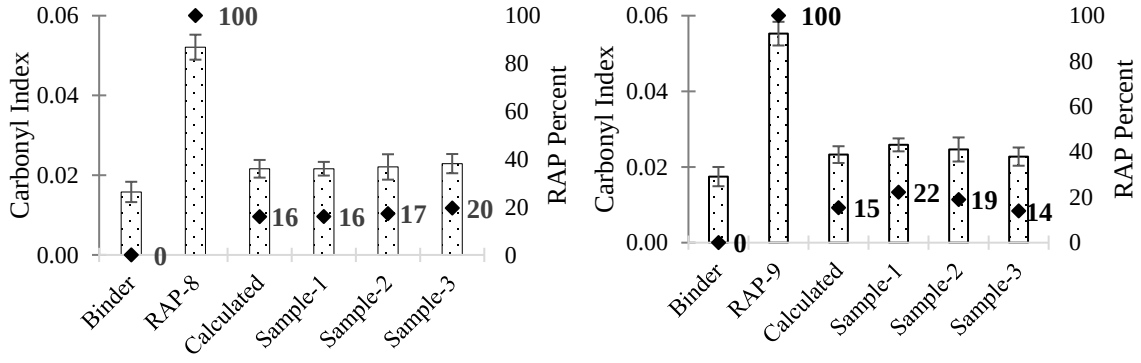

(a) (b)

Figure 3-11 Prediction and validation of RAP content in plant produced mix of (a) RAP-8 with 16% design RAP binder, (b) RAP-9 with 15.4% design RAP binder.

3.5 Validation of the Developed Method Using Plant Mixes

Ten different types of asphalt mixes were collected from five plants in northern Louisiana. The liquid binder was collected from the binder tank and RAP was collected from the RAP pile for each of the ten mixes. Details information of all the mixes is provided in table 3-2. The ATR-FTIRS was performed on the unaged binder, binder

residue obtained from the RAP and mix samples FT-IR spectra were recorded. Binder residues were prepared by the quick extraction process and the FT-IR spectra were recorded. Three to five samples for each plant mix were tested. The result provided here is the average of ten spectra for each sample.

Table 3-2 Details information regarding the plant mix.

	Mix Designation								
	A	B	C	D	E	F	G	H	I
NMS (inch)	0.5	0.5	0.5	0.5	0.5	0.75	0.5	1.0	0.75
RAP %	15.0	14.3	14.3	14.2	15.0	23.8	14.2	19.0	14.9
Design Asphalt %	4.8	4.7	4.7	5.0	4.6	4.6	5.0	4.2	4.6
Binder from RAP %	0.8	0.7	0.7	0.8	0.7	1.2	0.8	1.0	0.8
RAP to Binder Ratio	0.167	0.149	0.148	0.160	0.152	0.260	0.160	0.238	0.174
Binder PG	67-22	64-22	70-22	64-22	67-22	76-22	64-22	70-22	70-22
Virgin Binder I_{CO}	0.0219	0.0167	0.0283	0.0196	0.0200	0.0193	0.0209	0.0190	0.0190
RAP Binder I_{CO}	0.0758	0.0667	0.0689	0.0697	0.0577	0.0924	0.0725	0.0722	0.0722
Mix Collected From	Drum	Truck	Drum	Drum	Truck	Drum	Drum	Truck	Truck

3.5.1 Different Calculation Methods of Carbonyl Index

Different amount of RAP was added in the laboratory and carbonyl index was calculated in six different methods. Carbonyl Index can be calculated considering the peak height or area under the curve at wavenumber 1696 cm^{-1}. The change in the carbonyl Index with the change of added RAP is shown in Figure 3-12. It is expected that the index will vary linearly with the addition of RAP. Carbonyl Index corresponding to zero percent and hundred percent RAP are connected by a straight line. The indices at intermediate RAP content are shown in the figure. Considering the straight line as a predicted index, root mean square errors are calculated using the equation:

$$RMSE = \sqrt{\frac{\sum[(Predicted - Measured)^2]}{Number\ of\ data\ points}}$$

The RMSE is then normalized by dividing it by the carbonyl index of the mix with zero percent RAP. This normalized RMSE is presented as percent in each figure. From Figure 3-12(f) it can be observed that normalized RMSE for the area ratio at 1696 cm^{-1} to 1456 cm^{-1} yields the lowest error. Although the area ratio at 1696 cm^{-1} to 1601 cm^{-1} also yields the same value, this ratio is not considered for further calculation as the previous one predicts more closely at lower RAP content. For the quantification of RAP content in the mix, the area ratio at 1696 cm^{-1} to 1456 cm^{-1} is considered in the later sections.

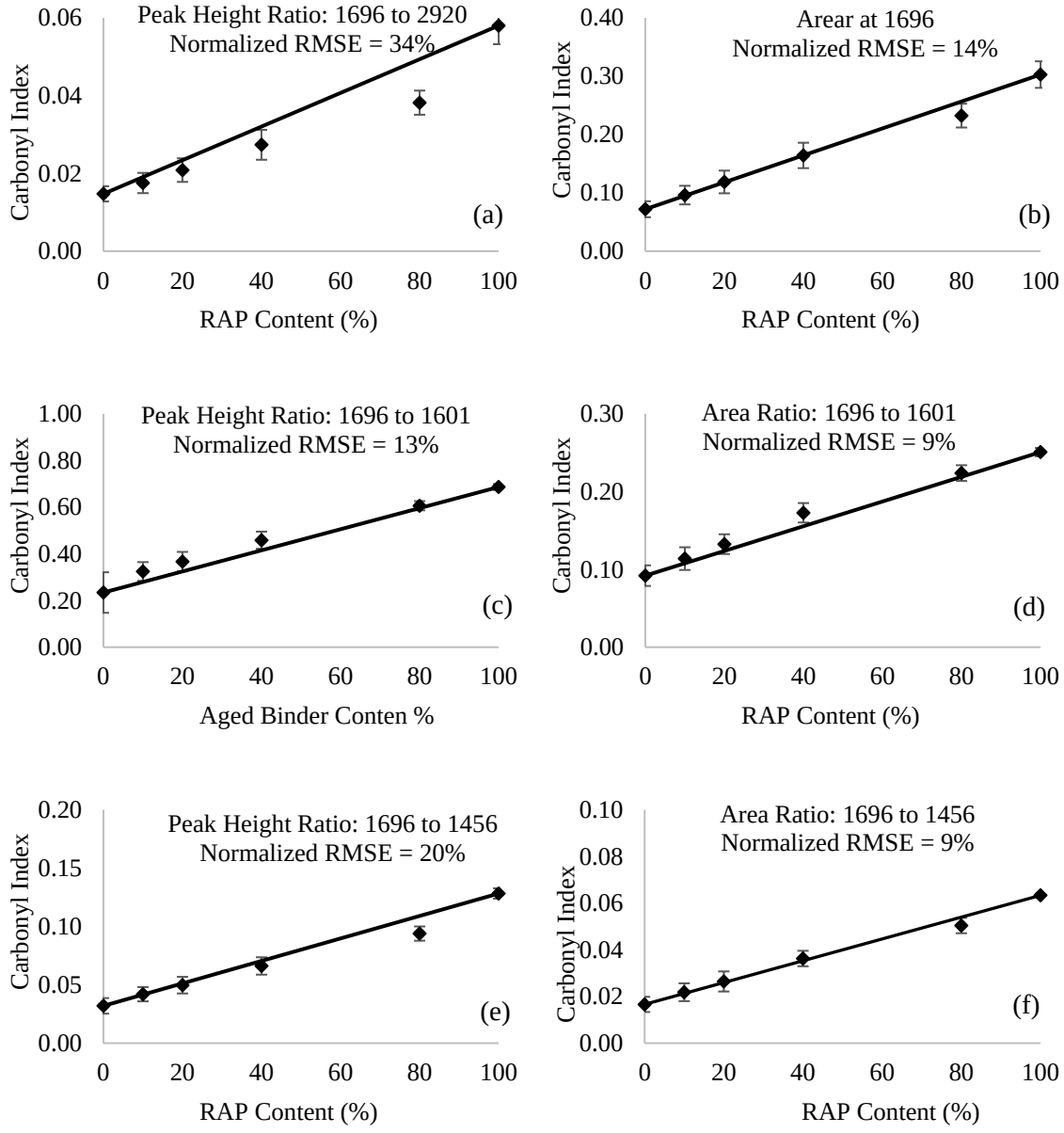

Figure 3-12 Change in Carbonyl Index for various amounts of RAP addition. Indices are calculated in six different methods and normalized Root Mean Square Errors are provided for each method.

3.5.2 Effect of Short-Term Aging in the Plant

All the mixes were collected from two different locations in the plant: the 'drum' and the 'truck'. The carbonyl indexex were measured for all the mixes and based on this measurement, the percentage of RAP could be determined. In figure 3-13, the carbonyl

indexes of four mixes are shown where ‘mix D’ is collected from the drum and the remaining three were collected from the truck. The bar charts are representing the carbonyl index of the unaged binder, used RAP, and predicted value of carbonyl index if designed RAP were used. For example, the carbonyl index of unaged binder and RAP in ‘mix D’ has the carbonyl index of 0.0196 and 0.0697 respectively. The predicted carbonyl index of the mix made of 16% of the RAP binder was calculated to be 0.0276 by the following equation where RBR stands for RAP to total Binder Ratio:

$$I_{CO-Mix} = I_{CO-Binder} * (1 - RBR) + I_{CO-RAP} * RBR \qquad \text{(Eq 3.4)}$$

Except ‘mix D’ all other mixes showed a significant increase in the carbonyl index than the predicted value. It can be mentioned that ‘mix D’ was collected from the drum whereas, the other three mixes were collected from the truck. There is a chance that ‘mix B’, ‘mix E’, and ‘mix H’ were short-term aged when they were being stored in the silo. If the carbonyl indices were used to calculate the RAP percent in the mix it would give a much higher percentage although RAP content might be in the design limit. So, it is important to choose the location from where the sample should be collected. In the case of ‘mix D,’ the carbonyl index was obtained around the predicted value. So, ‘mix D’ and other mixes collected from the drum were used to determine the RAP content in the mix. Further study will be conducted to investigate the effect of short-term aging of mix in the silo.

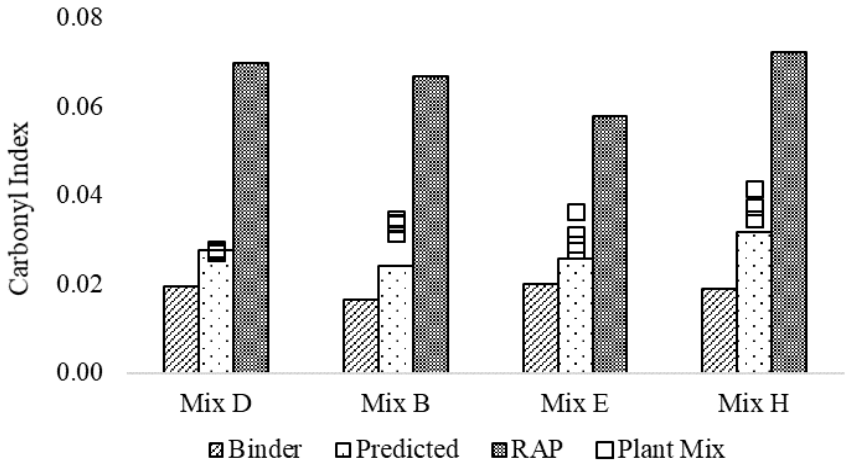

Figure 3-13 Carbonyl Index of short-termed aged mixes in the plant.

3.5.3 RAP Content in Fresh Plant Mix

Figure 3-14 is the RAP content of six different plant mixes collected from the drum. Three to five samples of each mix were extracted and tested in FT-IR to determine the RAP content in the plant. Design RAP content for each mix is shown on the horizontal axis. The carbonyl indexex for different samples of the same mix are slightly different which can be used to calculate the corresponding RAP binder percent in the mix. For example, unaged binder and RAP in 'mix A' have carbonyl indexes of 0.0220 and 0.0758, respectively. The carbonyl index of one sample from 'mix A' was found to be 0.0285. If I_{CO} of the unaged binder corresponds to 0% and I_{CO} of RAP binder corresponds to 100% RAP binder, for a given value of I_{CO} of 0.0285, the percentage of RAP binder in the mix was found to be 12% by the following equation:

$$RAP\% = \frac{I_{CO\,(Mix)} - I_{CO\,(Unaged\ bInder)}}{I_{CO\,(RAP)} - I_{CO\,(Unaged\ bInder)}} * 100 \qquad \text{(Eq. 3.5)}$$

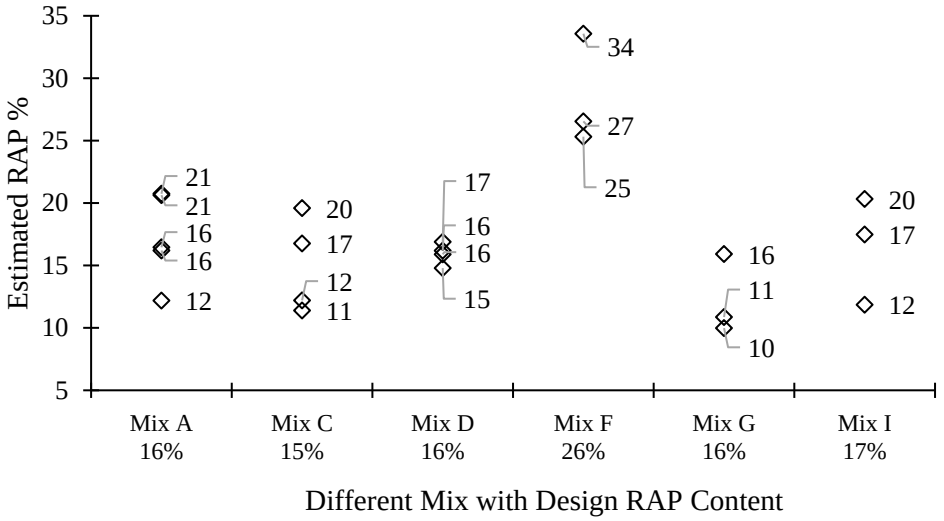

Figure 3-14 RAP content determined by handheld FT-IRS in the plant.

Percentage of RAP in the ‘mix A’, varies from 12% to 21% where the design RAP was 16% (Figure 3-14). For all the mix tested here, the RAP content was found within ±5% range, with the only exception of one sample from ‘mix F’. There might be a probability of using a higher amount of RAP in the mix or the RAP was not properly blended from where the sample was collected. Whatever the reasons are, the FT-IRS can detect the variation in the carbonyl index and dictates the investigation of the mix production anomaly.

3.6 Conclusions

The study is conducted to implement the handheld FT-IR as a quality control tool in the field by monitoring the quantity of added RAP. FT-IR spectral analysis was performed on plant produced mix as well as RAP to estimate the RAP content in a fresh mix. Laboratory aged binder and mix were analyzed at the beginning to comprehend and

compare the aging processes in terms of carbonyl index. From this study following conclusions can be drawn:

- Carbonyl index can successfully quantify binder and mix aging. For all four types of laboratory aging methods, the carbonyl index gradually increases with the duration of aging. The rate of increase of I_{CO} is not linear it rather slows down while the aging progresses.
- Change in concentration of sulfoxide with the extent of asphalt binder or mixture aging is not consistent. At some point in aging, the concentration of Sulfoxide stars to drop. The rate of change in the Sulfoxide index largely depends on the method of aging. Even after 24-hours of RTFO aging, the Sulfoxide index cannot reach a similar index value if it is aged in PAV. Moreover, in the case of mixture aging, the index values are influenced by the fines present in the mixture. Therefore, the Sulfoxide index should not be considered a reliable indicator to quantify the aging rate of an asphalt binder or mixture.
- PAV aging of binder and oven aging of mix at 135 ºC exhibit a comparable relationship. 1-PAV, 2-PAV, and 4-PAV can produce a similar aging effect which is resulting from mix aging of 2 hours, 4 hours, and 12 hours, respectively.
- Generally available RAPs possess a much higher carbonyl index than that of the laboratory aged binder or mix. But laboratory aged asphalt shows higher stiffness than the RAPs at similar carbonyl content. FT-IR can be used for screening of RAP based on their extent of aging.
- A quick extraction process developed in this study can produce enough binder from the mix for testing in FT-IR. The process is very simple and time-saving.

- The amount of RAP in the plant mix can be determined by spectral analysis of fresh mix provided the carbonyl index of unaged binder and the RAP are already determined. FT-IRS can successfully determine the RAP content in the mix within the ±5% range of the design RAP content. Mix sample should be collected from the outlet of the drum before it reaches to the silo to minimize the effect of short-term aging.
- This study indicates that handheld FT-IRS has the potential to be used as an effective quality control tool.

CHAPTER 4

EVALUATION OF BIO-BASED AND PETROLEUM-BASED REJUVENATORS BASED ON CRACKING SUSCEPTIBILITY OF HOT MIX ASPHALT[†]

4.1 Introduction

Environmental benefits and economic savings are the main inspiration behind the promotion of repetitive use of high reclaimed asphalt pavement (RAP) in hot mix asphalt (HMA). Although more than 40 states allow the use of over 30% RAP in HMA the actual use of RAP varies from only 10 to 20% [4.1]. Higher variability in RAP and lack of properly defined mix design hinder the increased use of RAP. National cooperative highway research program (NCHRP) first addressed this issue and developed AASHTO M 323 standard to incorporate RAP in HMA mix design which was then revised and improved later [4.2, 4.3]. West et al.'s (2011) study of long-term pavement performance revealed that cracking is more frequently occurring distress in the pavement with high RAP content [4.4]. The several modes of asphalt pavement cracking—thermal, reflection, fatigue, and top-down—are all affected by the high use of RAP if proper considerations are not made during the mix design.

[†] This chapter or portions thereof has been presented previously in the 98th Annual Meeting of Transportation Research Board, Washington D.C., 2019. The current version has been formatted for this dissertation.

A low amount of RAP (10 to 20%) does not affect the intermediate and low temperature cracking potential as well as fatigue resistance of pavement [4.3, 4.5]. However, a high amount of RAP (over 25%) can significantly increase the stiffness as much as 60% that leads to a cracking susceptible mixture [4.3, 4.6]. Overlay test, semi-circular bending test (SCB), indirect tension test (IDT) were utilized by several researchers to evaluate the cracking susceptibility of the mixture at an intermediate temperature [4.6-4.8]. With no exception, a high amount of RAP makes the mixtures prone to cracking at intermediate temperatures. Cracking susceptibility at low temperature can be evaluated by SCB test at low temperature, bending beam rheometer (BBR), disk shape compact tension (DCT), thermal stress restrained specimen test (TSRST), IDT test. All the studies reported increased cracking susceptibility at a higher amount of RAP in the mixture [4.3, 4.5, 4.8]. Except for some contradictory findings where inclusion of RAP improved the fatigue resistance, most of the studies reported deteriorated performance of RAP mixes evaluated through four-point beam fatigue, direct tension fatigue tests as well as indirect tension test. [4.5, 4.9-4.11**].** Aged binder in RAP makes the mixture stiffer and escalates the cracking susceptibility of the mixture at intermediate and low temperatures, for this reason, the agencies are reluctant to incorporate a higher amount of RAP [4.6, 4.9]. Special considerations must be taken to design mixture with a higher amount of RAP and thorough laboratory investigation should be performed before being implemented in the field.

When RAP is included in HMA, it is intended to stay for another pavement service life, and the mixture is expected to perform better or at least equal to the virgin mix [4.1]. Several approaches are being practiced offsetting the higher stiffness of binder

from recycled asphalt to make the mix resistant to cracking. One approach is to use a softer virgin binder according to the blending chart to achieve the design binder grade of the binder blend [4.2]. Another option is to make a rich asphalt mixture with a lower design air void. The most suitable strategy is to use rejuvenators that are rich with dispersing agents which helps keep the asphaltene dispersed thus restore the rheological properties of recycled aged binder [4.12]. Softening agents apparently reduce the viscosity of aged binder but rejuvenators are more effective to reversing the stiffness of aged binder both physically and chemically by deagglomeration of asphaltene [4.13]. Overcoming the restriction of RAP amount and precisely controlling the required doses are the main benefits of rejuvenator over the softer binder [4.14]. Commercially available rejuvenators are primarily classified into six categories: paraffinic oils, aromatic extracts, naphthenic oils, triglyceride & fatty acids, and tall oils [4.15]. The first three are petroleum-derived oils that supply the maltene as dispersing agent while the last two are agricultural-derived compounds that provide the fatty acids and/or ester as a dissolution media [4.16]. Among all those types, aromatic extracts are traditionally used rejuvenators which is a refined crude oil product and a major fraction of asphalt binder. Recently, different types of modified vegetable oils, bio-based oils, and organic oils are tested and commercially available which are gaining popularity as being more environmentally friendly [4.17]. Those types of rejuvenators fall into the category of triglycerides and fatty acids and tall oil group. Tall oil contains a straight chain of fatty acids while in other types of rejuvenators, fatty acids and glycerol react together to form eater. This study is focused on evaluating the performance of petroleum-based aromatic oil and plan-based bio-oil (fatty acid and triglyceride) types of rejuvenators.

Zaumanis et al (2014) investigated the effectiveness of aromatic extracts and vegetable oil to restore the rheological and mechanical properties of RAP binder [4.14]. Change in chemical fractions in aged asphalt binder is the main reason for the stiffening effect of RAP binder which was estimated by combined rheological (DSR and BBR), chemical (SARA), and morphological (AFM) investigation. Rejuvenators can alter the chemical fractionation and thus restore the mechanical properties. A significant change in SARA fractionation due to the addition of rejuvenators was also reported by Yu et. al (2014) [4.18]. Rejuvenated binders show lower hardness and increased fatigue life through the LAS test [4.13]. The level of interaction of RAP binder and virgin binder in a mixture is not completely known. When rejuvenators are used the major concern arises is the blending of RAP binder and rejuvenator and the time of diffusion [4.20]. For mix design purposes, it is statistically reasonable to assume the total blending although total blending is very unlikely. So, the application of rejuvenators should not rely on rheological can chemical tests only. The performance of a rejuvenated mixture must be evaluated before the implementation of the rejuvenator in the field.

In a study, Zaumanis et al. (2014) compared recycling agents with 100% RAP mixtures. Both conventional petroleum and bio-based recycling agents were tested, including plant-based oil, aromatic extract, waste engine oil, distilled tall oil, waste vegetable oil, and waste vegetable grease [4.21]. The author believed that by optimizing the rejuvenator dosages most of the products in that study can be used. In another study, similar types of rejuvenators were used where aromatic extract showed higher fracture energy in comparison to the plant-based oil [4.22]. Saha et al. (2020) investigated the effect of the use of bio-oils (waste cooking oil and soy oil). Up to 70% RAP mix showed

satisfactory resistance against fatigue and low temperature cracking when modified with bio-oils [4.23]. In a study, Hajj et al. (2013) evaluated the performance of Bitutech RAP which is a kind of plant-based (basically tall oil type) rejuvenator [4.24]. Mix with 50% RAP showed improved resistance to moisture damage after freeze-thaw cycles and restored the low-temperature properties in TSRST. Tran et al. (2012) conducted a laboratory study on aromatic extract type rejuvenator with 50% RAP and reported higher energy ratio indicating improved resistance to top-down cracking of rejuvenated mixture than the RAP only mixture [4.25]. Low-temperature cracking resistance was also improved evaluated by the fracture energy parameter obtain through the IDT test. A similar conclusion is valid for intermediate temperature cracking in the overlay test. Improvement is more pronounce is mix with lower RAP content. But in both cases, the improvement was not up to the level of virgin mix. Tran et. al (2015) conducted another study to evaluate the effectiveness of the rejuvenator in the high (50%) RAP mixture [4.26, 4.27]. A pine-sourced liquid product (tall oil type) was used as a rejuvenator. The addition of rejuvenator can lower the high-temperature grade of the recovered binder and improve the low-temperature grade. Intermediate and low temperature cracking performance of rejuvenated mix after short-term aging was close to the virgin mix. It was found that the virgin and rejuvenated mix were more susceptible to RAP mix without rejuvenator based on the dynamic modulus testing. Ali (2015) studied the effect of ten rejuvenators including bio-based and petroleum-based rejuvenators [4.9]. Based on different physical properties aromatic oil and bio-based rejuvenators were ranked among the top five. Aromatic type rejuvenators helped slow down the aging while bio-based one accelerated the long-term aging. Because of aging susceptibility of the rejuvenated

mixture, a mixture can perform worse in the long run although initially it might pass the performance grading requirement. The diminishing efficiency of rejuvenators to reduce the stiffness and to improve the cracking resistance of the mixture with long-term aging is also reported by other researchers [4.28, 4.29].

The use of rejuvenator improves the thermal cracking temperature but it might come with increased susceptibility of rutting [4.19]. The softening effect of rejuvenator can be compensated by the addition of polymers [4.30]. Based on test results of 0, 15, and 30 percent RAP mixture, Hajj et al. 2009, concluded RAP can be a partial replacement for polymers to get a fatigue-resistant mixture [4.31]. Mogawer (2013) found the polymer modification as an effective measure to improve the fatigue resistance of the rejuvenated asphalt mixture but improvement of low-temperature cracking resistance was not reported [4.32]. In this study, limited tests were performed to investigate if a polymer modified binder has the potential to improve the low temperature cracking resistance through the SCB test at low temperatures.

Cracking is a primary mode of distress for flexible pavement and it is more pronounced when a higher amount of RAP is used. In this study, comprehensive laboratory experiments were conducted to investigate the cracking potential of the RAP mixed asphalt with and without rejuvenating agents. A set of performance-related tests were conducted to particularly assess the susceptibility to cracking at intermediate low and temperature, along with resistance to rutting and moisture-induced damage. A wide variety of laboratory tests and models to assess the cracking potential of asphalt mixtures are in practice and quite a few are recommended for routine use. For example, Louisiana DOTD requires for J_c parameter from the intermediate temperature SCB test, Texas DOT

put overlay test in their standard specification, Illinois DOT implemented a balanced mix design method where flexibility index parameter from intermediate temperature SCB test is utilized. In this study, these three types of tests along with SCB at low temperature is performed on unaged and long-term laboratory aged specimens. Because of variation in RAP binder grade and a wide variety of rejuvenators it is necessary to develop a procedure of mix design and selection of the optimum doses. This study is intended to address this mix design issue and to evaluate the performance of a traditional (Aromatic Oil) and recently become popular (Bio-based oil) rejuvenators through different cracking tests.

4.1.1 Objective

The overall objective of this study is to evaluate the bio-oil and aromatic oil rejuvenator based on cracking susceptibility of hot mix asphalt with high RAP content. This objective will be achieved by accomplishing the following tasks:

- Determination of optimum rejuvenator contents based on high-temperature grading of the RAP binder.
- Application of the Superpave mix design method addressing the asphalt content and gradation of the RAP as well as the rejuvenator amount.
- Evaluation of the effect of rejuvenator on rutting and moisture-induced damage.
- Determination of short-term and long-term aging effect on the rejuvenated mix.
- Investigation of the susceptibility of RAP mixed asphalt to different types of cracking: cracking at an intermediate temperature, reflective cracking, and low temperature cracking.

4.2 Materials and Experimental plan

4.2.1 Asphalt Binder, Aggregate and RAP

Reclaimed asphalt pavement used for this study was collected from Madden Contracting Company LLC, Minden, LA. The RAP was fractionated and was stored under the shed. To prepare the regular HMA crushed granite and manufactured sand was used with PG 67-22 binder.

4.2.2 Rejuvenators

Two types of rejuvenating agents were evaluated: plant-based bio-oil (‘B’) and petroleum-based aromatic oil (‘A’). Both are commercially available and were directly supplied by the manufacturer. Generally, rejuvenators are maltene rich substances which help to restore asphaltene to maltene ratio diminished because of the aging process of asphalt binder [4.12, 4.33]. Maltene facilitates the asphaltene to disperse uniformly and consequently reduce the stiffening effect of aged binder. Aromatic oil is a traditionally used rejuvenator whereas, bio-oils are recently gaining more popularity as rejuvenators. Aromatic oil is refined crude oil contains highly polar aromatic rings works as a dispersing agent for asphaltene. Bio-oil used in this study is a proprietary material produced from plant-based oil with other added modifiers which creates a strong dispersing media for asphaltene. Details physical properties of the rejuvenators can be found elsewhere [4.34]. Both the rejuvenator specimens were investigated using a Fourier Transformed Infrared Spectroscopy with Attenuated Total Reflectance (FTIR-ATR) and the spectrum in the fingerprint region (wavenumber 650 to 1800 cm-^{1}) is provided in figure 4-1. Bio-oils show distinct peaks at wavenumber 1746 cm^{-1} and 1163 cm^{-1} which

corresponds to -C=O and -C-O stretching respectively present in triglycerides. Unlike bio-oil, aromatic oil does not show any additional peaks in comparison to virgin asphalt binder. In fact, aromatic oil is a constituent of the virgin asphalt. So, the spectra of aromatic oil are a subset of the asphalt binder. Due to the presence of aromatic oil, at wavenumber 1600 cm^{-1} in the absorbance spectra, a peak corresponds to the aromatic functional group (aromatic -C=C-) is pronounced. With the help of FTIR-ATR, the rejuvenator used for this study can be categorized into two different rejuvenator types mentioned by NCAT [4.15].

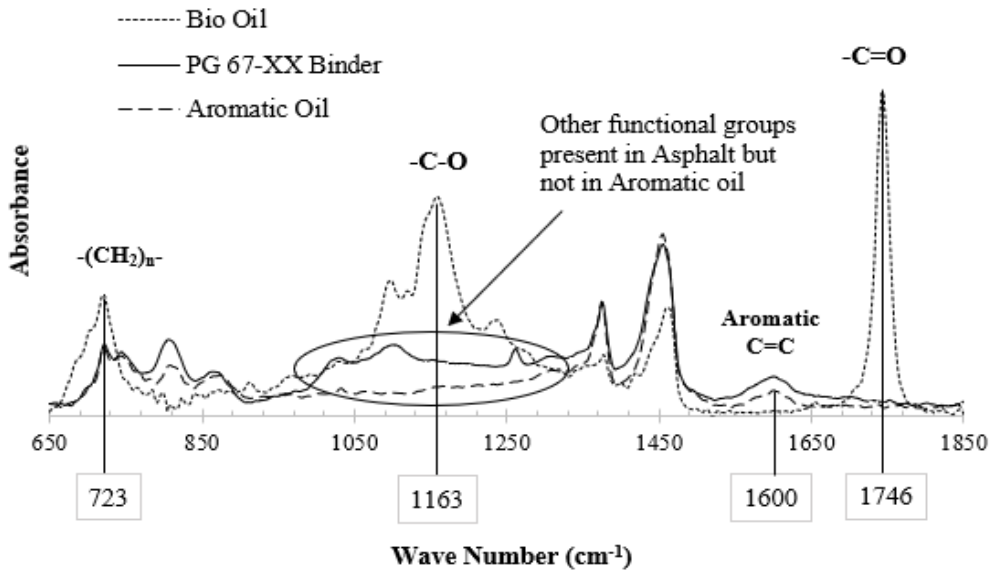

Figure 4-1 FTIR-ATR spectra of the binder and rejuvenators.

4.2.3 Experimental Plan

The study started with the proper characterization of RAP. The asphalt content of the RAP was determined by extraction (ASTM D 2172) and recovery (ASTM D 5404) as well as by using the ignition oven (ASTM D 6307). Gradation and physical properties of RAP aggregate were determined using the aggregate obtained from the ignition oven

after burning the asphalt. Both the recovered and virgin binders were tested in DSR to determine the high-temperature grade with and without the addition of different percentages of rejuvenators. Mix testing was performed on a control mix (0%R), a mix made of 15% RAP (15%R), and a mix made of 30% RAP (30%R). 15% (based on RAP binder) 'B' rejuvenator was added to the 15%R mix and it was named as 15%R-0.15B. Similarly, 30%R-0.15B and 30R-0.30%B mixes were prepared with 15% and 30% 'B' rejuvenator, respectively. Another mix was prepared with 35%'A' rejuvenator with 30% RAP which was named 30%R-0.35A. So, a total of seven different types of unaged (short-term aged) mixes were evaluated for cracking resistance. Selected four mixes were evaluated for rutting susceptibility and moisture-induced damage. Four mixes: 0%R, 30%R, 30%R-0.15B, and 30%R-0.35A were subjected to long term aging and were tested for cracking susceptibility. Loose mix was aged in the forced draft oven at 135 ºC for 12 hours to simulate long term aging [4.35]. The temperature was raised to 150 ºC and maintained for an hour before compaction. Figure 4-2 shows the detailed experimental plan executed in the study. A limited number of low SCB tests at low temperatures were also performed on a long-term aged rejuvenated mix made of polymer modified binder (PG 76-22).

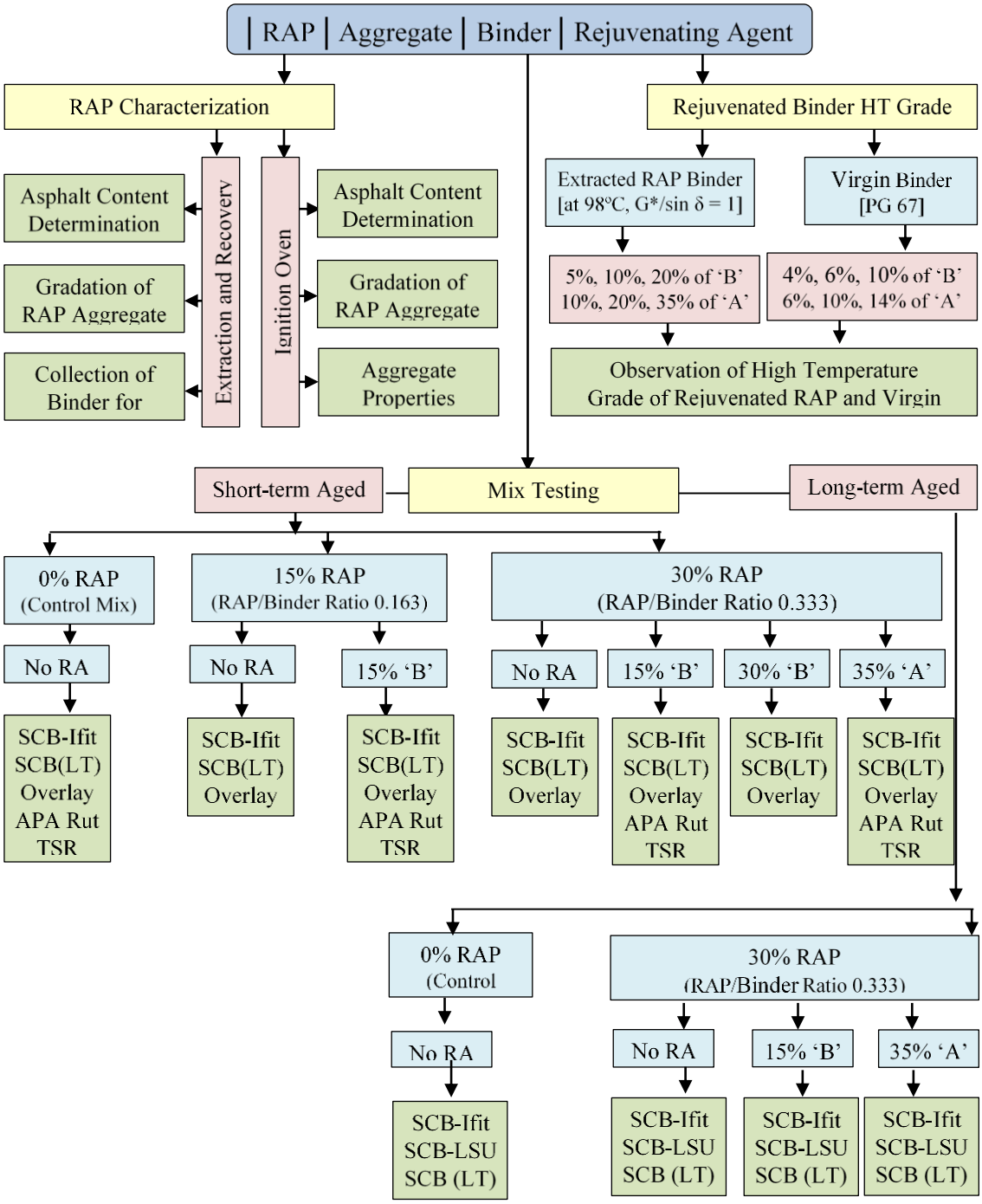

Figure 4-2 Detailed experimental plan of the study.

4.3 Methodology

4.3.1 Characterization of RAP

Characterization of RAP involved the determination of percent asphalt content, determination of binder high-temperature grade, and the aggregate gradation of (coated) RAP as well as RAP aggregate. The average asphalt content of RAP obtained from two different methods was 5.0%. The high-temperature grade was found to be 98. The gradation of the RAP aggregate along with virgin aggregate for the mix design is provided in figure 4-3. RAP (coated) gradation was performed using selective sieves (3/8 inch, #4, #8, #40, #100, and passing #100) and the RAP was stored in different buckets based on sieve sizes. Gradation of RAP aggregate was determined using all the standard sieves. The relation between the RAP gradation and RAP aggregate gradation was established so that the actual aggregate amount can be determined from the RAP collected from the bucket.

4.3.2 Mix Design of HMA with RAP

The control mix used in this study was designed according to AASHTO R 35. Crushed granite and manufactured sand were used as the aggregate conforming to the gradation requirement of table 502-4 of the Louisiana Standard Specifications for Roads and Bridge [4.36]. Optimum asphalt content was determined as 4.6%. Mix was produced at 163 °C and aged at 150 °C for 2 hours in an oven for volumetric calculations. At a design gyration of 100, the air void was found 3.89%. Voids in mineral aggregate (VMA) and voids filled with asphalt (VFA) were 13.5% and 69%, respectively.

To accommodate the different amount of RAP in the HMA, the original mix design and the mixing process was needed to be modified. The RAP was preheated at 110

ºC for two hours and then heated at mixing temperature (163 ºC) for one hour. The RAP was then mixed thoroughly with the heated aggregate. The RAP and aggregate mixture were placed in the oven for 30 more minutes before the addition of the liquid binder. Inclusion of 15% RAP did not require the change in asphalt content used for the control mix. The optimum asphalt content was verified by checking the air void after 100 gyrations. Inclusion of 30% RAP required the reduction of asphalt content from 4.6 to 4.5% based on the 4% air void at design gyration. To get the optimum mix design, the gradation of the mix was kept unchanged even after the addition of RAP. So, the gradation of virgin aggregate was altered so that the mixture of RAP and the virgin aggregate possessed the same gradation as of the control mix. Figure 4-3 shows the required granite gradation for 15% and 30% added RAP.

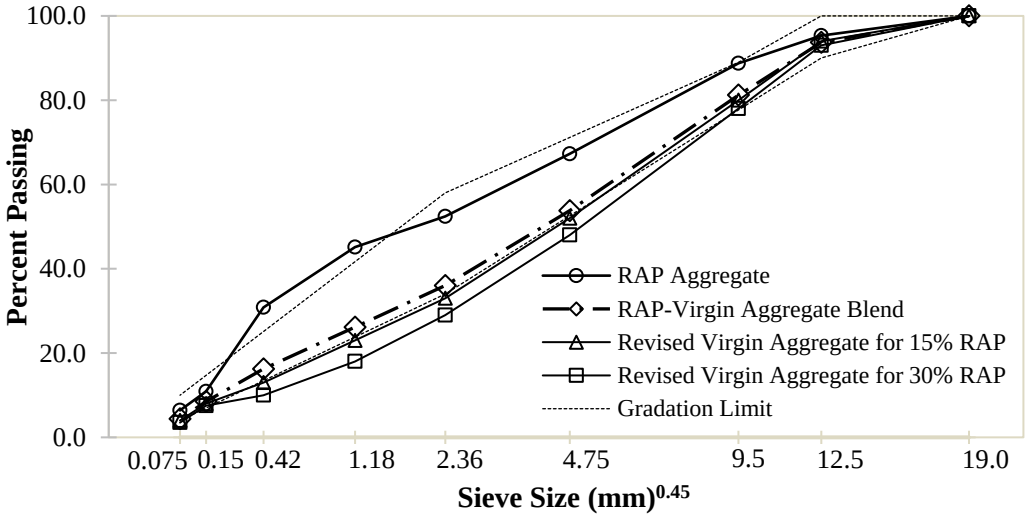

Figure 4-3 RAP and virgin aggregate gradation required for HMA design.

RAP Binder Ratio (RBR) is defined as the ratio of the RAP to the total binder in the mix. Calculated RBR for 15% and 30% RAP was 0.16 and 0.33, respectively. If the

RBR is over 0.25 it can be considered as high RAP content [4.3]. So, this study includes both low and high RAP content.

When the rejuvenator was needed to be included in the mix, it was added to the liquid binder. Rejuvenator ‘B’ is a low viscous liquid and was added at room temperature. The rejuvenator ‘A’ is much viscous and was heated for 15 minutes at 163 ºC before mixing. The required amount of rejuvenator was measured separately and added to the hot binder. A mechanical mixer was used to mix the rejuvenator homogenously into the hot binder. The mixing process was continued for 5 minutes before making each specimen. Detail information regarding the proportioning of RAP, virgin aggregate and binder, and rejuvenators for several different mixes are given in table 4-1. It can be noted that the rejuvenator percent is determined based on the RAP binder, but it was mixed with the virgin binder based on the quantity of virgin binder in the mix.

Calculation of required virgin binder is done based on the assumption that all the aged binder from the RAP is contributing to the new mix. Although the extent of interaction between the RAP binder and the virgin binder is not certainly known, it is customary to assume that all the RAP binder is fully available in the new mix [4.37].

Table 4-1 Proportioning of RAP, virgin aggregate and binder, and rejuvenator for seven different mixes.

	0%R	15%R	15%R -0.15B	30%R	30%R -0.15B	30%R -0.30B	30%R -0.35A
Total Mix	5000	5000	5000	5000	5000	5000	5000
RAP %	0	15	15	30	30	30	30
Added RAP	0	750	750	1500	1500	1500	1500
Target AC% in Mix	4.6	4.6	4.6	4.5	4.5	4.5	4.5
Total Asphalt	230	230	230	225	225	225	225
Asphalt from RAP	0	38	38	75	75	75	75
Asphalt to be added	230	192	192	150	150	150	150
Rejuvenator % of RAP	0	0	15	0	15	30	35
Rejuvenator Req.	0	0	5.6	0	11.3	22.5	26.3
Rejuvenator% of Virgin Binder	0	0	2.9	0	7.5	15.0	17.5
RAP to Binder Ratio	0	0.16	0.16	0.33	0.33	0.33	0.33
% of RAP Aggregate	0	14.9	14.9	29.8	29.8	29.8	29.8
% Virgin Aggregate	100	85.1	85.1	70.2	70.2	70.2	70.2
Binder% (including Rejuvenator)	4.6	4.6	4.7	4.5	4.7	4.9	5.0

4.3.1 Binder Testing

High-temperature performance grading of both extracted RAP and virgin binder with and without rejuvenator was determined using a DSR according to AASHTO T 315. 25 mm parallel plate geometry with a 1 mm gap was chosen for the test. The temperature sweep test was performed at a 10 rad/sec angular frequency and a 12% strain where the temperature was varied at 6 °C intervals to find the high-temperature grade.

Frequency Sweep tests were conducted on unaged and extracted aged binders to construct a complex modulus (G*) master curve. The angular frequency was selected from 1 to 100 rad/sec at a fixed strain rate of 0.1% and frequency sweep was conducted from 4 to 82 ºC at 6 ºC temperature increment. Below 46 ºC temperature 8 mm parallel plate with a 2 mm gap and above that temperature 25 mm parallel plate with a 1 mm gap was used for the test. At 46 ºC, both the geometries were used. Complex modulus results were shifted to 22 ºC reference temperature using the time-temperature superposition

principle to construct the master curve. The Williums-Landel-Ferry equation (eq. 1) was used to compute the shift factor and the shifted complex modulus was fitted using Christensen-Anderson (CA) model (Eq. 2) [4.38]. The model consists of a glassy modulus (G_g), cross over frequency (ω_c), and rheological index (R) parameters. The shift factor was determined at each test temperature by repeatedly fitting the curve in eq. (2) with the additional segment at each temperature. Finally, C_1 and C_2 were determined by fitting all the shift factors using the eq. (2). It is customary to assume the G_g value as 1 GPa for unmodified asphalt binder.

$$\log a_T = \frac{-C_1\left(T - T_{ref}\right)}{C_2 + \left(T - T_{ref}\right)} \quad \text{(Eq. 4.1)}$$

$$G* = G_g\left[1 + \left(\frac{\omega_c}{\omega_r}\right)^{\log 2/R}\right]^{-R/\log 2} \quad \text{(Eq. 4.2)}$$

4.3.1 Mix Testing

4.3.1.1 *Resistance to Rutting*

Rut resistance testing was performed on short-term aged laboratory compacted specimens using an Asphalt Pavement Analyzer (APA). Control and selected rejuvenated mixes were compacted at 35 gyrations (resulting in targeted air void of 7%) and 75 mm height. The testing temperature was fixed at 67 °C. The testing was conducted at 100 psi (689 kPa) hose pressure and 100 pounds (444.8 N) vertical wheel load. Rut depth was measured manually after 8000 cycle wheel-passes.

4.3.1.2 *Resistance to Moisture Induced Damage*

A mix must pass the criteria set by Superpave specification to resist the moisture-induced damage. The tensile strength ratio (TSR) was determined by following AASHTO T 283. Indirect tensile strength of unconditioned and conditioned cylindrical specimens was determined under 50 mm/min monotonic compressive loading. The peak load was recorded and the ratio of the indirect tensile strength of conditioned to the unconditioned specimen was reported as TSR.

4.3.1.3 *SCB at Intermediate Temperature (AASHTO TP 124)*

Semi-circular bend (SCB) test at intermediate temperature has the potential to evaluate the fracture properties of the laboratory compacted specimens. Specimen fabrication and the test was performed according to AASHTO TP 124. The 50 mm thick semicircular specimen with a notch in the flat side was positioned in the loading fixture. Load line displacement was maintained as 50 mm/min throughout the test. Fracture energy and flexibility index were calculated from the load-displacement plot. The test was performed at 25 ºC on short-term and long-term aged binders.

4.3.1.4 *SCB at Intermediate Temperature (ASTM D 8044)*

SCB test was performed on long-term aged laboratory compacted specimen at binder's intermediate temperature. The intermediate temperature is defined as, [PG HT + PG LT]/2 + 4 in degree Celsius. For the control and rejuvenated mix, the test temperature was set as 26.5 ºC and for 30% RAP mix the temperature was set as 34 ºC. A 57 mm thick semi-circular specimen was loaded monotonically at a 0.5 mm/min constant deformation rate until the fracture failure occurred. The test was repeated for three

different lengths of notch depths to compute the critical strain energy release rate (J_c) of the mix.

4.3.1.5 *Overlay Test for Reflective Cracking*

The resistance of the mix to reflective cracking was evaluated using an overlay test at 25 ºC with significant modification of Tex-248-F. To expedite the test, the loading frequency was selected as 0.5 Hz which is five times faster than the rate specified by the standard, yet it is slower than the NCAT-OT which is performed at 1 Hz [4.39]. Maximum displacement was set as 0.7 mm which was found to be large enough to distinguish among different mixes in 500 to 600 loading cycles. The specimen for the test was fabricated in accordance with Tex-248-F.

4.3.1.6 *SCB at Low Temperature*

Low-temperature cracking of the asphalt mix was evaluated by the SCB test at -12 ºC which is 10 ºC above the lower PG grade of the binder. Sample preparation was performed according to AASHTO TP 105. It can be mentioned that the standard specifies to apply the load in such a way that the crack mouth opening rate is kept constant at 0.0005 mm/sec. The test was conducted at a 0.005 mm/sec load line displacement rate. It was investigated that the vertical loading rate of 0.005 mm/sec creates an initial crack mouth opening at a rate of 0.0005 mm/sec. Fracture energy and fracture toughness were computed from the load-displacement plot up to the fracture failure. The test was performed on short-term and long-term aged specimens. Two rejuvenated mix made of polymer modified binder was also evaluated by the SCB test at low temperature.

The four types of cracking tests mentioned above were performed using an MTS loading machine. The machine was equipped with an environmental chamber where the low temperature was achieved using liquid nitrogen. Different test fixtures were accommodated to the loading frame to perform different tests. Figure 4-4 shows the loading machine and test set up used for the cracking tests.

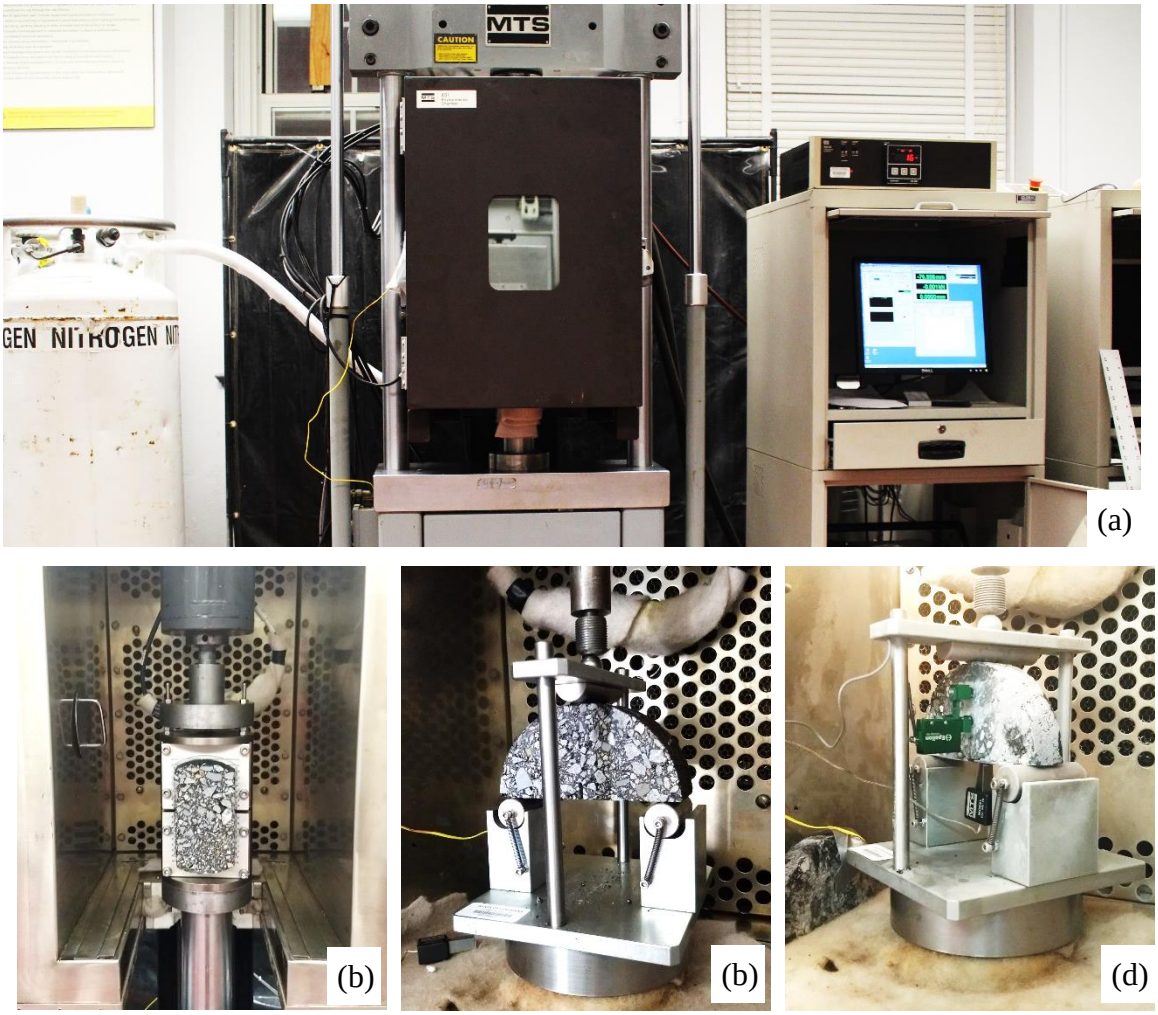

Figure 4-4 Test set up for cracking resistance testing. (a) Universal testing machine from MTS, (b) Test jig for overlay test, (c) Test fixture for SCB test at an intermediate temperature, (d) Test set up for SCB at low temperature.

4.4 Results and Discussions

4.4.1 Binder Test Results

4.4.1.1 *Effect of Rejuvenator Doses on Binder High-Temperature Grade*

Two different types of rejuvenator: ‘A’ and ’B’ at different percentages based on the weight of RAP binder were blended with the extracted RAP binder. High-temperature grade was determined at each rejuvenator content and is plotted in figure 4-5(a). It can be observed that change in high-temperature grade follows a linear relationship irrespective of the rejuvenator type. “B’ rejuvenator seems to be more effective in lowering the high-temperature grade with a higher slope than that of ‘A’ rejuvenator. For this study, a PG 67-22 binder is used as a virgin binder. To make the RAP binder compatible with the virgin binder, the rejuvenator content is chosen in such a way that it lowers the RAP binder grade to PGH 67. As recycling agents are more effective to low-temperature performance grade selecting the dose to match the high-temperature grade will automatically restore the low-temperature grade [4.12, 4.40, 4.41] For rejuvenator ‘B’ the optimum amount is determined as 15% but for ‘A’ this amount is 35% of the RAP binder.

Rejuvenator was added to the virgin binder before mix preparation. How the presence of rejuvenator changes the grade of the virgin binder was evaluated in a similar manner followed for the RAP binder. In this case, rejuvenator ‘B’ lowers the binder grade more rapidly than the rejuvenator ‘A’. The slope of the line for the RAP binder is higher than the slope of the line drawn for the virgin binder. This means rejuvenator is more effective in lowering the binder grade with higher initial grade.

The grade of the blended binder can be predicted using the following equation modified from West et al (2013 [4.3]. In the following equation T stands for high-temperature grade, RBR stands for RAP Binder Ratio.

$$T_{Blend} = T_{Virgin} * (1 - RBR) + RBR * T_{RAP} \quad \text{(Eq. 4.3)}$$

Figure 4-5(b) shows the binder grade of the rejuvenated virgin binder before mixing. Predicted grade of the binder blend is plotted there too. This binder grade can be achieved if and only if 100% proper blending of RAP and virgin binder occurs. Throughout the paper, the addition of the rejuvenator is expressed as a percent of the RAP binder. If the RBR increases, the percentage of the rejuvenator based on RAP binder does not increases but the total amount of rejuvenator in the mix increase. As a result, the rejuvenated virgin binder grade lowers when higher RBR is used.

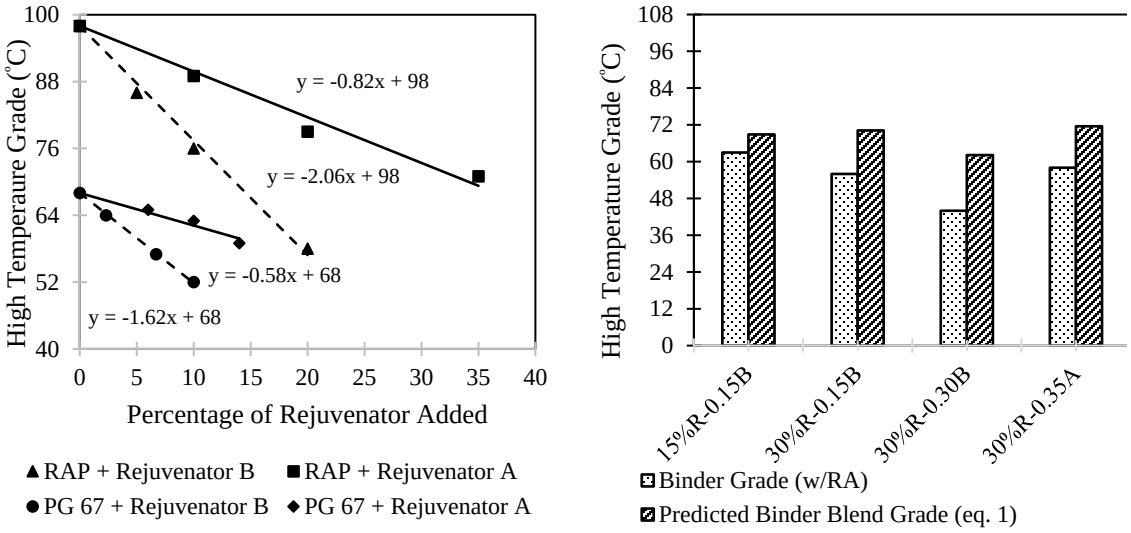

Figure 4-5 (a) Change in the high-temperature grade of the RAP and virgin binder with addition of rejuvenating agent, (b) Rejuvenated virgin binder grade and predicted binder blend grade.

4.4.1.2 *Effect of Rejuvenator on Binder Aging*

Master curve of the complex shear modulus (G*) was constructed for unaged and aged control binder, 30% RAP binder, and two rejuvenated binders. Aged binders were extracted from the corresponding oven aged mix. The parameters, cross over frequency (ω_c), and rheological index (R) used in master curve parameters according to Christensen-Anderson model, have some specific physical significance. Lower ω_c value corresponds to a harder binder and it is expected that ω_c would decrease after aging. Higher rheological index (R) indicates wider relaxation spectra indicating a more gradual transition from elastic behavior to steady-state flow. R is normally higher for an aged binder which contributes to a flatter master curve. Figure 4- 6(a) shows the master curve for the four types of binders (aged and unaged) and the parameters ω_c and R, and the shift factors are plotted in figure 4-6(b), (c), and (d) respectively. By looking at the shape of the master curve it can be noted that the 30% aged binder is much stiffer than the control binder as expected. The rejuvenated binders show almost similar rheological properties as the unaged control binder. It is also observed that, if the rejuvenator dose is selected to match the high-temperature grade of the control binder it will be soft enough in low temperature (higher reduced frequency). A closer look at the parameters reveals that the control binder possesses a higher reduced frequency and lower rheological index than the rejuvenated binder which implies that the control binder is overall softer than the rejuvenated binder.

The scenario of the aged binder is not the same as an unaged binder. The Control binder is affected more than the rejuvenated binder or the 30% RAP binder. The aromatic rejuvenated binder is the softest one after aging which is followed by the bio rejuvenated

one. Among all the binders, the aromatic rejuvenated binder possesses the most amount of aromatic fraction in the binder which helps to make it less aging susceptible. A quantity ‘aging index’ can be used to quantify the aging susceptibility of the binders. Zaumanis et al. (2014) defined the aging index as the area between the aged and unaged binders in the master curve [4.14]. The computed aging index is showing in figure 4-6(e). It is evident that the control binder is the most affected by the aging and the aromatic rejuvenated binder is least affected. Bio rejuvenated binder has a higher aging index than the 30% RAP one. RAP is already aged which makes it less susceptible to further aging in comparison to its initial aging state which corroborates to the findings from [4.42].

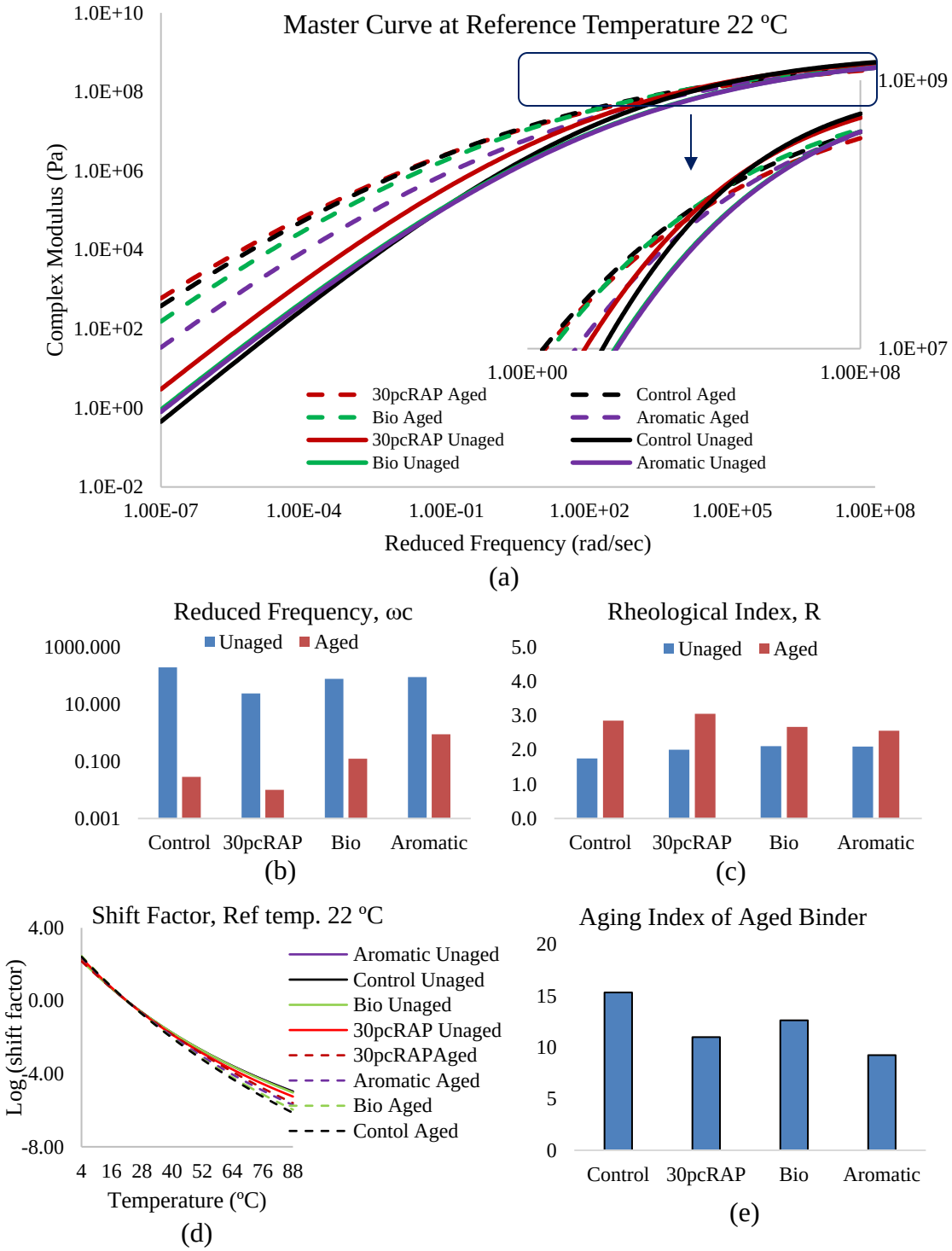

Figure 4-6 (a) Master curve of unaged and extracted aged binder with and without rejuvenators; (b) Reduced Frequency and (c) Rheological Index; (d) Shift factors at different temperatures; (e) Aging Index of aged binder calculated from the master curve.

4.4.2 Mix Test Results

4.4.2.1 *Resistance to Moisture Induced Damage*

Indirect tensile strength was determined for unconditioned and moisture conditioned specimens to find the tensile strength ratio (TSR). All the tested rejuvenated mix passed the minimum TSR value set by Superpave criteria and exhibited higher TSR value in comparison to the control mix. However, the unconditioned tensile strength of the specimens was lower than that of the control mix (figure 4-7). It can be mentioned that the same amount of compaction effort was applied to control and rejuvenated mixes, but the rejuvenated mix possessed a little lower air void. Lower air void might be the cause of higher TSR results. As rejuvenator was added in addition to the required amount of binder, the total binder content (if we consider rejuvenator as a part of the binder) of the mix might have increased a little. Asphalt rich mix possesses lower tensile strength but higher resistance to moisture-induced damage.

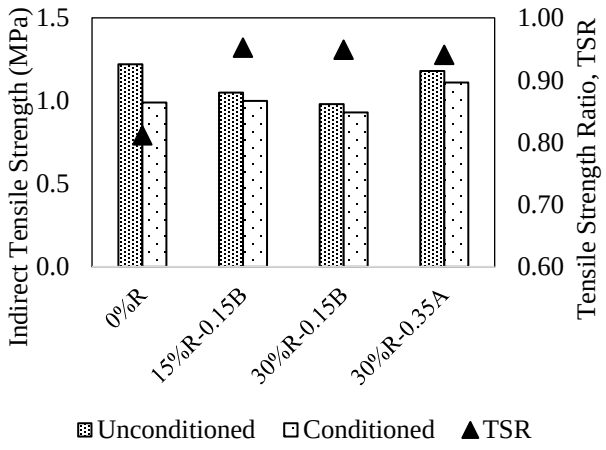

Figure 4-7 Indirect tensile strength for dry and conditioned specimens along with the tensile strength ratio (TSR).

4.4.2.2 *Resistance to Rutting*

If the RAP and the virgin binder are sufficiently blended, the mix will hardly be rutting susceptible. But rejuvenated mix might be prone to rutting. Rutting test was performed on the control mix, 15%R-0.15B, 30%R-0.15B, and 30%R-0.35A, and results are plotted in figure 4-8. There is a negligible difference in rut depth between control and 15%R-0.15B mixes. When 15% 'B' rejuvenator is added to 30% RAP the rut depth increased about 1 mm. It was reported in a previous study conducted by the authors that inclusion of rejuvenator increased the nonrecoverable creep compliance (J_{nr}) value of short-term aged binder although the high-temperature grade remained similar to the virgin binder [4.43]. For this reason, the mix made with a rejuvenated binder accumulates more permanent deformation under repeated wheel loading. It does not require to perform the test with 30% 'B' rejuvenator as it is comprehensible that the mix would be more rutting susceptible. Although 'A' rejuvenator was added by 35%, the rut resistance of the mix 30%R-0.35A is improved. A high amount of aromatic oil might result in better compaction and consequently the better rut resistance. As there exists a probability to get a rutting susceptible mix when rejuvenator is added the mix should be tested for rutting resistance if rejuvenator is used.

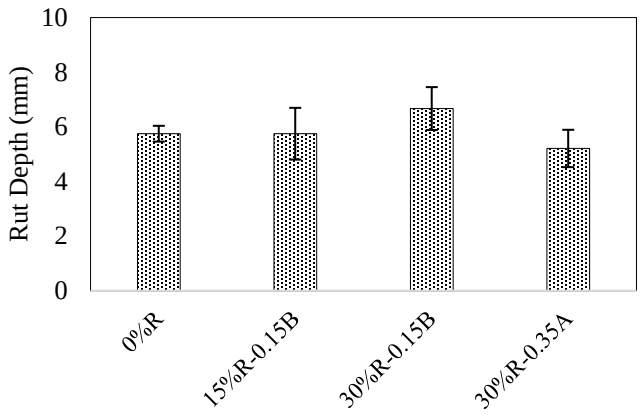

Figure 4-8 APA rutting test results for selected mixed.

4.4.2.3 *Cracking Test Results on Short-Term Aged Specimens*

4.4.2.3.1 Overlay Test

Overlay tests were performed on seven mixes to investigate the susceptibility to reflective as well as fatigue cracking. Mix with higher RAP content fails faster which can be prolonged by the addition of either type of rejuvenator at any amount (figure 4-9a). Failure of the specimen is defined as the number of cycles when the peak load reaches the 20% of the initial load which is named as the crack driving force. This definition of failure is fair enough to distinguish among the different mixes investigated for this study. In figure 4-9(a), the percentage of initial load after 500 cycles is also plotted which shows a good agreement with the definition of failure. The use of rejuvenator 'B' can increase the number of cycles to failure but still, the cycles are much lower than the cycle required for the failure of the control mix. The positive side of using the rejuvenator 'A' is that, it can increase the failure cycle beyond the cycle recorded for the control mix.

The crack resistance index (β) is also calculated from the overlay test data. Normalized peak load is plotted against the number of cycles which follow a power

relation: $y = x^{(0.0075\beta - 1)}$, with R^2 ranging from 0.78 to 0.96 except for 30%R-0.30B mix for which the coefficient of correlation was as low as 0.52. The cracking resistance index is plotted in figure 4-9(b) where a higher value indicates more resistance to cracking under repetitive loading. Figure 4-9(c) is the plot of the regression equation: $y = x^{(0.0075\beta - 1}$ up to 500 cycles. 30%R performs worst while 30%R-0.35A performs the best even better than the control mix.

A close look to figure.4- 9(b) tells that there exists an inverse relationship between the cracking resistance index and the cracking driving force. For all the mixes except 15%R and 30%R-0.30B, cracking resistance increases for the mix with a lower crack driving force. When a 30% rejuvenator (twice the optimum amount) 'B' is added to the mix made of 30% RAP, the virgin binder grade is lowered to 44. The resultant mix becomes very soft and cannot withstand repetitive loading. So, proper care should be taken to limit the maximum amount of rejuvenator even though theoretically the grade of the binder blend is not that much lower.

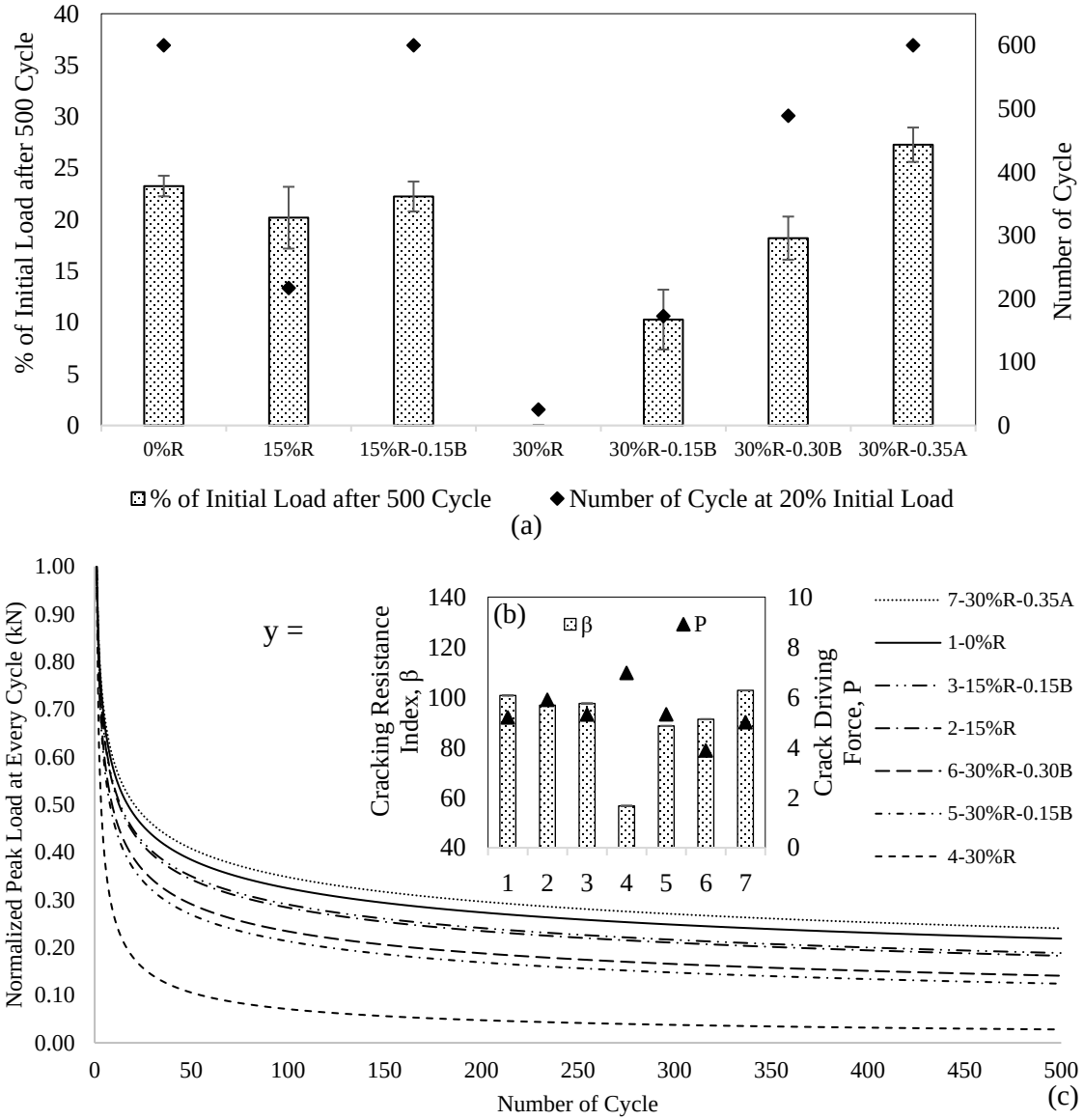

Figure 4-9 Overlay test results: (a) Percentage of initial load after 500 cycles and number of cycles at 20% of initial load; (b) Crack driving force and cracking resistance index for different mix; (c) Best fitted curve showing the change in peak load with the number of cycles.

4.4.2.3.2 SCB Test at an Intermediate Temperature (AASHTO TP 124)

SCB test according to AASHTO TP 124 is developed based on the linear elastic fracture mechanics (LEFM) where small scale yielding governs the fracture process [4.44]. Despite being viscoelastic material at the test temperature, the LEFM assumption

is valid for asphalt binder/ mix in this test procedure because of the higher loading rate. Several parameters can be derived from the load-displacement curve obtained from the SCB test. Among those parameters, Fracture Energy (G_f) in conjunction with Flexibility Index (FI) can distinguish between two different mixes based on their fracture potential. Inclusion of RAP in any amount reduces both the fracture energy and flexibility index which is an indication of increased brittleness resulting from the inclusion of a highly aged binder from RAP. Effectiveness of rejuvenator is obvious in 15%R-0.15B mixes which restore the fracture energy and flexibility index of the control HMA (figure 4-10).

The same percent of rejuvenator 'B' is not as effective when used in the mix made with 30% RAP. Both the fracture energy and flexibility index are much lower than the control mix. Although the rejuvenator content added in 30%R-0.15C is supposed to lower the RAP binder grade to the same extent as happened in the 15%R-0.15C mix, still it cannot restore the flexibility to the level of control mix. There is a chance that a higher amount of RAP might not be blended completely to the virgin aggregate which makes the mix more susceptible to cracking.

Increased amount (30% by weight of RAP binder) of 'B' rejuvenator makes the mix flexible enough compared to the control mix but it comes with a trade-off with the fracture energy which is not desirable. Increased fracture energy is resulted from higher peak load and/or higher displacement at peak load. Though a high amount of rejuvenator widens the range of displacement at peak load, it makes the mix so soft that the magnitude of the peak load is much lower. Peak load should not be directly correlated to the structural design of the pavement, but the mix should have a minimum stiffness. From this point of view a higher amount of rejuvenator is detrimental to the strength of the

pavement. An increase in RAP percent decreases the fracture energy which makes the mix susceptible to cracking. The addition of rejuvenator in any amount can reverse this process to some extent.

The mix named as 30%R-0.35A exhibited the highest fracture energy among four mixes made with 30% RAP even higher flexibility index than the control mix. Based on the SCB test results, it can be concluded that when 30% RAP is added to HMA, rejuvenator 'A' performed better though the amount of rejuvenator required is much higher than the rejuvenator 'B'.

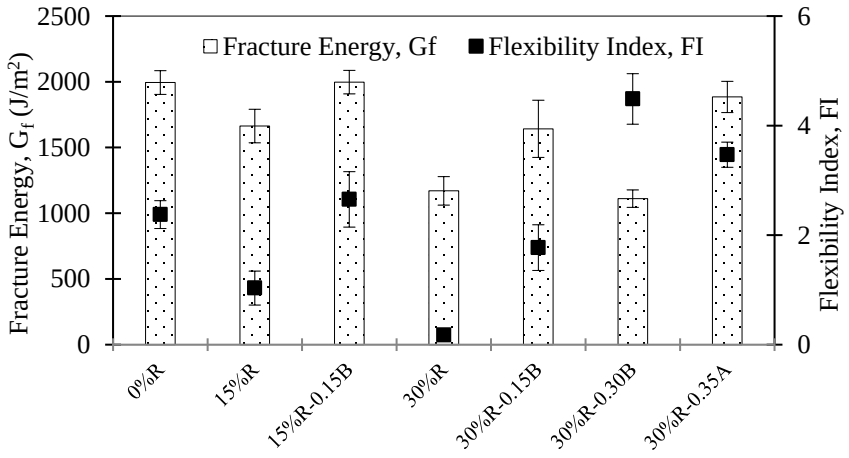

Figure 4-10 Test results: Fracture energy and flexibility index from SCB test at an intermediate temperature.

4.4.2.3.3 SCB at Low Temperature

Mixes were evaluated for resistance to thermal cracking using two parameters: Fracture toughness (K_{IC}), and fracture energy (G_f) obtained from semi-circular bend tests at low temperature. Test temperature was selected as 10 ºC above the low-temperature grade of the virgin binder, i.e. -12 ºC. Mixes with higher fracture energy and fracture toughness are expected to better resist low temperature cracking. Figure 4-11 is the plot of fracture toughness and fracture energy. It can be mentioned that fracture energy shown

in figure 4-11 is the energy up to the point of failure. Fracture toughness is directly related to peak load for a specific specimen geometry and it is a measure of the material's resistance to brittle fracture. Mix with an increased amount of RAP (w/o rejuvenator) exhibited lower fracture toughness which is an indication of brittle failure. Fracture toughness values were restored when the rejuvenators were introduced into the mix.

A similar trend is also observed in fracture energy quantity. The addition of rejuvenator helped increase the fracture energy of the mix which indicates better mix performance at low temperature. Fracture energy increases with the increased amount of rejuvenator 'B'. The addition of rejuvenator 'A' also improves the low-temperature performance but is not as effective as rejuvenator 'B'. Effective doses of rejuvenator cannot be determined by solely looking at the low temperature cracking test results. Because higher than the optimum amount of rejuvenator may improve both the fracture toughness and fracture energy of short-term aged mix.

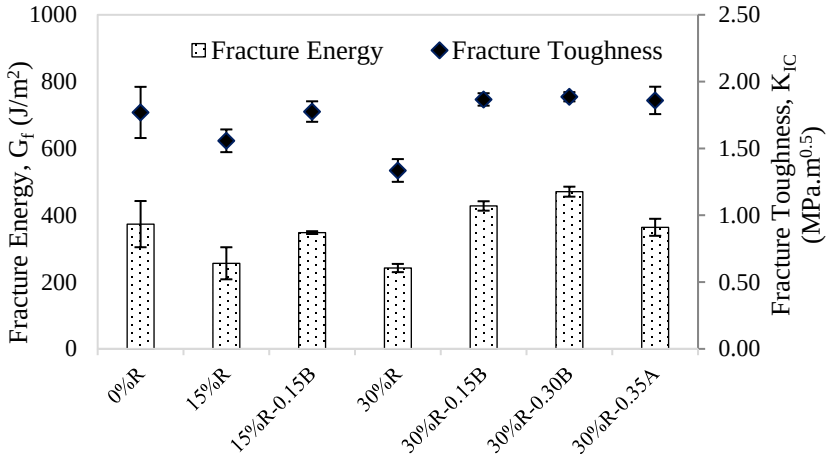

Figure 4-11 Low-temperature SCB-Ifit test results: fracture energy and fracture toughness of the mixes.

4.4.2.4 *Cracking Test Results on Long-Term Aged Specimens*

4.4.2.4.1 SCB Test at Intermediate Temperature (ASTM D 8044)

SCB test according to ASTM D 8044 was developed considering the larger fracture process zone for fracture assessment which conforms to the elastic-plastic fracture mechanics (EPFM). In this test, critical strain energy release rate (J_c) or *J* integral is computed from the load-displacement plot of mixes up to peak load with three different notch depths for each mix and then plotted against the notch depth. Mix with high J_c value performs better to resist fracture. Louisiana Department of Transportation requires a minimum J_c value of 0.50 kJ/m^2 to accept a mix for being used is a surface course [4.36]. For a given aggregate gradation the cracking resistance is a function of binder in the mixture. The use of aged RAP makes the mix brittle at an intermediate temperature which can be offset by adding rejuvenator into the mix. Figure 4-12(e) shows the change in strain energy with a notch depth of four mixes. The 30% RAP mix exhibited the lowest J_c value (0.24 kJ/m^2) as expected because of the presence of stiff binder in the mix. Both the rejuvenator could improve the cracking resistance of the RAP mixes but the aromatic one could restore the property to the same level as the control mix.

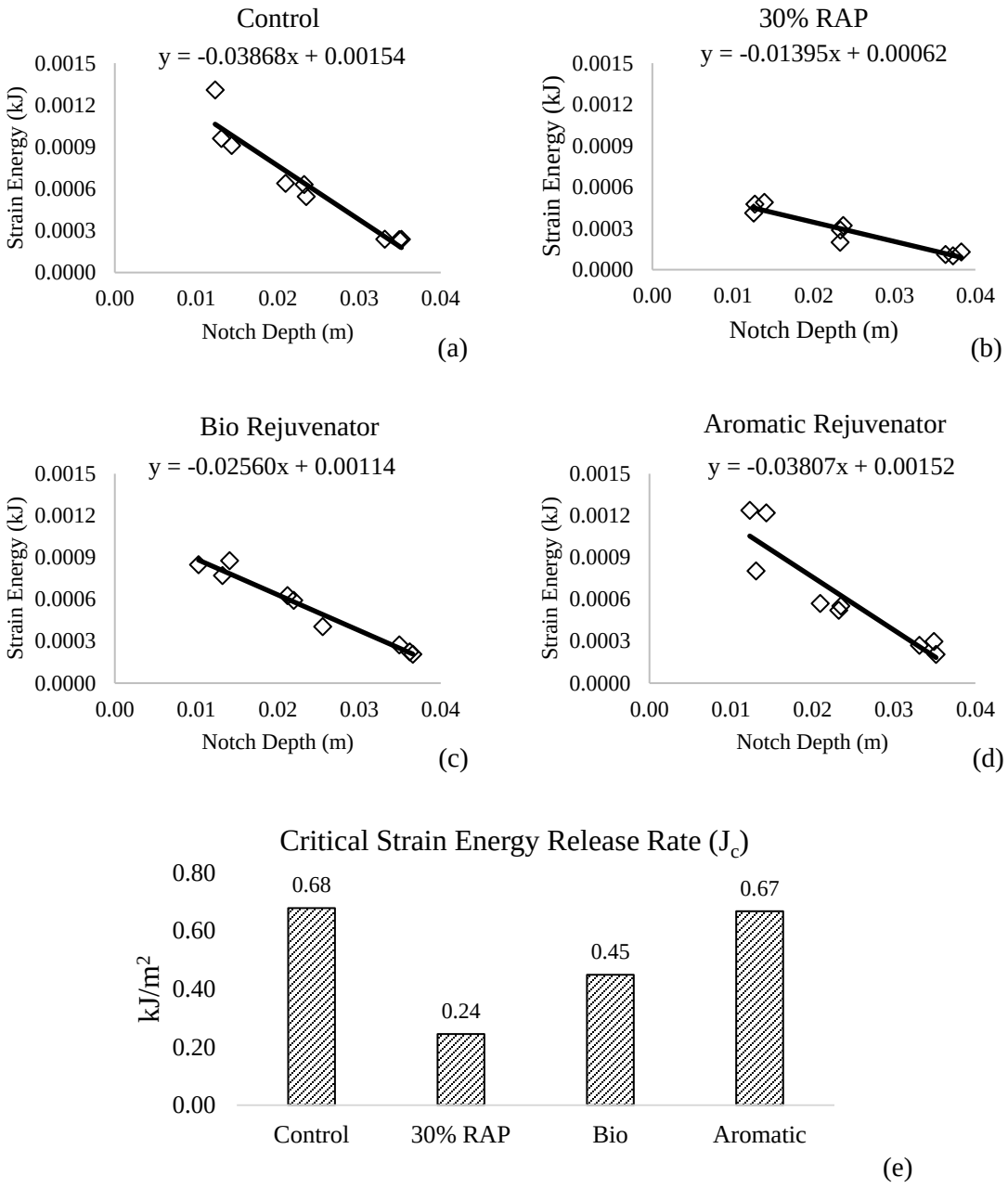

Figure 4-12 SCB-LSU test results for the long-term aged mix.

4.4.2.4.2 SCB Test at an Intermediate Temperature (AASHTO TP 124)

Fracture energy and flexibility index for selected long-term aged along with the short-term aged specimens are plotted in figure 4-13 (a) and (b). As anticipated, both the parameters for the control specimen reduced because of long-term aging. In fact, due to

the aging process, the binder (long-term aged) became stiffer at the same time it lost the strain tolerance. So, the fracture occurred at lower displacement in comparison to the unaged (short-term aged) binder and resulted in lower fracture energy. For the same reason, the slope of the portion of the load-displacement curve in the post-peak region is steeper which yielded to lower flexibility index (figure 4-13b). A similar analogy is applicable for 30% RAP mix and rejuvenated mix. The ranking of the mix based on fracture energy and flexibility index does not change because of aging. One unusual observation is noted in flexibility index value for a mix made with rejuvenator 'B'. The flexibility index did increase after aging. The increase in flexibility index is largely contributed by the smaller post-peak slope of the aged mix. Statistically, these two values are not significantly different.

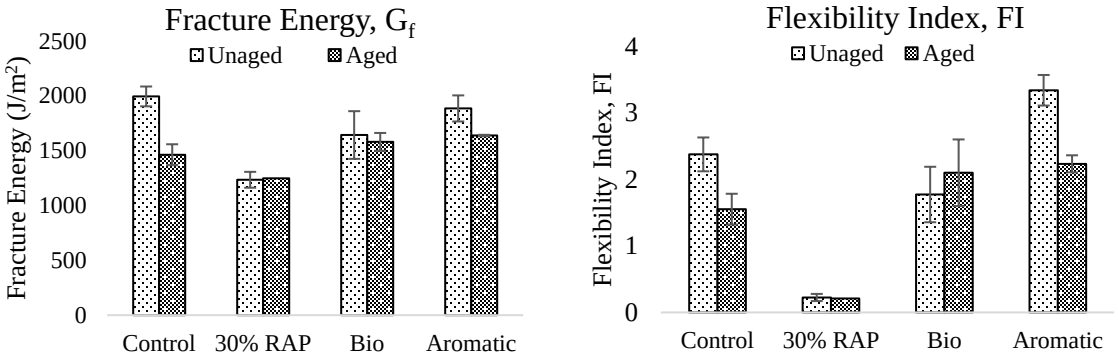

Figure 4-13 SCB-Ifit test results for the long-term aged mix: (a) Fracture Energy; (b) Flexibility Index.

4.4.2.4.3 SCB at Low Temperature

SCB test at low temperature (-12 ºC) showed that the fracture toughness diminished for all the aged specimens except the 30% RAP mix. That indicates, the mixes became prone to brittle failure after the aging process. Contrary to the general

conception, the fracture energy for all the mixes except the bio rejuvenated mix is higher in aged specimens (figure 4-14a). Fracture energy is computed as the area under the load-displacement plot. Either increase of peak load or displacement at peak load can contribute to higher fracture energy in this test and mix with higher fracture energy is more resistant to low temperature cracking. In this study, the displacement at peak load for aged control and aromatic rejuvenated specimens was found to be higher (figure 4-14a) than the unaged one although the specimens failed at lower peak load. It is possible that because of the aging the binder became more elastic and at the testing temperature, it can stretch more before failure in comparison to the unaged binder. Bio rejuvenated mix and the 30% RAP failed at lower displacement (figure 4-14a) and resulted in a decrease in fracture energy probably because of possible adhesion as well as cohesion loss due to aging. The control binder and aromatic rejuvenated binder contained much more aromatic constituent in comparison to the 30% RAP or bio rejuvenated binder. It can be hypothesized that higher aromatic fraction help improves the fracture energy in a long-term aged mix. Further investigation is required to prove this hypothesis.

Fracture toughness is of the mixes are plotted in figure 4-14(b). Fracture toughness of control and rejuvenated binders decreased indication of more brittle failure after long-term aging as expected. Ranking of the mix based on low-temperature SCB test is changed after long-term aging. Bio-oil rejuvenator is most adversely affected by aging. It lacks the maltene which is responsible for fluidity and adhesion of the asphalt matrix. Although bio rejuvenator did not lose its softness more than the control binder it lost the adhesive and cohesive properties with aging. Proper laboratory investigation on the effect of aging must be conducted before using bio rejuvenator in the asphalt mix.

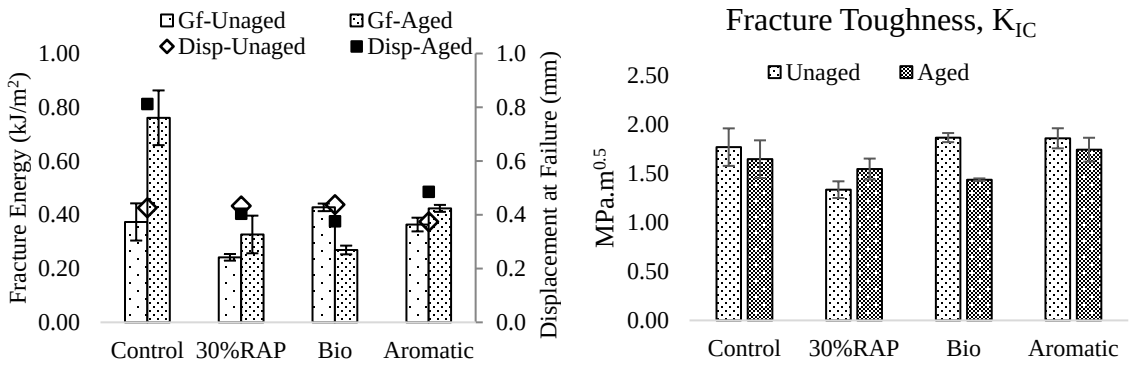

Figure 4-14 SCB test at low temperature for the long-term aged mix: (a) Fracture Energy and Displacement at Peak Load; (b) Fracture Toughness.

Two mixes made of polymer modified binder (PG 76-22) were tested at low temperatures after long-term aging to get an idea if polymer in conjunction with rejuvenators has any positive effect on mix cracking resistance. It was found that both the fracture energy and the fracture toughness parameters are higher in the mix made of polymer modified binder (figure 4-15). So, a polymer modified binder has the potential to make the mix more resistant to cracking than the unmodified binder when used with a rejuvenator. But, the improvement of the thermal cracking resistance is not up to the level of the control binder.

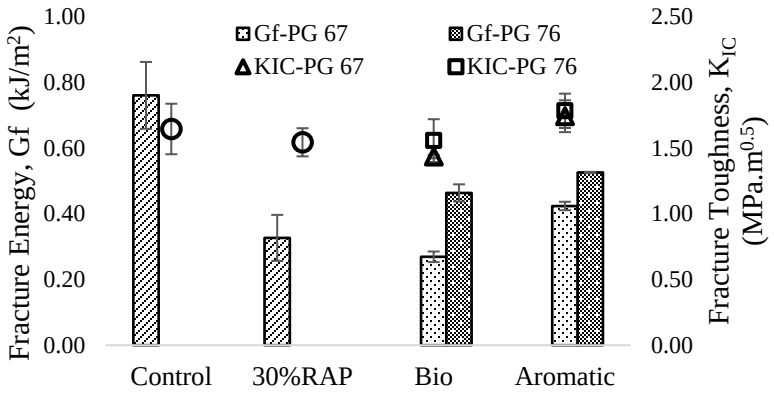

Figure 4-15 SCB test at low temperature for a long-term aged mix made of polymer modified binder.

4.4.2.5 *Summary of Mix Tests Results*

Between plant-based bio-oil ('B') and petroleum-based aromatic oil ('A') rejuvenators, the bio-oil requires less amount to lower the binder grade to a certain level. Though aromatic oil rejuvenator requires a larger amount, it exhibits better performance based on all the cracking tests performed in the study. Bio-based one can perform better at low temperatures after short-term aging, but its effectiveness diminishes with the duration of aging. From the study, it can be concluded that petroleum-based rejuvenator is more desirable for making a cracking as well as rutting resistance mix in comparison to bio-based rejuvenators. Rejuvenators are capable of completely restoring the cracking resistance when RAP is added at a lower amount (15%) but for a higher amount of RAP (30%), except the SCB-LSU test, the rejuvenated mix could not restore the cracking resistance to the level of control mix.

4.5 Conclusion

In this study, two completely different categories of rejuvenators were chosen, and dosages were selected based on the properties of RAP. Mix design of hot mix asphalt was modified because of the inclusion of RAP and rejuvenator at a different amount. The effect of aging on rejuvenated mix and efficiency of the rejuvenators to reduce cracking susceptibility was investigated through several cracking tests. The following conclusions can be drawn from the study:

- The inclusion of RAP at high amounts requires the modification of the HMA mix design. For this study, the addition of 15% RAP does not change the optimum asphalt content but the addition of 30% RAP reduces the optimum asphalt content from 4.6 to 4.5%. Proper characterization of RAP is important to determine the required virgin aggregate gradation and to obtain the optimum amount of rejuvenator.
- A bio-based rejuvenator requires less amount to lower the RAP binder grade to the desired level. It has a more softening effect and has inferior rutting resistance than the petroleum-based rejuvenator although both pass the high-temperature performance grade.
- Rejuvenator can effectively restore the cracking potential of the short-term aged HMA prepared with 15% RAP content based on cracking test.
- Bio-based rejuvenator is more susceptible to long-term aging in comparison to the petroleum-based one.
- Petroleum-based rejuvenators performed better than the bio-based rejuvenator after long-term aging of high RAP mix. But one test, it was not possible to restore

the original mix properties using a high amount of rejuvenator in HMA with higher (30%) RAP content.

CHAPTER 5

COHESIVE ZONE MATERIAL MODEL FOR CRACK SIMULATION IN SEMI-CIRCULAR BEND TEST

5.1 Introduction

5.1.1 Background

Cracking is the most common form of distresses for asphalt concrete pavement and good fracture resistance is an essential requirement for longer-lasting pavement. Cracking can occur due to a severe temperature drop (low-temperature cracking) or repetitive loading at intermediate temperature (fatigue cracking). Sound understanding of the cracking mechanism can help to design a mix with higher cracking resistance. The asphalt mix is a heterogeneous material where aggregates are coated with the asphalt layer. Failure in the asphalt mix occurs in the form of fracture that initiates between the aggregate and thin layer of asphalt binder as well as fine aggregate mastic (FAM). Being a viscoelastic material, the fracture of asphalt concrete shows both the brittle and quasi-brittle manner. At a higher loading rate or low temperature, the linear elastic fracture mechanics (LEFM) can a reasonable approach to predict the crack growth. But, at an intermediate temperature and slow loading rate the fracture process zone ahead of the crack tip is no longer an elastic region and requires different considerations than the LEFM. Cohesive Zone Material (CZM) model is an efficient and powerful approach to

model crack initiation and propagation which considers the inelastic fracture process zone [5.1, 5.2].

To analyze the crack that propagates through asphalt binder or mastic, several researchers modeled the material as cohesive zone material (CZM) which can be implemented in both homogeneous and non-homogeneous material [5.3-5.8]. It can easily be implemented in finite element and discrete element methods. It has the potential to model both the brittle and ductile failure which are observed in asphalt material. Another advantage of the CZM method is that it can model cracks along the asphalt-aggregate interface (biomaterial interface) which are often considered the weak zone susceptible to cracking. By properly defining the CZM parameter, it is possible to model both the brittle and ductile failure, which are frequently encountered in the asphalt mixture.

One of the early applications of CZM in asphaltic material is to simulate the mode I crack propagation in an indirect tension test [5.9]. Several other researchers have applied CZM and provided substantial contributions in demonstrating its applicability for modeling of fracture in asphalt mixtures. Song et al. (2006) simulated mode I and mixed-mode crack propagation of laboratory fracture tests, e.g., the single-edge notched beam (SE(B)) test, using a potential-based cohesive zone model and investigated various aspects of fracture behavior in conjunction with experiments [5.3]. Aragao and Kim (2011) implemented CZM to characterize the fracture properties of asphalt mixtures in combination with experimental tests and computational models for a wide range of loading rates at intermediate temperatures on SCB geometry [5.4]. Le and Marasteanu (2005) studied a low-temperature cracking mechanism in asphalt pavement employing a

zero-thickness interface element to implement CZM in the finite element model [5.5]. Pirmohammad et al (2014) investigated the binder type and air void percent on the cohesive zone parameter by calibrating a finite element model with laboratory SCB test at low temperature [5.6]. Kim et al (2008) utilized the cohesive zone fracture model in the discrete element method to investigate the mechanism of fracture [5.7]. Dave and Buttlar (2010) used temperature-dependent CZM for low-temperature cracking simulations in asphalt pavements [5.8].

An important input parameter for the CZM model is the cohesive properties (traction, separation, and/or fracture energy) of the interface material. Although aggregates are coated by this asphalt film the crack may not propagate through the asphalt-aggregate interface rather it can propagate through the fine aggregate mastic. So, the determination of the cohesive properties is a challenge to implement the CZM model. Researchers calibrated the finite element model with the laboratory tests and by matching the global response of the specimen the cohesive material properties are calibrated [5.3, 5.5, 5.6]. Several researchers have attempted various testing configurations, such as the indirect tension (IDT) test, the single-edge notch beam (SEB) test, the disk-shaped compact tension (DCT) test, and the semi-circular bending (SCB) test, with different measuring systems [5.3, 5.5, 5.9, 5.10]. Several researchers determined the cohesive properties of adhesive directly by laboratory tests or using both the laboratory tests and finite element models. A double cantilever beam (DCB) test is the most common and convenient laboratory test to extract the traction-separation behavior of cohesive material. Harvey extracted the traction-separation relationship of asphalt film by tensile tests on butt joints and on double cantilever beams at a wide range of temperatures (-30 to 20 ºC)

and strain rates [5.11]. Rajan et al (2017) used digital image correlation techniques to find the cohesive properties of polymer modified asphalt at room temperature [5.12]. Kim et al (2018) developed an experimental procedure to characterize the ductile viscoelastic damage behavior using a non-linear viscoelastic cohesive zone model [5.13]. Although cohesive properties of asphalt binders are determined those were not further applied to verify if they are reliable enough to predict the mix's response.

The success of numerical modeling in the CZM model is directly related to proper identification of the cohesive properties of the media of fracture propagation. If the relation of mix test geometry on the cohesive properties of FAM can be established, the mix fracture behavior can be predicted without performing the mix test. A wide variety of laboratory tests and models to assess the cracking potential of asphalt mixtures are in practice and quite a few are recommended for routine use. For example, Louisiana DOTD requires for *Jc* parameter from the intermediate temperature SCB test (ASTM D 8044) which is a measure to quantify the cracking resistance of a mix. A mix must pass this test before the application in the field. This test is performed at an intermediate temperature and at a 0.5 mm/min loading rate. At this temperature and loading rate, the mixture is subjected to quasi-brittle failure. Crack in the mix propagates through the fine aggregate mastic (FAM) and the crack path avoids any large particle on its propagation. So, it can be considered that the critical fracture energy release rate (*Jc*) should be a function of the FAM. It should be possible to model the fracture behavior of asphalt mix in the SCB test by knowing the properties of FAM. If the model is properly calibrated, the *Jc* value can be predicted even without performing the SCB in the lab. Viscoelasticity of the binder or FAM can be overlooked as the scope of the study is narrowed down by

focusing on a specific loading rate and test temperature to replicate the ASTH D 8044 test result.

The objectives of the study are to:

- Establish the applicability of CZM model to describe the fracture behavior of asphalt mix in SCB test performed at a slow loading rate and at an intermediate temperature
- Determine the CZM properties of FAM by comparing the results of the laboratory performed DCB test and finite element model of DCB
- Investigate if material heterogeneity in the mix can be avoided in the model by properly calibrate the material properties of FAM and asphalt mix modulus

5.1.2 Cohesive Zone Material (CZM): Fundamentals and Application

The development of the CZM model is based on the work of Dugdale and Barenblatt [5.14, 5.15]. In the cohesive zone material (CZM) model, the formation of fracture is considered as a gradual phenomenon where the separation of the surfaces takes place across an extended crack tip and is resisted by cohesive traction. Within the cohesive zone, there are active traction stresses between the cohesive surfaces, and interaction is governed by a traction-separation law. Before loading is applied, a CZM element is said to be undamaged, while a fully damaged element has been completely separated, and does not produce any force interactions between the cohesive surfaces. The traction-separation relationship of material must be known to implement the CZM model to analyze fractures. The traction σ is exerted by the interface until the interfacial separation u reaches a critical value u_c. σ is a function of u given by traction-separation law. As the element becomes damaged, the area beneath the traction-separation law is the

mechanical work needed to separate the elements. Thus, the area beneath the traction-separation law is equivalent to fracture energy *Gc*. When peak traction is known, and the fracture energy has calculated the shape of the traction-separation curve has little effect on the ultimate result [5.10]. It is the matter of numerical computation and convergence issue which model should be used. In this study, the cohesive property of FAM is assumed to follow a bilinear CZM model which is shown in figure 5-1.

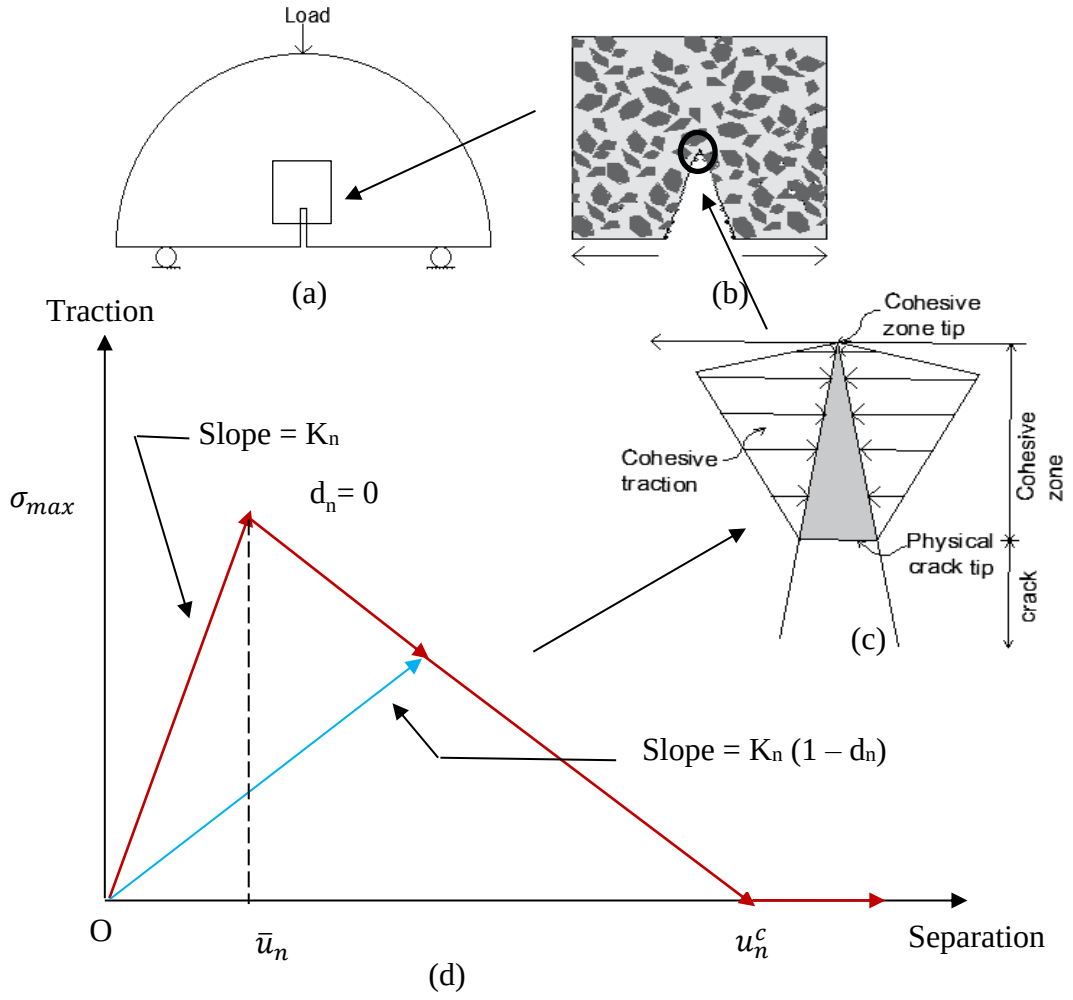

Figure 5-1 Schematic elastration of the CZM model: (a) SCB specimen with crack; (b) Close view of the crack; (c) Fracture process zone ahead of a crack tip; (d) Idealized Bilinear Cohesive Zone Material (CZM) Traction-Separation curve, reproduced from ANSYS instruction manual.

The bilinear CZM model is based on the model proposed by Alfano and Crisfield [5.16]. The figure shows linear elastic loading (OA) followed by linear softening (AC). The maximum normal contact stress is achieved at point A. Debonding begins at point A and is completed at point C when the normal contact stress reaches zero value; any further separation occurs without any normal contact stress. The area under the curve OAC is the energy released due to debonding and is called the critical fracture energy. The slope of the line OA determines the contact gap at the maximum normal contact stress and, hence, characterizes how the normal contact stress decreases with the contact gap, i.e., whether the fracture is brittle or ductile. After debonding has been initiated it is assumed to be cumulative and any unloading and subsequent reloading occur in a linear elastic manner along the line OB at a more gradual slope.

The debonding parameter for mode I debonding is defined as:

$$d_n = \left(\frac{u_n - \bar{u}_n}{u_n}\right)\left(\frac{u_n^c}{u_n^c - \bar{u}_n}\right)$$

The value of *dn* = 0 when, $u_n < \bar{u}_n$, and *dn* = 1 when, $u_n > \bar{u}_n$,

The normal critical fracture energy is defined as:

$$G_C = \frac{1}{2}\sigma_{max} u_n^c$$

A double cantilever beam (DCB) test is one of the most widely used tests to extract the traction-separation relationship as CZM parameter. There are two approaches to determine the CZM parameter from the laboratory tests: direct and iterative method [5.17]. The direct method provides the result based on measured displacement and

rotation of the beams which is highly susceptible to the accuracy of the measurement device. The energy release rate (J-integral) for the crack growth in a symmetrical DCB specimen subjected to mode I loading, considering the finite rotation of the adherent at the crack tip, can be expressed by the following equation developed by Hogberg et al (2007) [5.18]:

$$J = 12\frac{P^2a^2}{Eh^3} + P(\theta_1 - \theta_2)$$

Where, *P* is the applied load per unit width of the beam, *a* is the crack length, *E* is young's modulus of the substrate, *h* is the thickness of the beam, and θ_1 and θ_2 are the in-plane rotation of top and bottom adherent at the crack tip. Again, the J-integral containing traction-separation relation can be expressed as:

$$J = \int_0^{u_n} \sigma(u)du$$

Differentiation of J gives the expression of the traction-separation:

$$\frac{dJ}{du_n} = \sigma(u_n)$$

Rajan et al (2017) implemented those equations where the digital image correlation technique was utilized to directly extract the cohesive parameters of polymer modified binder [5.12]. Dastjerdi and Barthelat (2013) performed a DCB test with a rigid substrate that eliminates the measurement of the substrate rotation [5.19]. Traction-separation relation was determined by the following equation: Where, L is the total length of the beam and $\triangle$ is the opening at the front edge of the beam.

$$\sigma(u) = \left(\frac{L}{(L-a)^2}\right)\left(2P + \triangle\frac{dP}{d\triangle}\right)$$

In the iterative method, a numerical model is prepared using proper elements and laboratory test conditions. Cohesive parameters are assumed for the specific shape of traction-separation law. The numerical and experimental results are iteratively compared until a satisfactory match of the global load-displacement curve is obtained. For the bilinear traction-separation relation two input parameters are required: maximum traction (σ) and either maximum separation (u) or fracture energy (G_c). In this study, the iterative method is used to determine the cohesive properties of FAM using the contact debonding feature of ANSYS Workbench where CZM material is defined by traction and fracture energy.

5.2 Outline of the Study

In this study, the CZM properties of FAM were determined by matching the load-opening curve of simulated and laboratory test results for three different binders. Traction and fracture energy were iteratively assumed for the DCB model and when the simulated and test results match, the input parameters were recorded as the CZM properties of the FAM. In the next step, the SCB model was run using the traction and a factored fracture energy to match the load-deflection curve of simulated and test results. This match was performed by both matching the peak load and strain energy up to the fracture of the specimen. It was observed that the factor is dependent on the modulus of the mix obtained by direct compression at the test temperature. A regression equation was developed to relater the factor with the mix modulus.

ASTM D 8044 test determines the critical energy release rate (Jc) of asphalt mixture at intermediate temperature by semicircular bend (SCB) test. The goal of this study is to get the Jc value for a mix using a finite element model utilized the contact debonding feature for fracture analysis in ANSYS by adopting the bilinear cohesive zone material (CZM) method. CZM properties of the FAM in an asphalt mix are determined by the DCB test at intermediate temperature. The traction is directly used as an input parameter for the SCB model. The fracture energy is multiplied by a factor that depends on the asphalt mix modulus is then used as another input parameter. Together the CZM properties of FAM and the asphalt mix modulus can predict the Jc value of the mix.

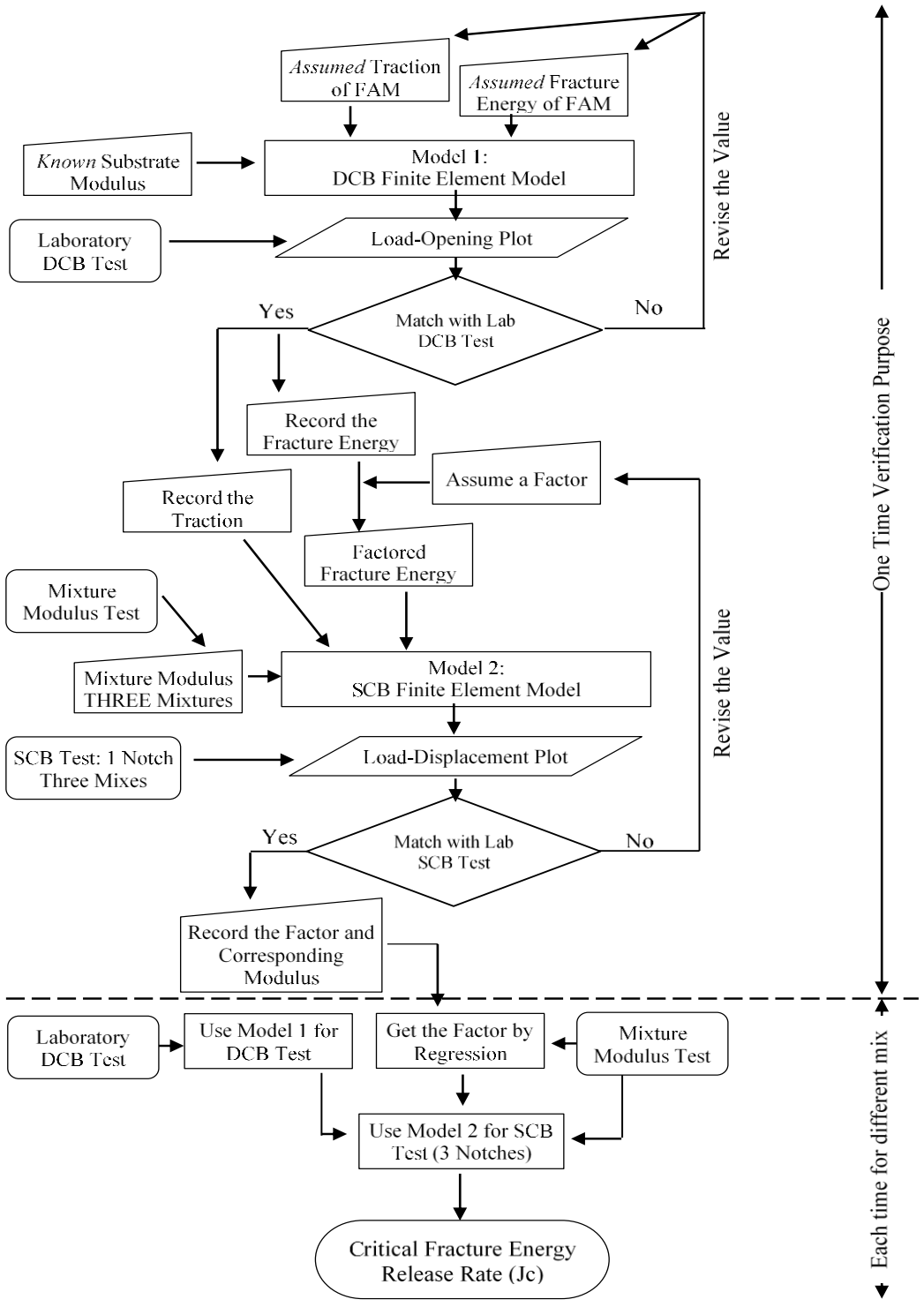

Figure 5-2 Outline of the study.

5.3 Materials and Experimental Method

5.3.1 Asphalt Binder and Aggregate

Three asphalt binders of different performance grades were used in this study: PG 58-28, PG 64-22, and polymer modified binder PG 70-22. ½ inch NMS of granite and manufactured sand was used as aggregate. FAM was prepared with aggregate passing #50 sieve but maintaining the same proportion as present in the mix. Aggregate gradation and volumetric properties of the mix is provided in table 5-1.

5.3.2 Double Cantilever Beam (DCB) Test

CZM properties of the FAM was determined using the DCB test performed in the laboratory. Two steel plates of 200 mm long, 38 mm wide and 6 mm thick were used cantilever beams. FAM was placed in between two plates as cohesive zone material which was 2-mm thick [Figure 5-3(a)]. The specimen was subjected to tension by a loading frame of a servo-hydraulic machine. The test result was recorded as a Load-Opening curve.

5.3.2.1 *Designing of Fine Aggregate Mastic (FAM)*

Observation of the number of fractured specimens in the SCB test indicates that the crack propagates through the asphalt mastic of the mix. No large particles are broken during the test rather the crack path deviates to avoid the larger stones. For the experimental purpose, the fine aggregate mastic (FAM) was prepared using the particles finer than the #50 sieve. The fine aggregates were proportioned in a way that they maintained the same proportion as present in the whole mix. The average asphalt film thicken was calculated using the method proposed by the Minnesota DOTD [5.20] and

was found to be 7.6 microns. Generally, the film thickness of fine aggregate is higher than the average film thickness. Assuming the film thickness as 11 microns, the required asphalt content for the FAM was calculated to be 18.2% of the total mastic. The FAM was prepared at 163 ºC and was kept in the oven for 10 hours at 135 ºC to simulate the long-term aging.

Table 5-1 Calculation of asphalt film thickness and required asphalt content for FAM.

Aggregate Gradation			Aggregate and Mix Volumetric Properties	
Sieve	% Passing			
	Mix	FAM		
3/4 in	100		Sp. Gr. Comb. Agg., Gsb	2.527
1/2 in	94		Sp. Gr. Smaller#4. Agg., Gsb(-4)	2.534
3/8 in	81		Eff. Sp. Gr. Agg., Gse	2.604
#4	54		Max. Sp. Gr. Of Mix, Gmm	2.43
#8	36		% Asphalt Binder in Mix, Pb	4.6
#16	26		% Stone in Mix, Ps	95.4
#30	19		Binder Sp. Gr., Gb	1.02
#50	16	100	Eff. Asphalt Content, Pbe	3.8
#100	8	50	% Absorbed Asphalt, Pba	0.85
#200	3	19	Asphalt Film Thickness, AFT (μ)	7.6

5.3.2.2 *Specimen Preparation*

Steel plates used as cantilever beams were sanded properly to remove any coating on the surface and to create surface roughness for better adhesion of the FAM with the substrate [figure 5-3(b)]. The surface was cleaned with acetone and preheated at 163 ºC before the application of FAM which was also heated in the oven at the same temperature for 1-hour after long-term oven aging. The consistency of the FAM is shown in figure 5-3(c). Although it contains 18.2% asphalt it looks very similar to the fine part of the whole mix. The FAM was spread evenly on both of the steel plates with a metal spatula and the excess amount was trimmed from all the sides. 1-mm thick silicon mat was placed at both

the ends of both the plates to ensure the thickness of the CZM material [figure 5-3(d)]. The steel plates with FAM on it was placed in the oven for 1 more hour at 163 ºC [figure 5-3(e)]. The two plated were then pressed to each other and a five-pound metal disk was placed on the specimen which was left in the oven for 6 more hours to get the desired thickness of the CZM material [figure 5-3(f)]. The excess material was trimmed from all the edges of the specimen. The specimen was left overnight for curing and it was then ready for testing.

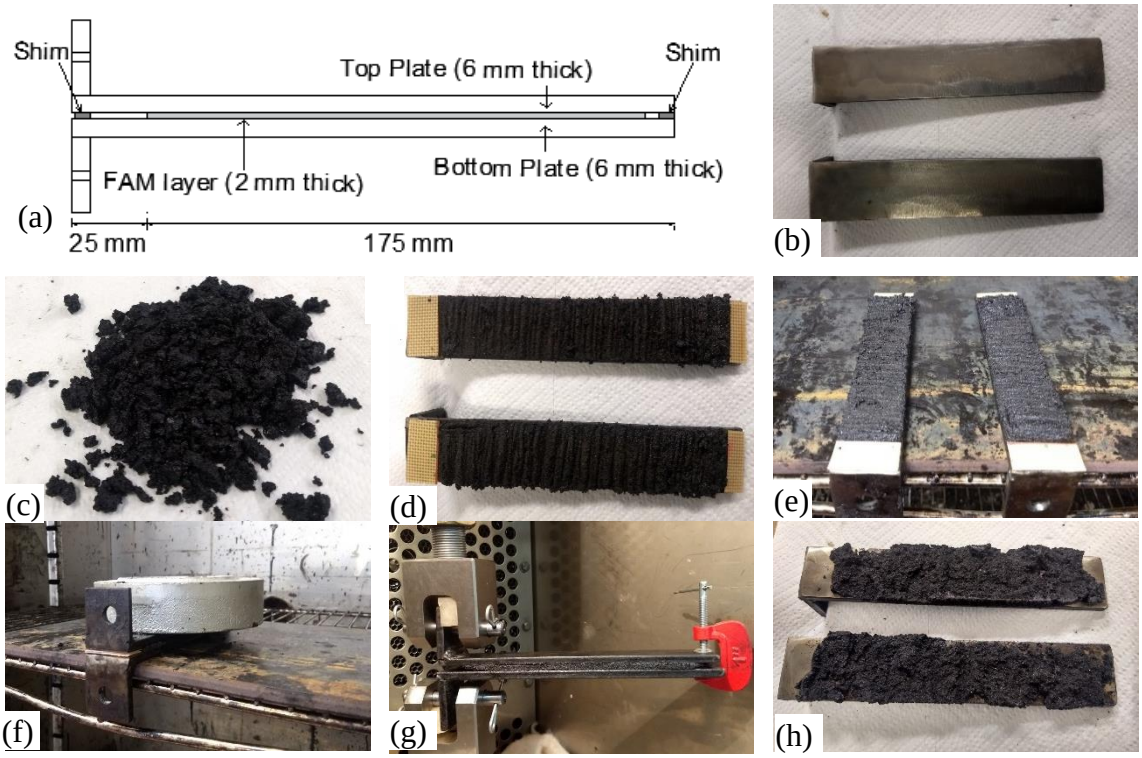

Figure 5-3: DCB specimen preparation and test set up. (a) Schematic diagram of DCM specimen; (b) Clean steel plates before specimen preparation; (c) Fine Aggregate Mastic (FAM) used as cohesive material; (d) FAM is spread over the steel plates; (e) Steel plates with FAM on top of it are placed in the oven before being pressed to each other; (f) Load is applied on the DCB specimen; (g) The specimen is under monotonic tensile loading; (h) Failed specimen after testing.

5.3.2.3 *Testing*

The monotonic tensile load was applied at a rate of 1.0 mm per min rate using a servo-hydraulic loading machine. The end of the DCB was clamped using a C-clamp to restrain the rotation at the end. Two steel plates having ½ inch hole were welded at another end of the beam to hook it up with the grip. The test set up is shown in figure 5-3(g). The test continued until the separation at the end reached up to 1.5 mm. The separated beams at the end of the test are shown in figure 5-3(h). It can be observed that the failure occurred in the FAM as expected.

5.3.3 Semi-Circular Bend (SCB) Test

5.3.3.1 *Specimen Preparation*

SCB test was performed according to ASTM D 8044. The loose mix was aged for 12 hours at 135 ºC to simulate long-term aging. It was then compacted at 7% air void [figure 5-4(a)]. The semi-circular shaped specimen was prepared from gyratory compacted 150 mm diameter and about 120 mm thick cylindrical specimen. The sample was cut along its central axis into two equal semi-circular shapes. The semi-circular specimen was trimmed to 57 mm thickness. A straight vertical notch was cut along the symmetric axis of the specimen at the straight end. Depth of the notches were 15, 25, and 37 mm [figure 5-4(b)]. Tests were performed on three replicates for each notch depth.

5.3.3.2 *Testing and Data Analysis*

The test was performed at binder intermediate temperature which is defined as 4 ºC higher than the average of high and low-temperature grade. The specimen was loaded under displacement control loading at a rate of 0.5 mm/min. Figure 5-4(c) shows the test

set up for the experiment. The time, force, and displacement were recorded up to the point when the applied load decreased to 25% of peak load. The critical strain energy release rate (Jc) is determined using the equation (1) where *b* is the thickness of the specimen and *a* is the notch depth.

$$J_c = -\frac{1}{b}\left(\frac{dU}{da}\right)$$

The strain energy (U) is calculated as the area under the load-displacement curve for three different notch length. The slope of the strain energy-notch depth plot is the change in strain energy with the notch depth which is denoted by *dU/da*.

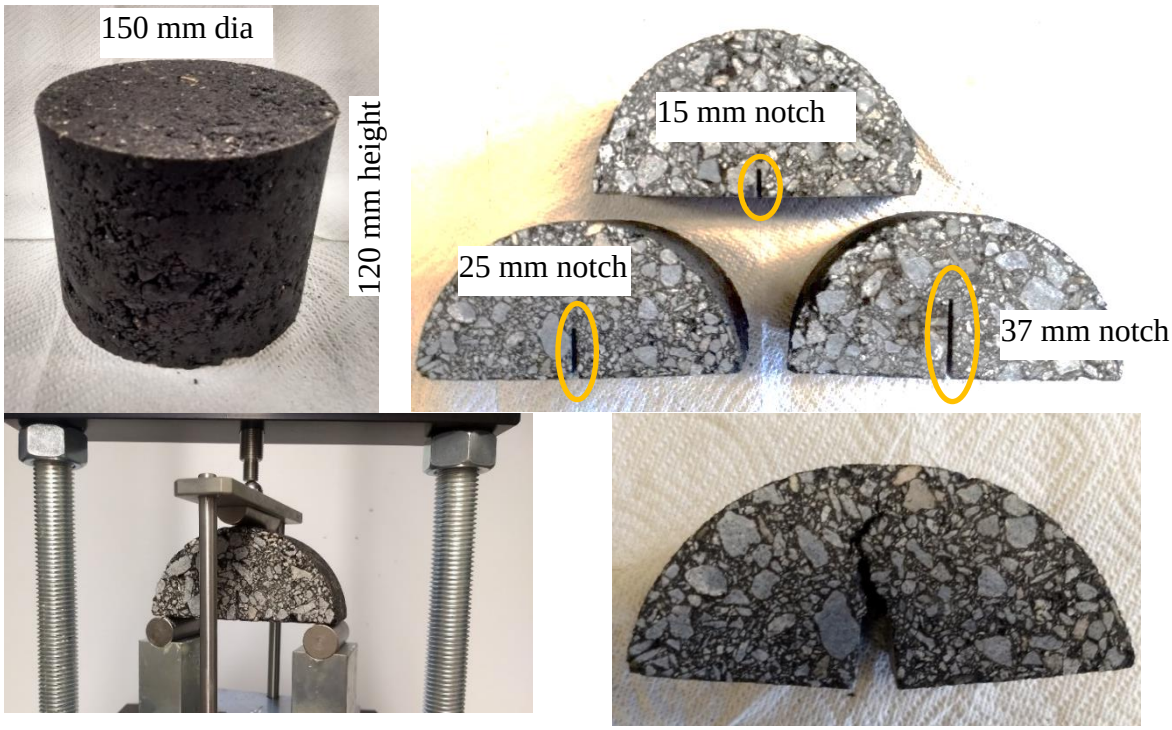

Figure 5-4 SCB specimen preparation and test set up: (a) Compacted specimen; (b) SCB specimen with three different notch depth; (c) SCB test set up; (d) Specimen after the failure.

5.3.4 Asphalt Concrete Modulus Testing

Modulus of asphalt mix was determined under direct compression loading. A 75 mm cylindrical specimen was subjected to direct compression at a rate of 0.5 mm/min. The load was applied up to 30 kN. Three consecutive cycles of loading were applied, and the load-displacement reading was recorded for the third cycle. The slope of the end portion of the load-displacement curve was considered as the modulus of the asphalt mix.

5.4 Finite Element Modeling

5.4.1 Double Cantilever Beam Test Model

A 2-D finite element model of DCB specimen was developed according to the experimental set up employing the ANSYS Workbench suit. The steel beams were modeled using the PLANE183 element which considers the plane strain condition. CONTA172 and TARGET169 were used at the interface of the two beams where CZM is applied to simulate contact-based debonding. The CZM approach introduces fracture mechanics by adopting a softening relationship between traction and separation. One end of the DCB is fixed and on the other end an equal but opposite displacement is applied for mode I crack simulation. The model requires the material properties of steel which is considered to be known. Young's modulus and Poisson's ratio of steel is 200 GPa and 0.25 respectively. The traction and fracture energy of CZM is unknown. Those two values are varied iteratively to match the simulated and laboratory test results.

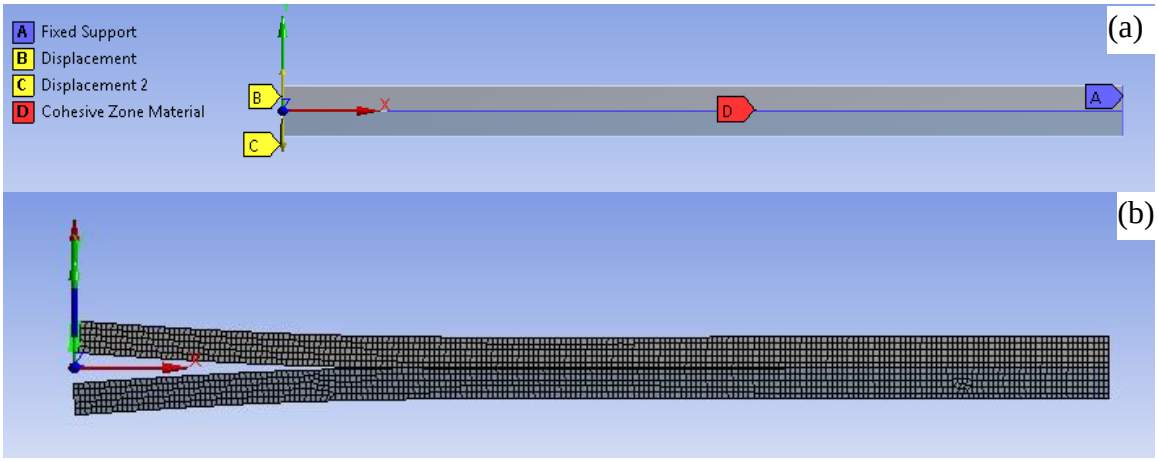

Figure 5-5 Finite element model of the DCB test: (a) DCB model with support condition and CZM element; (b) Model with generated mesh.

5.4.2 Semi-Circular Bend Test Model

In this section, a 2-D model is created in ANSYS to simulate the mode I crack growth in a semi-circular asphalt mix specimen. The dimension of the SCB specimen used in the numerical model is the same as the specimen in the laboratory experiment except the model is a 2-D one. The diameter of the semi-circular specimen is 150 mm with three different notch length of 15 mm, 25mm, and 37 mm. The specimen is simply supported with a span of 128 mm and the top is considered as fixed. An equal ramped vertical displacement is applied at both the simple supports.

The cohesive zone material is incorporated using the contact element. The contact debonding feature of the ANSYS Workbench 19.0 was utilized to create the numerical model. CONTA172 and TARGET169 were used as contact and target elements between the isotropic PLANE183 element that represents the asphalt mix. Figure 5-6(a) shows the geometry of the model and the generated mesh for this model is shown in figure 5-6 (b). It was generated automatically using the minimum mesh dimension of 0.5 mm in the vicinity of CZM as well as along the edge of the specimen.

Four material properties are required for the model: Youngs modulus and Poisson's ratio for the bulk material (asphalt mix); and traction and fracture energy for cohesive material (FAM). The bulk material is assumed as linear isotropic material with Young's modulus equal to the modulus determined by the direct compression test of asphalt mix. The Poisson's ratio was assumed to be 0.35. Traction of CZM obtained from the DCB test is directly used for the SCB model and the fracture energy from the DCB test is factored and then used in the SCB model. The factor is determined by calibrating the laboratory and numerical model of SCB performed on three different mixes.

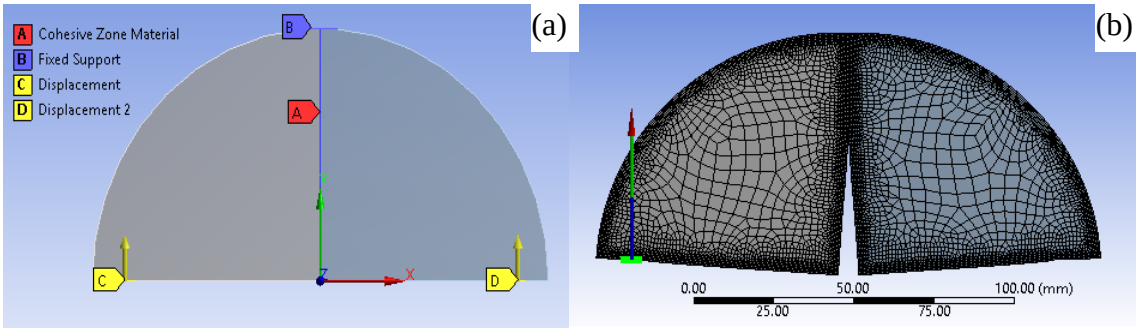

Figure 5-6 Finite element model of the SCB test: (a) SCB model with support condition and CZM element; (b) Model with generated mesh.

5.5 Results and Discussions

5.5.1 Determination of CZM Properties from DCB Test

DCB tests of FAM made of three binders were performed at 25 ºC. The Load-Opening plots for all three tests are plotted in figure 5-7. Plots for three replicates for each test is shown here. The finite element model required the structural properties of steel and cohesive properties of FAM as an input parameter. The modulus of elasticity of the steel is provided as 200 GPa. The traction (MPa) and fracture energy (J/m^2) are the two parameters that need to be determined by the test. The simulation was done by

providing initial assumed values for these two parameters. The finite element model for DCB is run iteratively until the experimental and numerical results are in good agreement. The comparison of the overall shape of the simulated results and the experimental data is performed by visual inspection in this study which is widely used by other researchers [5.5]. At this point, the traction and fracture energy provided as input parameters are recorded as the cohesive properties of the FAM which is provided in table 5-2.

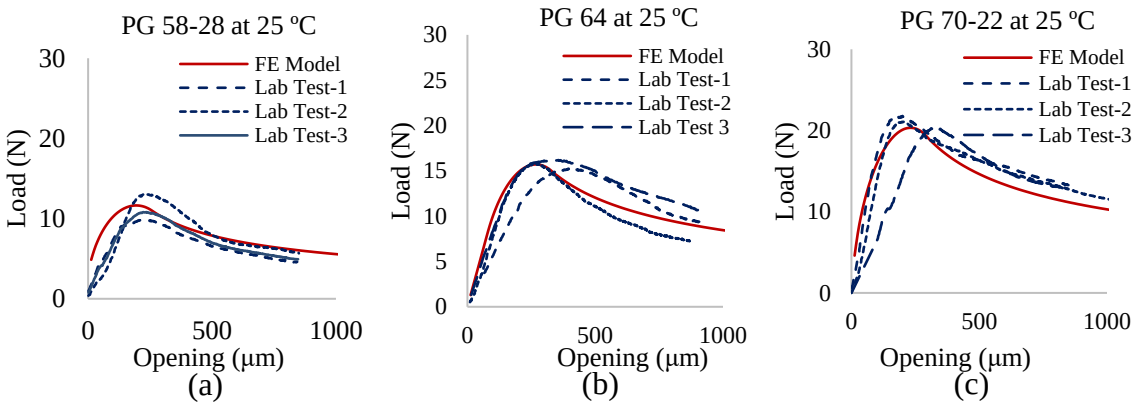

Figure 5-7 Comparison of DCB lab test data and finite element model: (a) PG 28-28; (b) PG 64-22; (c) PG 70-22.

Table 5-2 Material properties at 25 ºC from laboratory tests and finite element model.

Binder	Traction (DCB Model) MPa	Fracture Energy (DCB Model) J/m^2	Fracture Energy (SCB Model) J/m^2	AC Modulus MPa	Ratio of FE of SCB to DCB
PG 58-28	1.00	130	525	200	4.04
PG 64-22	1.50	225	975	275	4.33
PG 70-22	2.20	320	1400	325	4.38

5.5.2 Analysis of SCB Test

When cohesive properties of FAM are known, the finite element model of SCB is run using those parameters. The SCB model requires modulus of asphalt mix at test temperatures which were determined in the laboratory by separate tests. It is assumed that

as the material of FAM is not different from the one used in the DCB test the traction value will be the same for the SCB test. Because of the different geometry and load transfer mechanisms, the fracture energy of the FAM will be different than that obtained in the DCB test. The asphalt mix possesses much lower modulus than the steel and FAM is distributed all over the specimen. So, there is a chance that the FAM will deform much more before developing the full traction, and consequently, the fracture energy would be much higher. Fracture energy from the DCB test is multiplied by a factor and the load-displacement plot is compared with the laboratory test result. In this case, the comparison is made based on two factors: the peak load and the strain energy. Table 5-2 shows the input parameters for the SCB simulation and the table 5-3 shows the comparison of the simulated and test results. In most of the cases, the peak load and strain energy obtained by simulation are within 5% of the laboratory test results except the PG 70-22 binder where the strain energy of the simulated result is within 10% of the test result. Figure 5-8 is the graphical comparison of the simulated and tested results. It can be mentioned that the notch depth of the specimen for this test was 25 mm.

Table 5-3 Comparison of SCB laboratory test data and finite element model.

Binder	Peak Load (N)			Strain Energy (kj/m^2)		
	Lab Test	FE Model	% Difference	Lab Test	FE Model	% Difference
PG 58-28	10.32	10.87	5.3	0.3329	0.3467	4.1
PG 64-22	17.16	16.83	4.3	0.5995	0.6245	-1.9
PG 70-22	24.33	24.47	0.6	0.7891	0.8689	10.1

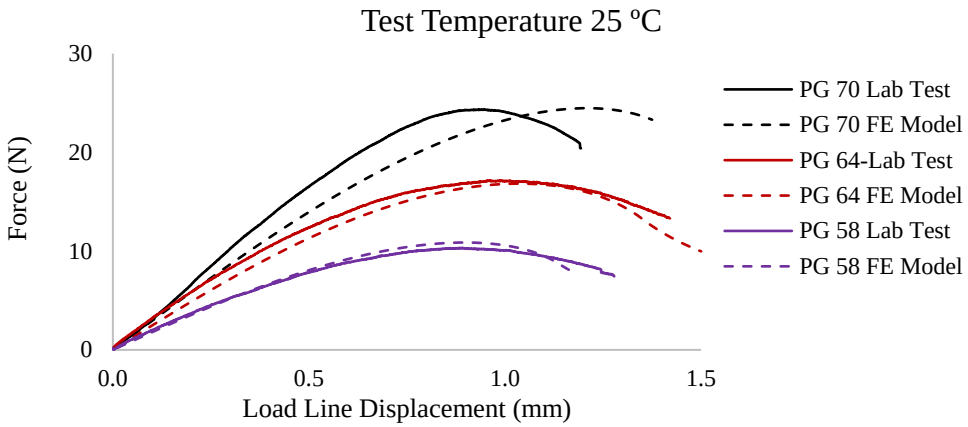

Figure 5-8 Comparison of SCB lab test data and finite element model.

Three SCB test results were compared with simulated results. Each time the multiplying factor was determined, and the asphalt mix modulus was tested. The multiplying factors are plotted against the mix modulus in figure 5-9. It can be noticed that there exists a linear relationship between the factor and the modulus of the mix. So, in the later section, this linear relationship will be used to determine the factor when the modulus of the mix is known for SCB simulation.

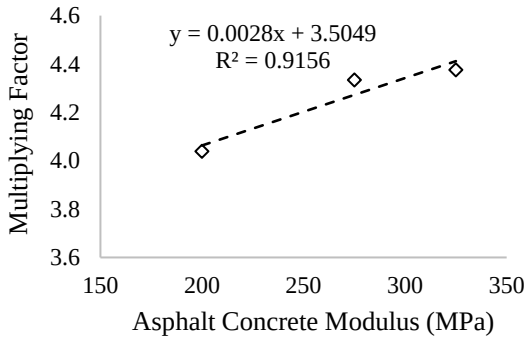

Figure 5-9 Determination of multiplying factor with mixture modulus.

5.5.3 Computation of Critical Fracture Energy Release Rate (*Jc*)

In this section, the Jc value from the finite element model, with the help of cohesive properties determined from the DCB test and mix modulus tested under direct compression, will be determined. The first DCB test was performed on three different FAM made of PG 58-28, PG 64-22, and PG 70-22 binders, and the test temperature was 19 ºC, 25 ºC, and 28 ºC respectively. The DCB simulated result and laboratory test results were compared and matched in a similar way described in section 1.6.1 and similar plots were obtained as shown in figure 5-7, of course, the values were different as the test temperatures are different (except the PG 64-22). Traction-Separation law for the FAM is shown in figure 5-10 and the values of traction and fracture energy are given in table 5-4. As the fracture energy is the area under the Traction-Separation cure, the maximum separation can be calculated from the fracture energy when the traction value is already known. The separation at peak traction depends on the initial slop of the line which is known as the contact stiffness (Kn). In ANSYS there is an option to vary the contact stiffness within a certain limit unless the convergence issue arises. The contact stiffness was varied up to a certain limit, to match the opening at which the peak load occurs in DCB simulations to laboratory test results. That slope is important to precisely express the traction-separation law, but it does not affect the traction or fracture energy of the FAM which will be used in further simulations.

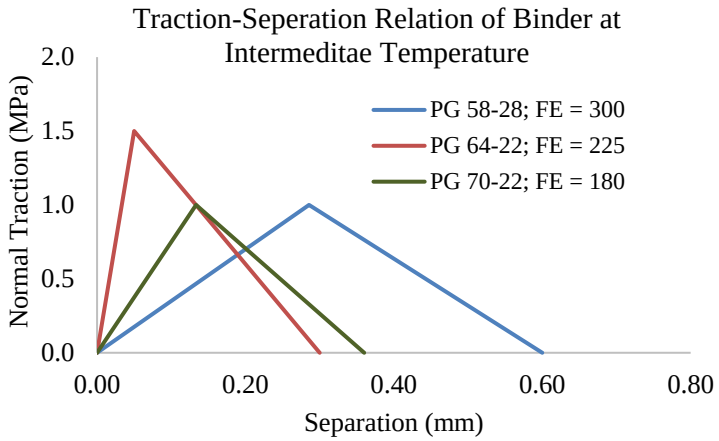

Figure 5-10 Traction-Separation relation of the FAM made of three different binders by DCB test performed at an intermediate temperature [Fracture Energy (FE) in the legend is mentioned in J/m^2 unit].

Table 5-4 Input parameters for SCB model at intermediate temperature.

Binder	Temperature ºC	Model from DCB Test		AC Modulus	SCB Model	
		Traction (MPa)	Fracture Energy (J/m^2)	(MPa)	Traction (MPa)	Fracture Energy (J/m^2)
PG 58-28	19	1.00	300	225	1.20	1230
PG 64-22	25	1.50	225	275	1.50	970
PG 70-22	28	1.00	180	250	1.00	750

In a separate laboratory test, the modulus of the asphalt mix was determined at the intermediate temperature where the mixes were made with the same aggregate gradation and air void, but the binders were different. The mix modulus is also shown in table 5-4. Using the regression equation shown in figure 5-9, the multiplying factor for fracture energy was calculated. The factored fracture energy was used as shown in table 5-4 for SCB simulation.

The plot for calculating the Jc value from simulated results for all three binders are shown in figure 5-11 along with the laboratory test results. Figure 5-11(a) is the plot of force-displacement for PG 58-28 binder for three different notch depths. It can be seen from the plot that, the specimen with shorter notch depth can resist more load before

failure. The laboratory and simulated load-displacement plots coincide point by point, but the strain energy values (figure 5-11(b)) do not differ that much. It is observed that the peak load in the laboratory test appears at shorter displacement than that in a simulated result. The strain energy which is the area under the curve up to the peak load is close for each notch depth. The strain energy is plotted against the notch depth in figure 5-11(b). The slope of the line is then used to calculate the Jc value. It can be noted that in figure 5-11(a) the force for the laboratory test specimen is divided by the thickness of the specimen and plotted as force per unit width (1 mm) of the specimen. When strain energy is calculated the thickness of the specimen is considered as 57 mm and is plotted in figure 5-11(b). Similar explanations hold for the other two types of specimens made of PG 64-22 and 70-22 binders.

Laboratory test results and simulated results for Jc values are shown in table 5. It can be observed that the ratio of the simulated to laboratory test results varies from 0.89 to 0.91. Every time the simulated results show a smaller Jc value than the laboratory test results. To adjust the simulated result, it is proposed to divide the simulated result by the average of the three ratios i.e. 0.90. This result is denoted as ‘Adjusted Simulated’ result. The last column of table 5 shows the values adjusted simulated to the laboratory test result, which is very close to 1.00.

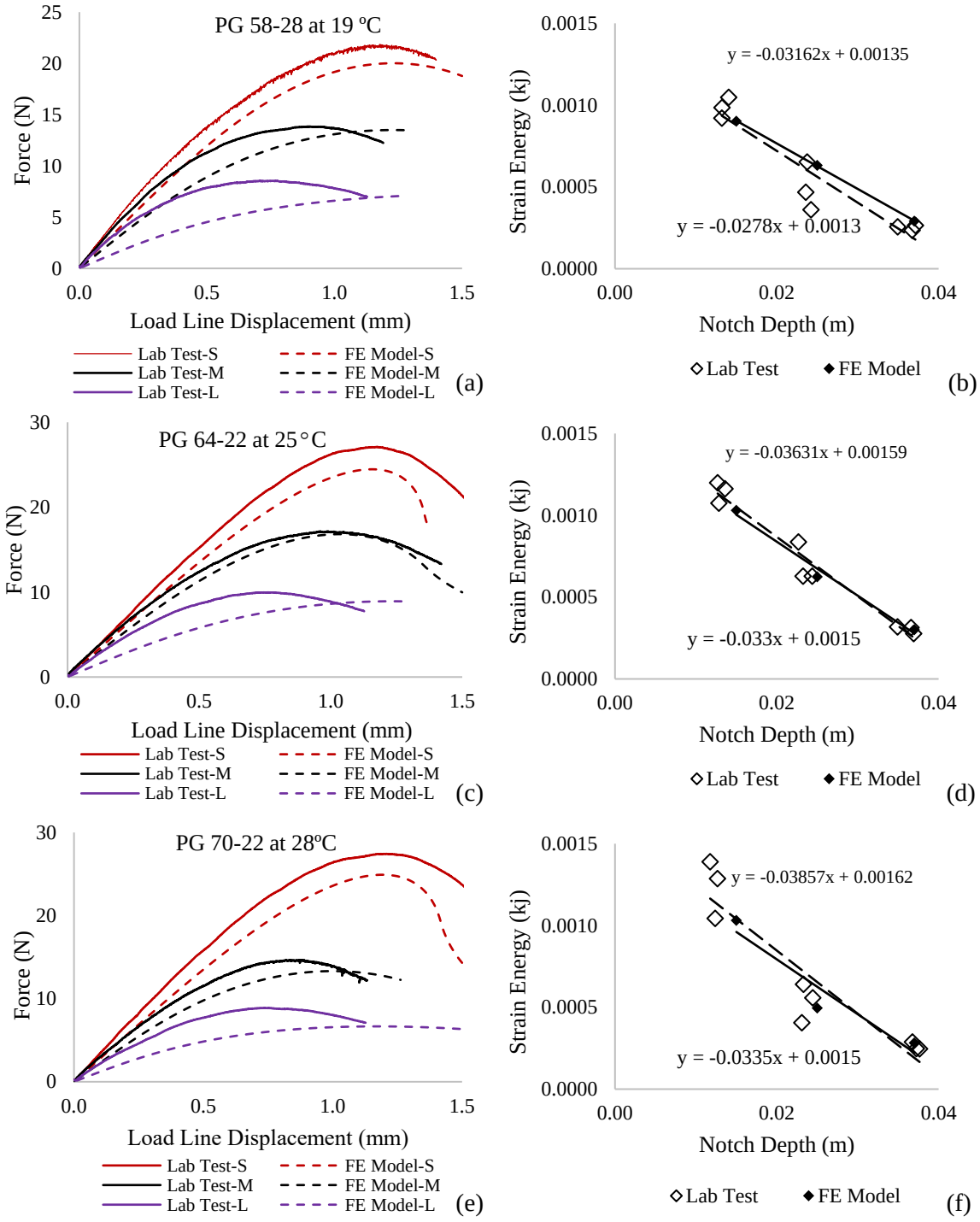

Figure 5-11 Computing critical strain energy release rate at intermediate temperature using the SCB model and comparison with laboratory test results: Force-Displacement plot for PG 58-28, PG 64-22 and PG 70-22 are shown in (a), (c) and (e) respectively; Change in strain energy with notch depth PG 58-28, PG 64-22 and PG 70-22 are shown in (b), (d) and (f) respectively.

Table 5-5 Comparison of critical strain energy release rate at intermediate temperature between laboratory test and finite element model.

Binder	Jc (kJ/m^2) Lab Test	Jc (kJ/m^2) Simulation	Simulated/ Lab Test	Average Ratio	Jc (kJ/m^2) Adjusted	Adjusted Simulated/ Lab Test
PG 58-28	0.55	0.49	0.89		0.54	0.989
PG 64-22	0.64	0.58	0.91	0.90	0.64	1.006
PG 70-22	0.65	0.59	0.91		0.65	1.005

5.6 Conclusion and Future Recommendations

In this study critical energy release rate (Jc) which can be determined by ASTM D 8044 test is calculated by utilizing a finite element model of SCB specimen incorporating the CZM model to simulate the fracture. The CZM properties are determined in the laboratory by a DCB test. The following conclusions can be drawn for the study:

- This study affirms that failure criteria in the SCB test at intermediate temperature can be modeled using the CZM model. The finite element model can successfully predict the critical fracture energy release rate (Jc) utilizing the cohesive properties measure in the DCB test.
- The purpose of the study is not to replace the SCB test but to establish that the fracture of the mix in SCB is dependent on binder properties if the gradation remains the same.

Although it may be premature to make definite conclusions from the limited test and simulation results presented in this study, the results shown in this paper demonstrate that the CZM model has the potential to simulate intermediate temperature cracking in the SCB test. Fracture behavior of asphalt mix in SCB can be characterized by connecting the cohesive properties of FAM by theoretically sound DCB test.

CHAPTER 6

SUSTAINABLE LIGNIN TO ENHANCE ASPHALT BINDER OXIDATIVE AGING PROPERTIES AND MIX PROPERTIES[†]

6.1 Introduction

Asphalt is one of the most widely used types of pavement, with 94% of roads in the United States paved with asphalt. In the world, over 86 million tons of asphalt binder per year are combined with gravel or sand to pave roads. It generates lower traffic noise, is lower cost, and is easier to repair when damaged than concrete. However, it is sourced from crude oil. Using non-renewable, limited resources to produce asphalt binder requires energy and generates greenhouse gases [6.1]. Also, advances in crude oil refining have decreased the amount of asphalt available for use in asphalt binders, increasing cost [6.2]. For these reasons, finding renewable, sustainable materials to replace asphalt binder has become a priority. However, trading performance for sustainability in paving our roads is unacceptable, as is worsening performance over time. Thus, it is essential to examine rheological properties and the oxidation/hardening aging behaviors of asphalt binders with alternative replacements.

[†] This chapter or portions thereof has been published previously in the Journal of Cleaner Production under the under the title as it is in chapter title. Volume 217 (2019), DOI: 10.1016/j.jclepro.2019.01.238. The current version has been formatted for this dissertation.

Lignin is the second most abundant biomass (plant) material available on our planet. Lignocellulosic biomass can be farm waste [6.3]. More attention is being given to using lignin, particularly when separated from waste agricultural products. For example, Mabrouk et al (2018) have performed an economic analysis of converting lignin from olive tree pruning to products [6.4]. Rice/paddy straw was used as a raw material in a direct process of simultaneous clean separation of small-sized nano-silica and lignin. Kauldhar and Yadav (2018) have used rice/paddy straw to produce small-sized nano-silica and lignin [6.5]. Since lignin-containing plants take in CO_2 when they grow, they reduce the amount of CO_2 in the atmosphere. If lignin separated from biomass is put into roads, it would sequester the carbon contained in the lignin. Using lignin in asphalt binder would also reduce the CO_2 generated when a petroleum-based binder is transported to paving sites, since local and sustainable lignin from biomass may be able to replace this fossil fuel derivative.

Lignin has gained a considerable amount of attention as a modifier for asphalt because of its potential to enhance the rheological properties of the binder. Lignin typically comes from pulp and paper mills that remove it from softwood to purify the cellulose they make into paper products. This Kraft lignin byproduct has been applied in asphalt binders, starting in 1979, but most of the studies have not been conducted until recently [6.6]. The role of lignin has been investigated as an antioxidant to resist aging, as well as a partial asphalt binder replacement. The rejuvenating effect of tall oil, which contains significant amounts of lignin, was also investigated by several researchers [6.7, 6.8]. It is worth mentioning that tall oil is obtained from Kraft liquor which is a byproduct of the paper manufacturing process. Tall oil was found to have potential in softening

reclaimed asphalt pavement (RAP) binder and could successfully restore the mechanical properties of RAP binder to some extent [6.7]. Improvement in mixture fatigue life was also observed in RAP mixes when tall oil was used as an additive [6.8]. Improvement of high-temperature properties of binder modified with lignin has been reported by several researchers, but binder modification compromised low and intermediate temperature properties [6.9-6.11]. At low lignin concentrations, binders showed limited improvement in aging resistance, and higher concentrations affected binders adversely [6.12]. However, an opposite conclusion was drawn in the study conducted by Hobson et. al (2017) where the action of lignin as an antioxidant was not supported and even the extracted binder was found to be slightly more oxidized [6.13]. Some researchers have used lignin in the Hot Mix Asphalt (HMA) as a partial replacement of the binder up to 25%, but neither the effect of the lignin in the binder nor mechanical properties were examined [6.13-6.14]. In one of the few studies performed with non-Kraft lignin, Sundstrom et al. (1983) reported that ductility decreased with increasing steam-exploded from aspen lignin content of asphalt binder [6.15]. In the most recently published article, Batista et al. (2018) found that Kraft lignin increased the Brookfield viscosity of binders mainly at 135 °C [6.16]. Lignin when added in asphalt binders gave a lower carbonyl index and thus a higher weathering aging resistance compared with a conventional binder and a content of 4 wt.% of lignin has increased thermal stability of binder after the Rolling Thin Film Oven procedure (RTFO) [6.16].

The contradictory findings may be due to different preparations and sources of the lignin used. The method of lignin de-polymerization and formation has been studied using density functional theory, which suggests that the H-bonding and π–π interactions

between the lignin monomers position the β carbon and oxygen atom to favor the formation of the β–O–4 linkage [6.17]. The prevalence of the linkage in separated lignins may affect the results when lignin is added to the asphalt. The findings point to a need to investigate the rheological properties and mix properties of different lignin-modified binders before their use in field application.

A particular lignin's physical and chemical behavior will be different depending on the original source and extraction method used [6.18]. Lignin in untreated biomass is a very high molecular weight polymer generally comprised of three possible monomers: paracoumaryl alcohol, coniferyl alcohol, and sinapyl alcohol; these are incorporated into lignin in the form of phenylpropanoids: p-hydroxyphenyl (H), guaiacyl (G), and syringyl (S), respectively. Lignins from different plant materials have differing proportions of the phenylpropanoids. For example, softwood lignin is almost exclusively guaiacyl, while grass-type plants have a mixture of all three. Softwood is generally used in the pulp and paper industry, so the lignin extracted from black liquor will be predominantly guaiacyl. As rice is a grass-type plant its lignin contains a mix of all three types.

Since wood has many uses, particularly in construction, using it to obtain lignin may not be an environmentally-conscious choice. Using wastes from food production to obtain lignin would prevent the landfilling of these wastes [6.19, 6.20]. Rice hulls, which are already transported to processing centers, are not as valuable as animal feed because of their high content of inorganic molecules (ash). Rice hulls have what is essentially silica "armor" on their exterior, so they are not useful as either animal feed, or even as compost materials [6.21]. Obtaining lignin from biomass in an environmentally-friendly way has been a continuing challenge to the pulp and paper industry. The widely-used

Kraft process requires caustics and sulfide, while other processes require other sulfur-containing chemicals, acids, or high pressure.

An exciting alternative type of lignin separation uses deep eutectic solvents (DESs). A eutectic system is a homogeneous mix of two solid-phase chemicals that forms a joint super-lattice at a particular molar ratio, called the eutectic composition. This super-lattice then melts at the eutectic temperature that is lower than the melting points of the individual components. DESs are formed by hydrogen bonding of the two components. The term "deep" is used because the melting point curve has a particularly deep crevice at the eutectic point. DES have low volatility and are non-flammable, non-toxic, biocompatible, and biodegradable [6.22]. They are easily synthesized from obtainable materials at high purities [6.23]. Also, DESs typically do not inactivate enzymes, making them valuable in biomass conversion [6.24]. They are not sensitive to water content, making their use more feasible with undried rice hulls [6.22]. Drying costs can be a substantial portion of pretreatment costs for biomass separation [6.25].

This work investigates the incorporation of three kinds of lignin from biomass into asphalt binder to determine its effect on the binder's properties. Lignin precipitated from black liquor ("B"), Kraft lignin that was commercially available ("C"), and lignin that was produced from rice hulls using DESs in the laboratory ("L") was added into asphalt binder. Extensive rheological testing of these binders was performed to reveal the enhancements possible with lignin addition. Asphalt mix prepared with a binder having lignin was tested for rutting, cracking, and moisture-induced damage susceptibility.

6.2 Materials and Methods

6.2.1 Materials

Rice hulls for “L” lignin were harvested in Louisiana and obtained from Falcon Rice Mill (Crowley, LA, USA). Formic acid was purchased from DudaDiesel (Decatur, AL). Choline Chloride (98%) and sulfuric acid (95-98%) were purchased from Sigma-Aldrich (St, Louis, MO). The commercial Kraft lignin (CAS 8068-05-01) was purchased from BOC Sciences (Shirley, NY, USA) and is referred to in this work as “C” lignin. “B” lignin was derived from black liquor from softwood Kraft processing, kindly supplied by Graphic Packaging International Inc (Monroe, LA). The three types of lignin used in this study are showing in Figure 6-1. The lignin is in powdered form and passing through #100 sieve, which means lignin particle size is below 0.15 mm. Asphalt binder used for this study was collected from Amethyst Construction, a local asphalt mixing plant in Ruston, LA. The original supplier of the binder was Ergon Asphalt and Emulsion, Inc, Vicksburg, MS. The binder is sold as PG 67-22. High-temperature grading of the binder was determined in the laboratory to be PG 68.

‘B’ Lignin ‘C’ Lignin ‘L’ Lignin

Figure 6-1 Physical appearance of the three types of lignin used in this study. Those are in powdered form and passed #100 sieve.

6.2.2 Experimental Plan

The base binder was modified with three types of lignin. Both “B” (from black liquor) and “C” were added to the base binder at 2%, 4%, and 6% while “L” lignin (extracted from rice hulls by the deep eutectic solvent) was added at 6% by weight of the binder. This study was conducted to investigate the binder properties as well as the behavior of the mix after lignin modification. Neat and modified binders were subjected to short-term and long-term laboratory aging before testing for rheological properties. High-temperature performance grading was performed on unaged and short-term aged binders. Percent recovery and non-recoverable creep compliance were determined by multiple stress creep recovery tests on short-term aged binders. Strain tolerance of the long-term aged binder was tested by strain sweep. Aging index was calculated for the unaged, short-term aged, and long-term aged binder based on rheological properties. The above-mentioned tests were performed in a Dynamic Shear Rheometer (DSR). Change in chemical composition because of modification was investigated by utilizing a Fourier Transform Infra-Red (FTIR) Spectroscopy.

Based on the rheological properties of modified binders, an optimum amount of suitable lignin was selected, and lignin modified Hot Mix Asphalt (HMA) was prepared. In this study, 6% of “B” lignin was chosen for mix preparation. A laboratory-developed mix design was used to make the control and lignin modified mix. An Asphalt Pavement Analyzer (APA) was utilized to determine the rutting resistance of the mixes. The cracking potential of the mix was investigated by Semi-Circular Bend (SCB) test. Figure 6-2 is the detailed experimental plan accomplished for this study.

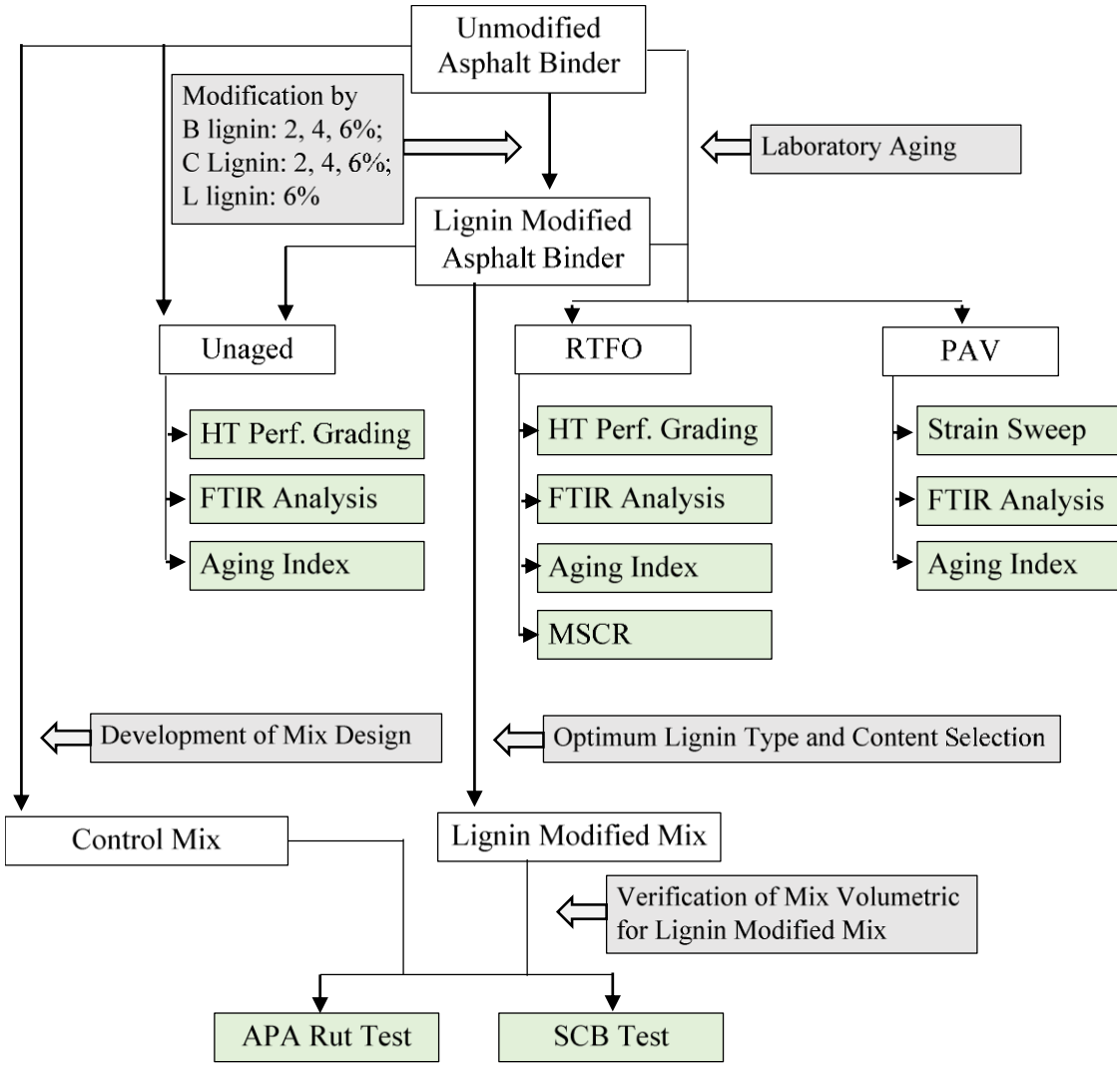

Figure 6-2 Experimental plan of the study.

6.2.3 Procedure for Obtaining "L" Lignin from Rice Hulls

The rice hulls were dried for 24 h at 105 ˚C and milled to a specific size (mesh 14-28, 1.168-0.589 mm in diameter) before DES pretreatment. The pretreatments were carried out using a biomass concentration of 10 wt% (3 g of dry biomass and 30 g of Formic Acid:Choline Chloride) in a flask that was immersed in an oil bath with magnetic stirring. The pretreatment of biomass with DES was conducted at 155 ˚C for 2 h. The

flask was connected to a condenser to precipitate the slightly volatile DES, to keep the solvent volume constant. After removal from the oil bath, vacuum filtering with a coarse nylon net filter separated solid biomass residue from DES. The solid biomass was then rinsed with ethanol and separated using the same coarse nylon filter. Following this, DI water was added to the filtrate to precipitate lignin. After precipitation, vacuum filtering with a nylon filter was used to separate the lignin. Additional DI water was used to wash the lignin to increase purity.

6.2.4 Procedure for Obtaining "B" Lignin from Black Liquor

The precipitation of lignin fraction through acidification of the black liquor was performed. After heating the black liquor to 60 ˚C, a 6 wt% sulfuric acid solution was added to precipitate the lignin. The precipitated lignin was collected after decantation and washing with additional DI water to remove any water-soluble impurity.

6.2.5 Fourier Transform Infrared-Attenuated Total Reflectance (FTIR-ATR) Spectroscopy

A Nicolet IR 100 FTIR (Thermo Scientific, Waltham, MA, USA) with a Diamond crystal using 24 scans per sample was used from 400 to 4000 cm^{-1}. FTIR analysis was performed on both fresh and aged samples, as well as on all different types of lignin, PG-67, and lignin incorporated in PG-67. Binder was heated in an 8 oz tin can on a hot plate at 100 ˚C for 20 minutes. When it was liquid enough, it was stirred by a spatula and a small drop (5 mm diameter) was poured on a silicone mold. At the time of testing the solid binder, the drop was placed on top of the diamond crystal using forceps for FTIR spectroscopy. For pure lignin, powdered samples were used.

6.2.6 Aging Procedure

Short-term aging of the neat and lignin modified binder was simulated in the laboratory using a Rolling Thin-Film Oven (RTFO) per AASHTO T 240. RTFO residue was then subjected to accelerated oxidative aging using pressurized air at elevated temperature in a pressurized aging vessel (PAV) according to AASHTO R 28.

6.2.7 Modification of Binder with Lignin

For this study, PG 67-22 binder was used as a base binder and three types of lignin were used as modifiers. The binder was heated at 180 °C in a forced draft oven until it became sufficiently liquid. Then a mechanical mixing blade was inserted into the asphalt and rotational speed was adjusted to make a vortex in the asphalt. The predetermined amount of lignin powder (passing #200 sieve) was then poured slowly into the vortex of the asphalt to promote rapid dispersion without agglomeration. The container was placed into a heating mantel where the temperature was precisely controlled at 180 °C. Mechanical mixing was continued for five minutes. A high shear mixer with a square hole high shear screen was then introduced into the binder. For the first 30 minutes, the rotational speed was set at 4000 rpm and for the next 30 minutes, it was set at 8000 rpm. Volumetric expansion was observed at the beginning of the mixing stage just after the addition of lignin. After 1 hour of blending at 180 °C, the lignin seemed to be well mixed with the asphalt.

6.2.8 Rheological Property Testing

High-temperature performance grading of the unaged and RTFO aged binder was performed according to AASHTO T 315. A 25 mm parallel plate and a 1 mm gap were

chosen for the test geometry. The test was performed at a 10 rad/sec angular frequency and a 12% strain where the temperature was varied from 64 to 82 °C at 6 °C intervals.

Aging Index (AI) of unaged, RTFO aged and PAV aged binder was determined using an 8 mm plate and a 1 mm gap. Angular frequency and the applied strain were the same as those for the high-temperature performance grading test. G*/sinδ parameters were recorded at 64 and 76 °C.

Percent recovery and non-recoverable creep compliance of asphalt binder were determined using a Multiple Stress Creep Recovery (MSCR) test on RTFO aged binder following the AASHTO TP 70 standard test method. The MSCR test was performed at 64 and 76 °C using a 25 mm plate and a 1 mm gap. The sample was tested in creep at 0.1 kPa and 3.2 kPa stress levels followed by recovery at each stress level. Creep portion of the test lasted for 1 second followed by a 9-second recovery.

Strain sweeps were performed on PAV aged binder at 64 and 76 °C. Initial and final targeted strains were 1% and 200%, respectively. Complex modulus (|G*|) and shear stress were recorded at each applied strain level. The geometry used for this test was an 8 mm plate with a 1 mm gap.

6.2.9 Mix Design

Asphalt mix used for this study was designed for a ½ inch wearing course subjected to level 2 traffic. It was designed according to AASHTO R 35 “Standard Practice for Superpave Volumetric Design for Asphalt Mixture." Crushed granite and manufactured sand were used as the aggregate conforming to the gradation requirement of table 502-4 of the Louisiana Standard Specifications for Roads and Bridges (2006). The nominal maximum size of the aggregate was ½ inch. Optimum asphalt content was

determined as 4.6%, according to the table 502-5 of section 502 of the standard specification. The mix was produced at 163°C and aged at 150°C for 2 hours in a forced draft oven for volumetric calculations. Lignin modified mix was prepared with binder modified with 6% lignin without altering the aggregate gradation, design asphalt content, and mixing temperature. Volumetric parameters for control and lignin modified mixes are tabulated in table 6-1.

Table 6-1 Mix parameters for control and lignin modified mix.

Mix Parameters	Control Binder	Lignin Modified Binder	Specified Limit
Asphalt Content, %	4.60	4.60	
Absorbed Asphalt, %	0.59	0.51	
Effective Asphalt, %	4.04	4.12	
Specific Gravity of Binder	1.020	1.034	
Maximum Specific Gravity	3.436	3.435	
Bulk Specific Gravity	2.336	2.326	
Air Void at 100 Gyration, %	4.14	4.46	2.5 - 4.5
Void in Mineral Aggregate (VMA), %	13.4	13.7	13 (min)
Void Filled with Asphalt (VFA), %	69.1	67.5	78 (max)
Resistance to Moisture Induced Damage	0.86	0.80	0.80 (min)

Some parameters in the lignin modified binder and mix are significantly different compared to the control mix. The specific gravity of the modified binder was found to be 1.034, but the specific gravity of the control binder was 1.020. Because of the higher specific gravity of lignin (1.342), more asphalt binder (in terms of volume) is replaced when the replacement is calculated by weight. Therefore, the VFA value of the lignin modified mix is lower than the control mix. Other than that, all other mix parameters are within the specified range according to the standard specifications. This is an indication of an acceptable mix design with a lignin modified binder.

6.2.10 Mix Property Testing

Rut resistance testing was performed on laboratory compacted specimens using an Asphalt Pavement Analyzer (APA). Control and lignin-modified mixes were targeted to compact at a 7% air void, which was attained at 35 gyrations. A certain amount of mix was taken for compaction so that after 35 gyrations the height of the compacted specimen became 75 mm. The testing temperature was fixed at 64 °C. Rut depth was measured manually after 8000 cycle wheel-passes.

The resistance to moisture-induced damage test was performed according to AASHTO T283. The indirect tensile strength ratio (TSR) of the moisture-conditioned samples and the dry samples must be a minimum of 0.80.

The semicircular bend test (SCB) test was performed according to AASHTO TP 124. A 50 mm thick semicircular disk was obtained from a 150 mm diameter gyratory compacted sample with a 7% air void. A 15 mm deep and 1.5 mm wide notch parallel to the loading axis was cut in the middle of the flat side of the SCB specimen. A load was applied along the vertical radius of the specimen at 50 mm/min rate and at 25 °C and the vertical displacement was measured during the entire duration of the test.

6.3 Results and Discussion

6.3.1 High-Temperature Grading

High-temperature continuous grading of unaged and aged binder was performed for both neat and modified binders and are plotted in Figure 6-3(A), 6-3(B), and 6-3(C). With increases in the percentage of lignin, the high-temperature grade increases irrespective of the type of lignin added. When the same amount of lignin is added, type "C" lignin is responsible for the greatest increase in stiffness, and type "L" is responsible

for the least increase. Figure 6-3(D) is the plot of the high-temperature performance grades of lignin-modified binders. If unaged and RTFO aged binders satisfy the minimum stiffness criteria at a slightly different temperature, the lower temperature is considered the high-temperature performance grade. Modification of lignin significantly improved the high-temperature grade of the binder from 68.5 °C to at least 74.5 °C or in some cases up to 82 °C. Modified binders thus have more stability at high temperatures and are likely to be more resistant to permanent deformation or rutting.

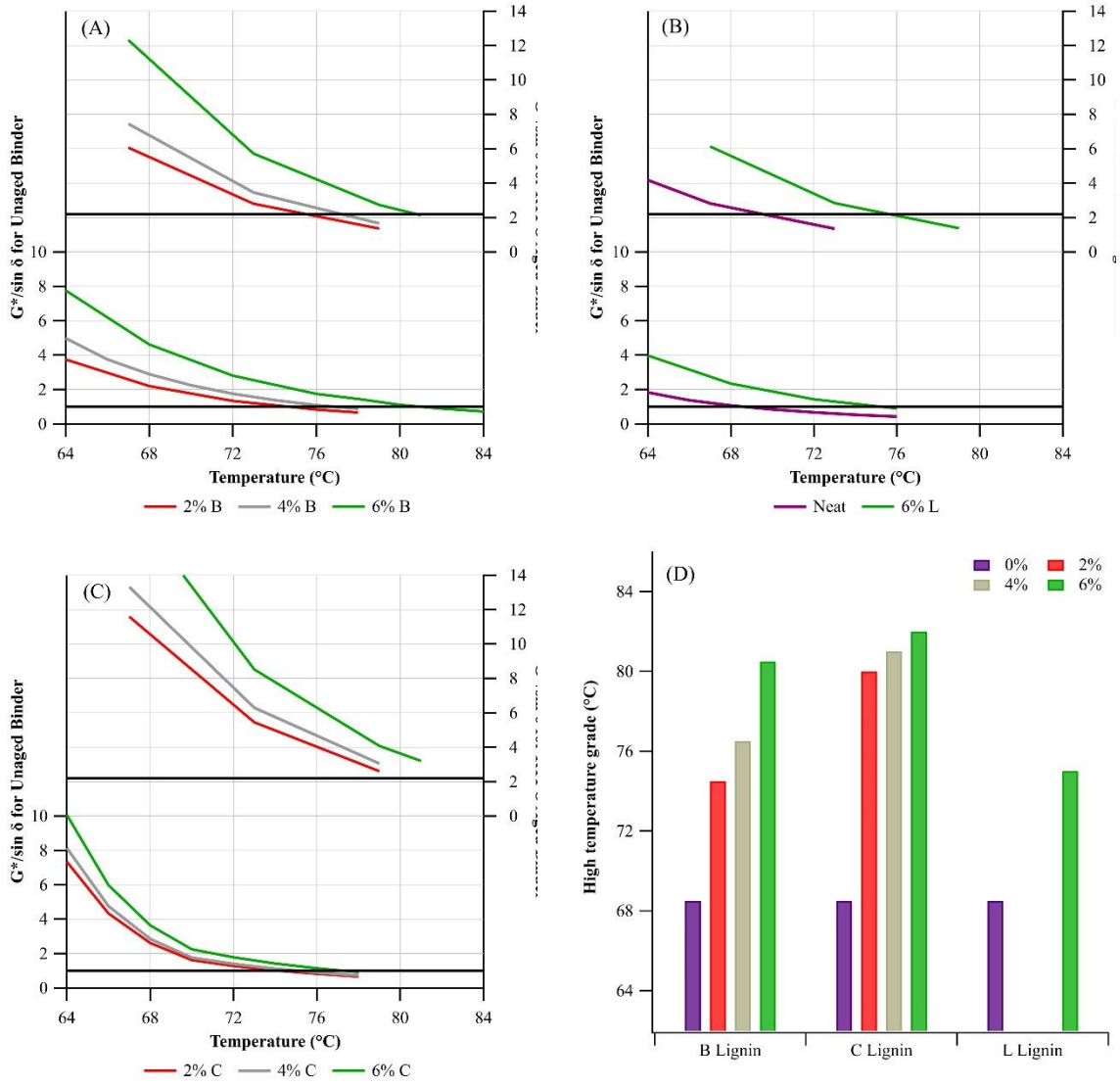

Figure 6-3 High-temperature performance grading of the neat and modified binder (a) High-temperature grading for binder modified with "B" lignin, (b) High-temperature grading for binder modified with "L" lignin, (c) High-temperature grading for binder modified witt "C" lignin, and (d) High temperature grade of lignin modified binder.

6.3.2 Grading According to Vehicular Loading Condition and MSCR Test Results

Performance grading of asphalt according to vehicular loading condition was performed per AASHTO MP 19. Asphalt binder is classified into four categories: Standard grade (S), High grade (H), Very high grade (V), and Extremely high grade (E)

based on the non-recoverable creep compliance (J_{nr}) value. The original binder was graded as "S" at 64 °C as it has a J_{nr} value of less than 4.0 kPa^{-1} when tested under 3.2 kPa stress level. At this temperature, all the modified binders have a J_{nr} value below that of the control binder (Figure 6-4(A)). At 76 °C, the binder modified with 6% 'C' lignin is classified as 'H' which is a real improvement. 6% of 'B' lignin and any percent of 'C' lignin could maintain the 'S' grade of the binder at a new high-temperature grade. This is an indication of the effectiveness of lignin as a binder modifier to improve the binder grade. But, 'L' lignin even at 6% could not satisfy the MSCR criteria (Figure 6-4(C)). Thus, compared to unmodified binder, the lignin modified binders (at certain percentage) were less likely to accumulate the permanent denting that eventually causes pavement damage.

In the MSCR test, responses of the binders were observed at 0.1 kPa and 3.2 kPa stress levels. $J_{nr\text{-}diff}$ is a parameter that expresses the percent difference in the J_{nr} value calculated at these stress levels. Figure 6-4(B) and 6-4(D) show the $J_{nr\text{-}diff}$ of all the binders at 64 °C and 76 °C, respectively. The maximum $J_{nr\text{-}diff}$ is observed at 16%, which is below 75%, the maximum allowable value allowed by the specification.

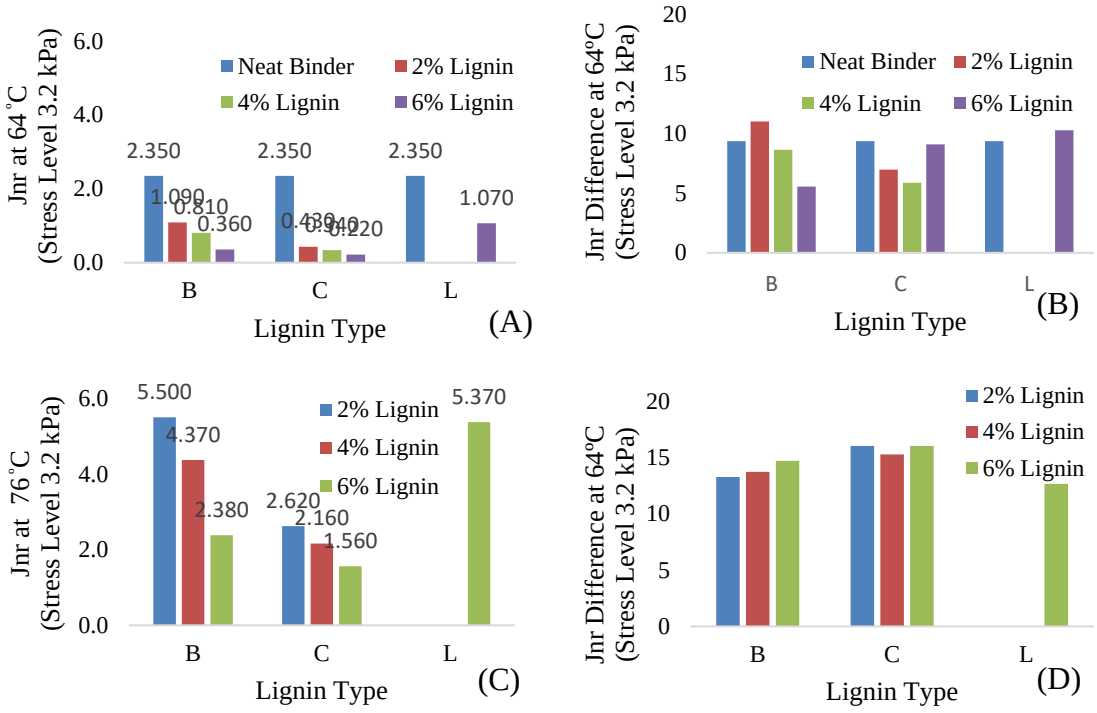

Figure 6-4 Non-recoverable creep compliance results from MSCR test (a) Jnr at 64 °C Stress level 3.2 KPa, (b) Jnr difference at 64 °C, (c) Jnr at 76 °C Stress Level 3.2 KPa, and (d) Jnr Difference at 76 °C.

Modification of binders with elastomeric polymers inhibit the binder from accumulating permanent deformation because of delayed elasticity [6.26]. The MSCR test also measures the recoverable portion of the strain in terms of percent recovery. Table 6-2 shows the percent recovery of all the binders at 64 and 76 °C under 0.1kPa and 3.2 kPa stress level. Unmodified binder did not have any recoverable portion of the strain at 64 °C, while modified binders exhibited up to 26% and 21% recovery at the 0.1 kPa and 3.2 kPa stress level, respectively. Binder modified with type "C" lignin possesses the highest percent recovery while type "L" possesses the least. Increases in added lignin increased the percent recovery of the binder. At 76 °C and 3.2 kPa stress level, not a single sample exhibits any recovery, while at 0.1 kPa stress level a maximum 8% recovery was found for binder modified with 6% "C" lignin.

Table 6-2 Percent recovery of the binder from the MSCR test.

Binder Type	64°C		76°C	
	0.1 kPa	3.2 kPa	0.1 kPa	3.2 kPa
Neat Binder	0.25	0	0	0
2% "B" Lignin	7.59	0.64	0.00	0
4% "B" Lignin	10.78	3.57	0.11	0
6% "B" Lignin	18.15	12.46	3.59	0
2% "C" Lignin	18.50	12.13	4.49	0
4% "C" Lignin	19.20	15.08	5.17	0
6% "C" Lignin	26.05	21.14	8.26	0
6% "L" Lignin	8.01	0.78	0	0

6.3.3 Analysis of Strain Sweep Test Data

Strain sweep test data was utilized to evaluate strain tolerance by the drop in complex modulus from its initial value, expressed as a percentage of initial complex modulus. A lower drop in complex modulus means higher strain tolerance before failure [6.27]. From the stress-strain plot of the binder at 64 °C (Figure 6-5(A)), peak shear stress was seen to occur above 51% for all samples. The initial and final values for strain were therefore chosen to be 1% and 51% stain. Figure 6-5(B) shows the complex modulus results with applied strain at 64 °C. Figure 6-5(C) is the plot of the percent drop in complex modulus of neat (PG 67) and modified binders at 64 °C. Increasing the lignin percentage in the binder caused a higher drop in modulus for “B” and “C” lignin. Lignin, “C” made the binder the least strain tolerant. Except for the binder modified with “C” lignin, all other binders modified with "B" and "L" lignin showed a modulus drop less than that of the unmodified PG 67 binder, indicating effective binder modification. "B" and "L" lignin binders, unlike the Kraft lignin “C”, thus would be able to endure a higher strain without failing, allowing a greater load on roads.

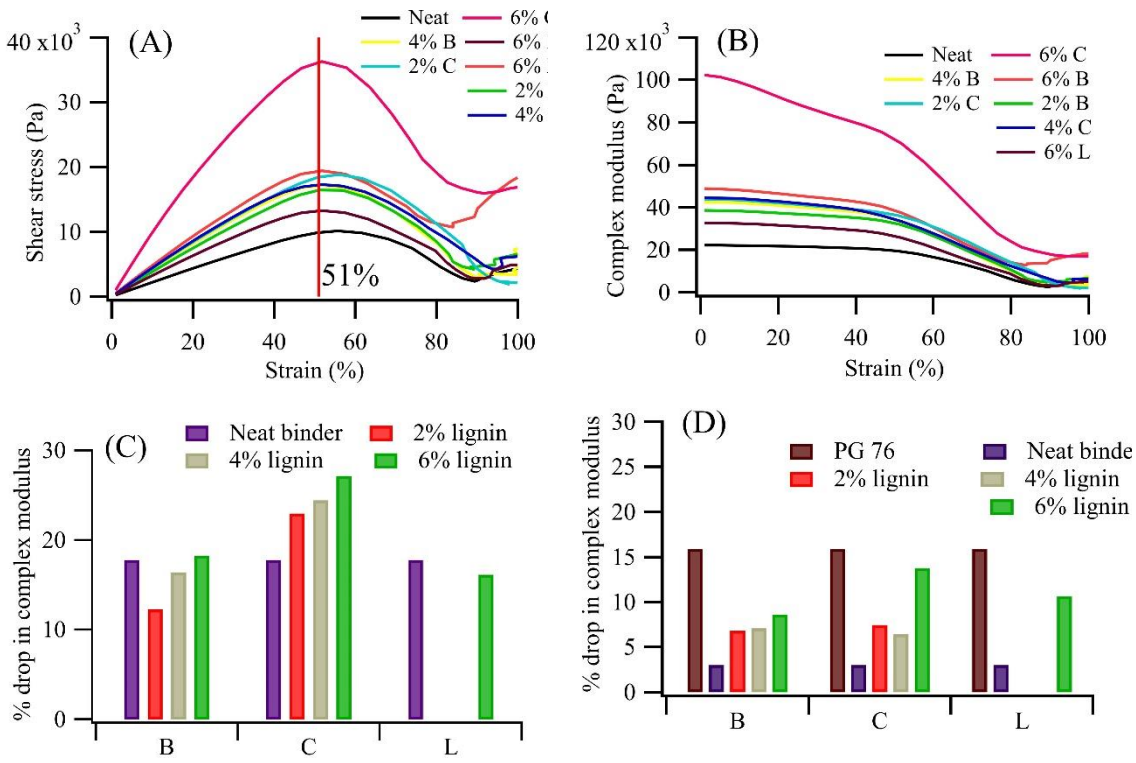

Figure 6-5 Strain sweep test results (a) Sheer stress (Pa) at 64 °C, (b) Complex modulus (Pa) at 64 °C, (c) % drop in complex modulus at 64 °C, and (d) % drop in complex modulus at 76 °C.

Figure 6-5(D) shows a similar trend in modulus drop at 76 °C, which is lower than the drop at 64 °C because at higher temperatures binders become more strain tolerant. All the lignin-modified binders had higher modulus drops compared to unmodified PG 67 binders, irrespective of modifier type or amount. As lignin modified binders possess a high-temperature grade of 76, it is not appropriate to compare the strain tolerance of those modified binders with a PG 67 binder. Figure 6-5(D) shows that all the lignin modified binders have lower modulus drop in comparison to the PG 76 binder. So, in terms of strain tolerance result, lignin modified binders perform even better than the PG 76 binder which is a polymer modified binder.

6.3.4 Improvement in Aging Index

Aging of asphalt binder is simulated with both short term and long-term conditioning, as described in section *6.3.6*. Increased stiffness indicates more aging. Aging index (AI) of a binder is defined as the ratio of stiffness ($G^*/\sin\delta$) of aged to unaged binder. A binder with an AI greater than 1.0 indicates that it is already aged. Stiffness and AI of binder modified with “B” lignin are plotted in Figure 6(A-C) for both RTFO and PAV aged binders. RTFO aged binders have slightly higher AI than that of an unmodified binder for any amount of added lignin. When 2% "B" lignin is added, the AI after long term aging becomes higher than the unmodified binder, but with increasing lignin percentage the AI decreases. When a binder is modified with “B” lignin, the stiffness of the unaged binder increases with an increased amount of added lignin (Figure 6(A)). When 6% "B" lignin is in the binder, the AI after long term aging at both temperatures is lower than the unmodified binder’s AI, indicating an improvement in aging resistance.

“C” lignin-modified RTFO aged binder showed similar aging susceptibility to "B", but “C” lignin-modified PAV binder behaved completely differently (Figure 6-6(D-F)). Increasing lignin increased the AI of PAV aged binder. Binder modified with 2 and 4% lignin has lower AI compared to the unmodified binder but 6% lignin addition results in a much higher AI, which is not desirable. Unlike the “B” lignin-modified binder, the stiffness of “C” lignin-modified binder increased after PAV aging at 6% added lignin, which caused an increasing trend of AI for “C” lignin-modified binder (Figure 6-6(D)). This result confirms that only a lower amount of "C" lignin is desirable as a modifier.

Figure 6-6(G) shows the AI of binder modified with the maximum percentage (6%) of the three different types of lignin. “B” lignin shows a desirable lower AI compared to the other lignins, and a lower AI than that of the unmodified binder. The “L” lignin from rice husks gave a similar AI to the unmodified binder, showing satisfactory aging performance.

From Figure 6-6(C), 6-6(F), and 6-6(H) it can be observed that at 76 °C, irrespective of lignin type and amount, the trends of change in AI remain the same, showing almost the same AI values. The incident of aging occurs when the binders undergo the RTFO and PAV processes. The test itself is to identify the changes that the binder experiences during the aging process. So, the AI of the binder at different test temperatures should yield a similar result, which is supported by Figure 6-6(G) and 6-6(H).

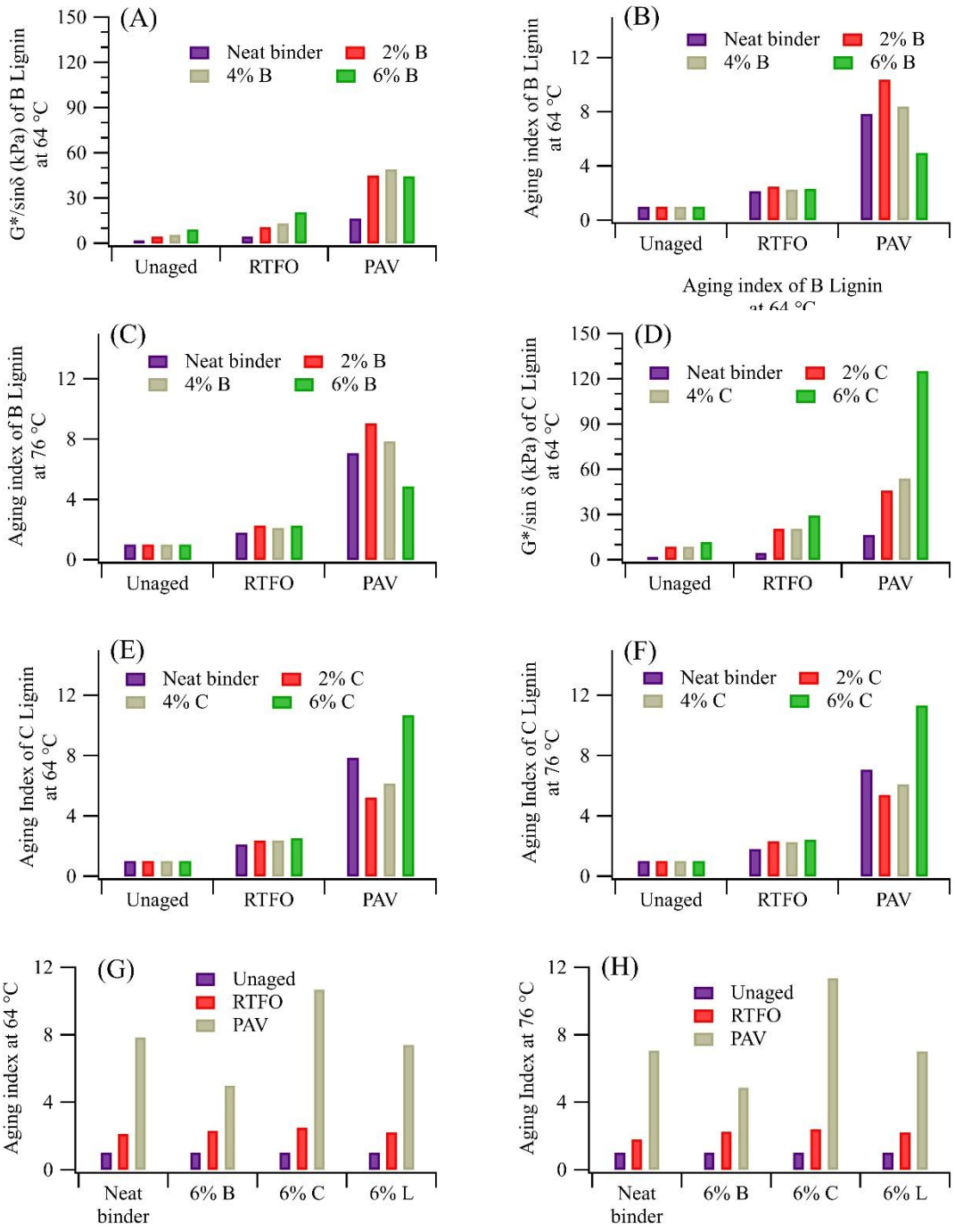

Figure 6-6 Aging Index data for neat and modified binders at different temperature (a) G*/ sinδ (kPa) of B Lignin at 64°C, (b) Aging index of B Lignin at 64°C, (c) Aging index of B Lignin at 76°C, (d) G*/sin δ (kPa) of C Lignin at 64°C, (e) Aging Index of C Lignin, (f) Aging Index of C Lignin at 76°C, (g) Aging index at 64°C, and (h) Aging Index at 76°C.

6.3.5 FTIR analysis of Aged and Unaged Samples of Lignin, Binder, and Binder with Lignin

Figure 6-7(A) shows the spectral differences between the three different types of lignin in the fingerprint region between 1800 and 800 cm^{-1} wavenumbers. All three lignin showed at 865 cm^{-1} vibrations associated with guaiacyl "G" lignin [6.28]. The lignin obtained from black liquor showed a more prominent guaiacyl methoxyl group peak at around 1260 cm^{-1} and a less intense C=O non-conjugated stretching vibration at 1703 cm^{-1} [6.29]. In the lignin obtained from black liquor, there is no vibration at 1154 cm^{-1}associated with C-O-C asymmetric stretching, found in Cellulose I and II [6.30]. The vibration at 1365 cm-1 related to C-H deformation from cellulose and hemicellulose is present in all three samples but less intense in “B” lignin (Boeriu et al., 2014) Thus, this precipitated "B" lignin may be somewhat purer than the commercial "C" lignin and the rice hull lignin "L." "B" lignin's purity may account for its slightly better performance in some binder properties.

Figure 6-7(B) shows the absorbance spectra of base binder partially replaced with varying percentage of “B” lignin from 2 to 6%. As the lignin concentration in the base binder increased, the intensity of the 1262 cm^{-1} absorption band and other lignin related peaks increased [6.29]. This shows that the binder was uniformly well-mixed. Similar findings were observed for base binder replaced with either “C” lignin or ‘L” lignin.

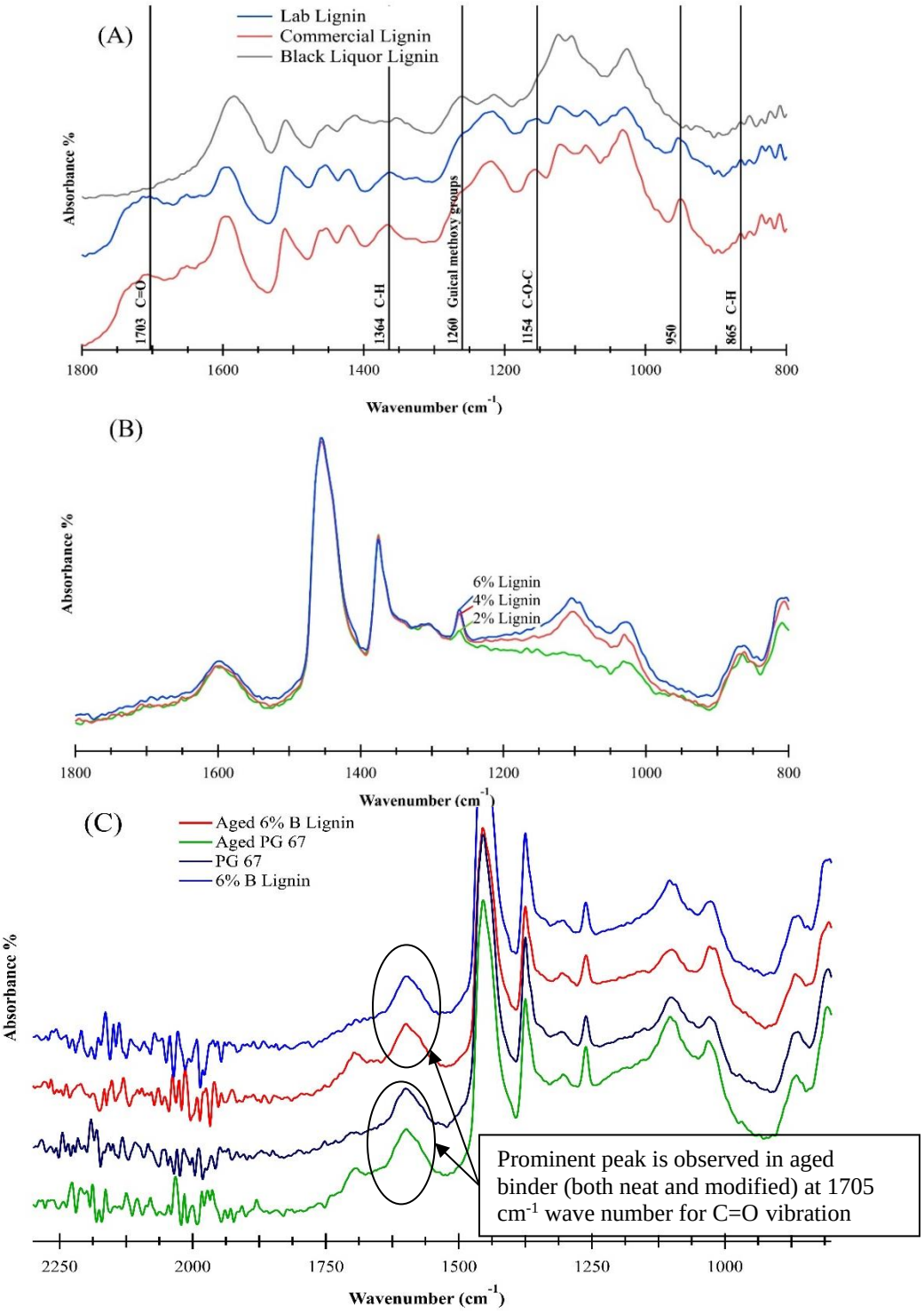

Figure 6-7 FTIR Spectra (a) FTIR Spectra of the three types of lignin in the biomass fingerprint region; (b) FTIR spectra of binder modified with varying percentage of "B" lignin; (c) FTIR spectra of unaged and aged neat and modified binder with 6% of "B" lignin.

The spectra of all the aged samples, regardless of whether they included lignin, showed an additional peak at the 1705 cm^{-1} vibration. This indicates that the vibration at the 1705 cm^{-1} absorption band comes from a base binder since the type of lignin had no effect. The 1705 cm^{-1} vibration is associated with carbonyl, C=O bonds [6.31, 6.32]. Also, in all samples that included PG-67 binder, with and without lignin, spectral differences were found in the 2000 cm^{-1} to 2200 cm^{-1} region. For the unaged samples, a vibration at 2000 cm^{-1} was more pronounced than that found for the aged samples. This phenomenon suggests that C=C=C allene bonds could be broken during aging, probably by being oxidized to become C=O bonds. At 2200 cm^{-1}, the vibration is again stronger for unaged compared to aged samples. It is thus likely that aging the binder breaks its C≡C alkyne bonds that vibrate at this wavenumber by oxidizing them to C=O Thus, oxidation is likely to be a prominent feature in aging of these binders.

6.3.6 Selection of Suitable Amount and Type of Lignin for Hot Mix Asphalt (HMA)

The objective of this study was to improve the binder properties by adding lignin as a modifier. Utilizing the highest amount of lignin possible was also an objective. Among the three types of lignin type, “C” improved the high-temperature grade and reduced the J_{nr} value most. However, "C" gave the least strain tolerance and highest AI, making it less desirable for use in asphalt binders. Type “L” gave the highest strain tolerance but did not improve the high-temperature grade as much as “B” or “C”. Producing sufficient amounts of "L" for mixing with aggregate to form asphalt pavement was a challenge that will be attempted in future studies. “B” lignin improved the high-temperature grade significantly and had a relatively high strain tolerance; most

importantly, it gave the lowest value for AI. For these reasons, we chose 6% of type “B” lignin to replace the control binder for mix preparation for further study. This mix includes both crushed granite and manufactured sand, similar to the asphalt used in pavement.

6.3.7 Improved Rut Resistance

Rut depths of 3 control mixes and 3 mixes prepared from lignin "B" modified binder are plotted in Figure 6-8. The pair of specimens plotted together are specimens that were tested in the same mold and under the same wheel of the tester. The pavement mix prepared with a lignin-modified binder exhibited 14% less rut depth than the control mix. The modified mix showed a lower standard deviation (0.23) than the control mix (0.66 mm), which is an indication of stability under wheel loading and consistency in compaction. Rut depth was measured at two points on each specimen. Considering these two values as different data points, a t-test was performed on the average rut depth of the specimens and a significant difference was found between the average rut depths of the control and modified mixes with a 95% level of significance having a p-value of 0.009 (< 0.05). Therefore, lignin modification of the binder can successfully improve the rutting resistance of the asphalt mix. As the addition of lignin increased the stiffness of the binder, lignin could have the potential to be used in Warm Mix Asphalt (WMA) production. The WMA process is more “green”, since it requires less energy consumption, reduces the release of volatile organic compounds, and generates less CO_2 than the Hot Mix Asphalt (HMA) process. Future work will investigate the effects of lignin binder on WMA properties.

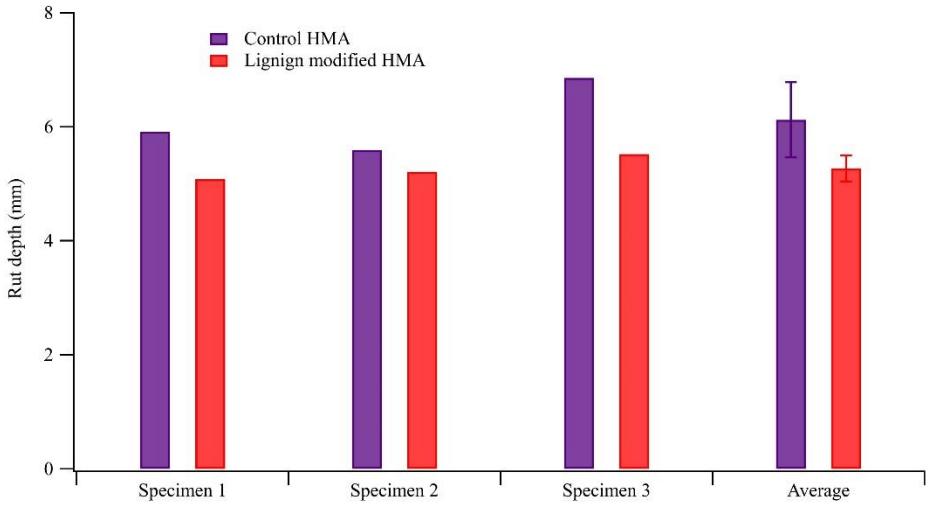

Figure 6-8 APA rut test result for control and lignin-modified mix.

6.3.8 Resistance to Moisture-Induced Damage Test

The control mix passed the resistance to moisture-induced damage test performed according to AASHTO T 283 with a Tensile Strength Ratio (TSR) value of 0.86. The loose mix was aged for 4 hours before compaction to test the mechanical property of the mix. Lignin-modified mix was produced without altering the gradation or asphalt content. The air void at design gyration was obtained as 4.46%, which is within the specified limit. The mix passed the moisture sensitivity test with a TSR value of 0.80. Although this value is lower than the control mix, it is within the specified limit set by the Superpave mix design.

6.3.9 Fracture Potential from SCB Test

Semi-circular bend (SCB) test results of control and 6% ‘B’ lignin modified binder after long-term aging is shown in figure 6-9. The area under the load-displacement curve is known as fracture energy and the fracture energy divided by the post-peak slope

is defined as flexibility index. Lignin-modified HMA can withstand a lower load that causes a 25% drop in fracture energy in the short-term aged mix. Fracture energy itself cannot independently determine the fracture potential of a mix. The fracture energy indicates the overall capacity of the asphalt mixture to resist fracture-related damage, but it should not be directly used in structural design and analysis of the pavement. Flexibility Index (FI) determined from the SCB test identifies brittle mixtures that are susceptible to premature cracking. An asphalt mixture can be ranked according to its FI. HMA with a lignin-modified binder showed higher FI, which indicates better cracking resistance than the control HMA at the intermediate temperature according to AASHTO TP 124 (Figure 6-9(B)). FI is proportional to fracture energy and inversely proportional to post-peak slope. The higher the value of post-peak slope, the lower the time it takes to propagate the crack. The same test is performed on long-term aged specimens. It is observed that the control mix loses 31% of its fracture energy due to long-term aging whereas, lignin modified binder loses 22%. That is an indication of the effectiveness of lignin as an antioxidant. The FI of lignin modified binder is still higher than the control mix after long-term aging.

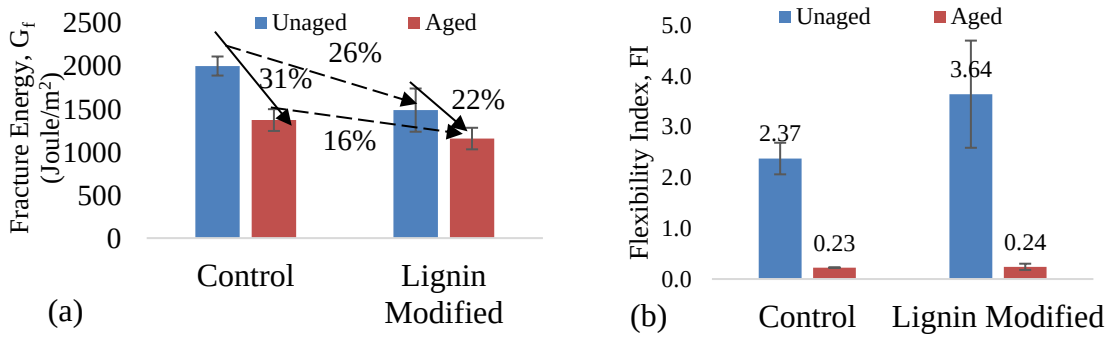

Figure 6-9 Semicircular bend (SCB) test results: (a) Fracture energy; (b) Flexibility index for unaged and long-term aged mixes.

6.4 Conclusions

- Commercially available Kraft lignin, lignin precipitated from black liquor in the laboratory, and lignin produced from agricultural waste rice hulls in the laboratory using a deep eutectic solvent partially replaced a standard asphalt binder (control).
- Lignin improved the high-temperature performance grade.
- Black liquor lignin and lignin produced from rice hulls improved the long-term aging index.
- Asphalt mix produced with 6% black liquor lignin modifying the binder met moisture-induced damage resistance specifications and improved rutting resistance.
- The 6% black liquor lignin binder mix gave lower fracture energy than the control mix, but it showed better cracking resistance and an improved flexibility index compared to the control.
- Replacing petroleum-based binders with up to 6% of lignin is likely to be feasible for asphalt pavements.
- Future work should be performed when more rice hull lignin is available to see the effect in binders of this waste residue on rutting and flexibility.

.

CHAPTER 7

QUANTIFICATION OF REDUCTION IN HYDRAULIC CONDUCTIVITY AND SKID RESISTANCE CAUSED BY FOG SEAL[†]

7.1 Introduction

A fog seal is a lightly sprayed application of diluted emulsion on an asphalt pavement surface that is usually aged and has become dry and brittle [7.1]. It is effective for maintaining pavements already in good condition. A fog seal is applied to the entire surface of the pavement and is usually used for pavements with no major structural deterioration. Relative low cost, effectiveness, and simplicity of application increased the popularity of this technique. Several studies report the possible functions of fog seal, including micro-crack sealing, filling of small voids, reduction of permeability, cessation of pitting and raveling, reduction of shrinkage tendencies, and lengthening the pavement surface life by slowing down the aging process of the binder [7.1-7.4]. However, fog seal does not correct severe distress such as rutting, aggregate loss, or major cracking [7.3]. While all agencies apply a fog seal to delay the deterioration of the pavement, most of

[†] This chapter or portions thereof has been published previously in the Transportation Research Record: Journal of the Transportation Research Board under the title "Quantification of Reduction in Hydraulic Conductivity and Skid Resistance Caused by Fog Seal in Low-Volume Roads." Volume 2657, Issue 1, (2017). DOI: 10.3141/2657-11. The current version has been formatted for this dissertation.

them reported that they also apply a fog seal for better appearance and aesthetic purpose [7.1].

Fog seal increases pavement life and postpones major rehabilitation. The life extension due to fog seal was reported 1 to 5 years by many agencies in SASHTO (Southeastern Association of State Highway and Transportation Officials) regions [7.1]. The effectiveness of the fog seal can be attributed to two different reasons. Firstly, a fog seal reduces the aging susceptibility due to binder oxidation; basically, this is achieved by reducing the stiffness of the existing binder. Another reason is that the fog seal reduces the permeability of the existing pavement. Less penetration of the water reduces the chance of moisture-induced damage. However, reported research efforts until now are not sufficient enough to decisively prove either of these concepts. Based on the rheological test on an extracted binder, Prapaitrakul et al. showed that the upper quarter inch of pavement was most likely affected by fog seal and there was no penetration of fog seal after that level [7.5]. Prapaitrakul et al. also used field core specimens for constant head permeability test and concluded that the fog seal treatments were usually effective, but not always [7.5]. Kim et al. reported a slight reduction of field permeability due to fog seal application based on the field evaluation of the three fog seal products on US-17 and US-27 [7.6]. Specific questions were raised on whether the increase of service life is due to the change of rheology or decrease in permeability. Very few studies were conducted to measure the effectiveness of the fog seal based on its capability to improve the permeability. To accurately quantify the field permeability using existing field permeameter on different pavement surfaces is a challenging task itself, let alone finding the improvement of permeability due to fog seal. Both lab and field data of permeability

are highly variable and the slight improvement of permeability made by fog seal may be lost inside the variance made by other parameters that control permeability, such as the interconnection of voids, voids arrangement, flow direction, etc.

It is therefore very important to test the same field core specimens before and after the fog seal application in the lab for permeability to properly understand the behavior of a fog seal. If measured correctly, the reduction of permeability may be a good parameter to measure the sealing potential of fog seal. Identifying fog seal effectiveness through permeability is critical to understand the fog seal working principle and to evaluate its performance.

Perhaps the most important trade-off that fog seal exhibits is the loss of friction of the surface. Qureshi et al. reported that fog seal without sanding on the OGFC surface reduces the friction by 2 to 24% based on the international friction index (IFI) parameter F60 [7.7]. An excessive amount of asphalt residue on the pavement would cause a slippery surface, which could lead to vehicle control difficulty, especially in wet weather [7.8]. Li et al. (2012) studied the effect of fog seal on the surface friction of two road sections of US-36 and US-231. The research shows that the average friction number fell from 61 and 58 to 28 and 23, respectively, after the application of the fog seal. The study also shows that it normally takes 18 months after fog seal application for the pavement to return to its original level of friction [7.9]. Another study made by the Florida Department of Transportation on US 17 and US 27 concluded that pavement friction drops immediately after fog seal application for all types of emulsion (Reclamite, E-Fog, and SealMaster AsPen AC) and is recovered between two weeks to three months [7.6].

Immediate loss of friction after application and friction recovery time varies by the product and application rate. Friction recovery time also depends on weathering and traffic. Over some time, the constant rubbing action between the tire and the aggregate surface allows the thin layer of fog seal on top of the aggregate surface to be worn out, which helps the surface to regain its micro-texture. But, for low volume roads, the rate of recovery of the friction may be very slow due to less rubbing action between fog sealed surface and tire. Very few studies addressed this particular issue of fog sealing on low volume roads. Therefore, considering a fog seal as a low-cost maintenance option for low volume roads, the friction characteristics of this surface after the treatment should be assessed thoroughly.

7.1.1 Objectives

The primary objectives of the study are 1) to quantify the sealing potential (if any) of fog seal by measuring the hydraulic conductivity of the field core specimens before and after the fog seal application, 2) to assess the effect of fog seal on surface friction characteristic over a prolonged period by evaluating international friction index parameter F60 as an indicator. To pursue these objectives, two asphalt emulsions, three application rates, and four different road surfaces were used.

7.2 Materials and Experimental Plan

In this study, four different roads in Caddo Parish, LA have been selected for the Fog seal application. All of these roads are low volume parish roads, having an Annual Average Daily Traffic (AADT) of less than 400. Before the application of a fog seal, the existing condition of the pavement surface was ascertained properly. Roads used in the

study had a dense HMA surface without any existing pretreatment (fog seal, chip seal, slurry seal, crack seal, etc.). The roads were structurally sound with minor hairline cracks. Rutting was very limited and completely absent in most cases. The road surfaces were free of other major distresses such as excessive raveling, alligator cracks, and potholes. The researchers were cautious about selecting the appropriate road surface to minimize the variable that could originate from the existing distress of pavement.

Two different types of emulsions, CSS-1H and E-fog (rejuvenating emulsion) were used in two lanes of each of those four roads. A 1300-foot section of the lanes was sprayed with fog seal. The 1300 feet sections were divided into three equal parts and three different application rates were used on each part. Typical application rates for a 50:50 diluted emulsion range from 0.03 to 0.22 gal/yd2, depending on the surface condition. Slightly higher application rates for CSS-1H emulsion were used because of the high dilution ratio. The application rate of CSS-1H emulsion was 0.2, 0.3, and 0.4 gal/yd2 at a dilution rate of 30:70 (Emulsion: Water). If these rates are converted to a typical 50:50 dilution ratio then they become 0.12, 0.18, and 0.24 gal/yd2, which is typical for the road surface used in the study. E-fog was sprayed at the rate of 0.1, 0.16, and 0.22 gal/yd2. This emulsion was diluted at the production plant. The residue content after the dilution of the emulsions was determined using ASTM D 6934, a high-temperature evaporative method for residue recovery. The residue content after dilution was 19.2% and 39.4% for CSS-1H and the rejuvenating emulsion, respectively. Table 7-1 shows the Summary of Materials and Experimental Plan.

The pavement surface was cleaned with a power broom. Before the fog seal application, the road surface was cleaned and completely dried. The minimum surface

(15°C) and air temperature (10°C) requirements have been met [7.8]. Figure 7-1 depicts the application of a fog seal.

Table 7-1 Summary of materials and experimental plan.

Road ID	Fog Seal Emulsions	Fog Application Rate (gal/yd^2)	Hydraulic Conductivity Reading on Field core Specimens		Short Term Friction Reading at 1 day, 7 Day, 1 month and 3 months after Fog Seal	
			Before Fog Sealing (Number of Specimens)	After Fog Sealing (Number of Specimens)	British Pendulum Tester (Number of Spot)	Sand Patch Test (Number of Spot)
1. Munnerlyn Chapel Road	CHFRS-2P (One Lane)	0.2	2	2	3	3
		0.3	NA	NA	3	3
2. Tacoma Blvd_PG 64		0.4	2	2	3	3
3. Tacoma Blvd_PG 70	E-Fog (One Lane)	0.1	2*	2*	NA	
		0.16	2*	2*		
4. Preston Road		0.22	2*	2*		

*For E-fog sections, change of hydraulic conductivity for before and after fog seal was evaluated on the same field core specimens.

Figure 7-1 Application of fog seal and measurement of friction parameter. (a) Cleaning of the surface with power broom, (b) Measurement of surface temperature, (c) Spraying of fog seal by a distributor truck, (d) Uncured fog seal, (e) Fully cured fog seal, (f) Use of British Pendulum Tester, (g) Measurement of mean texture depth the by sand patch.

7.2.1 Measurement of Hydraulic Conductivity

In the first phase of the core collection, 6-inch diameter core specimens were taken from each road before and after the fog seal application. After one lane was sprayed with CSS-1H emulsion, two core specimens were taken from the lowest application rate (0.2 gal/yd^2). At the same time, two more pavement cores were taken from the opposite lane that had not been fog sealed. The distance between these two sets of core specimens was kept to a minimum. Similarly, four more cores were taken from the highest application rate (0.4 gal/yd^2). In total, 32 cores were taken from the four roads and contained 16 specimens that were fog sealed and the 16 specimens that were not.
In the second phase, instead of comparing separate specimens, the same cores are tested for hydraulic conductivity before and after the fog seal application. 24 core specimens, two for each rate, and a total of six for each road were collected. The Karol-Warner permeameter was used to determine the hydraulic conductivity of field cores and was done per ASTM PS-129. This is a flexible wall permeameter, which determines the rate of flow of water through a saturated specimen. A summary of the steps to determine the hydraulic conductivity of the core specimen is given below.

- In most cases, the bottom of the core specimen was uneven and full of mud that could not be removed by cleaning with water. Therefore, the bottom of the specimen was sawed to make the surface even and clean.
- The specimen was then dried overnight at room temperature using a fan and the Bulk specific gravity of the specimen was determined per ASTM D 2726.
- The specimen was then vacuum saturated with a residual pressure of approximately 525 mm hg for 5±1 minutes.

- The specimen was placed inside the permeameter and a pressure of 12±1 psi was applied around the sidewall.
- The graduated standpipe was filled to the top with water and allowed to drain for 15 minutes for better saturation of the specimen.
- The standpipe was refilled with water to the upper trimming mark (75 cm from the top of the specimen), and the time was counted until it reached the lower timing mark (55 cm from the top of the specimen).
- The coefficient of permeability or the hydraulic conductivity is determined by using Darcy's law.
- Then the specimen was returned to the road right before the application of fog seal. The bottom side of the Core specimens was covered by the aluminum foils and duct tape so that fog seals seeping through the side crevice could not clog the bottom of the core. After fog sealing, the core specimens were brought back to the lab to test for hydraulic conductivity. Figure 7-2 depicts some important steps followed in the study to measure the hydraulic conductivity.

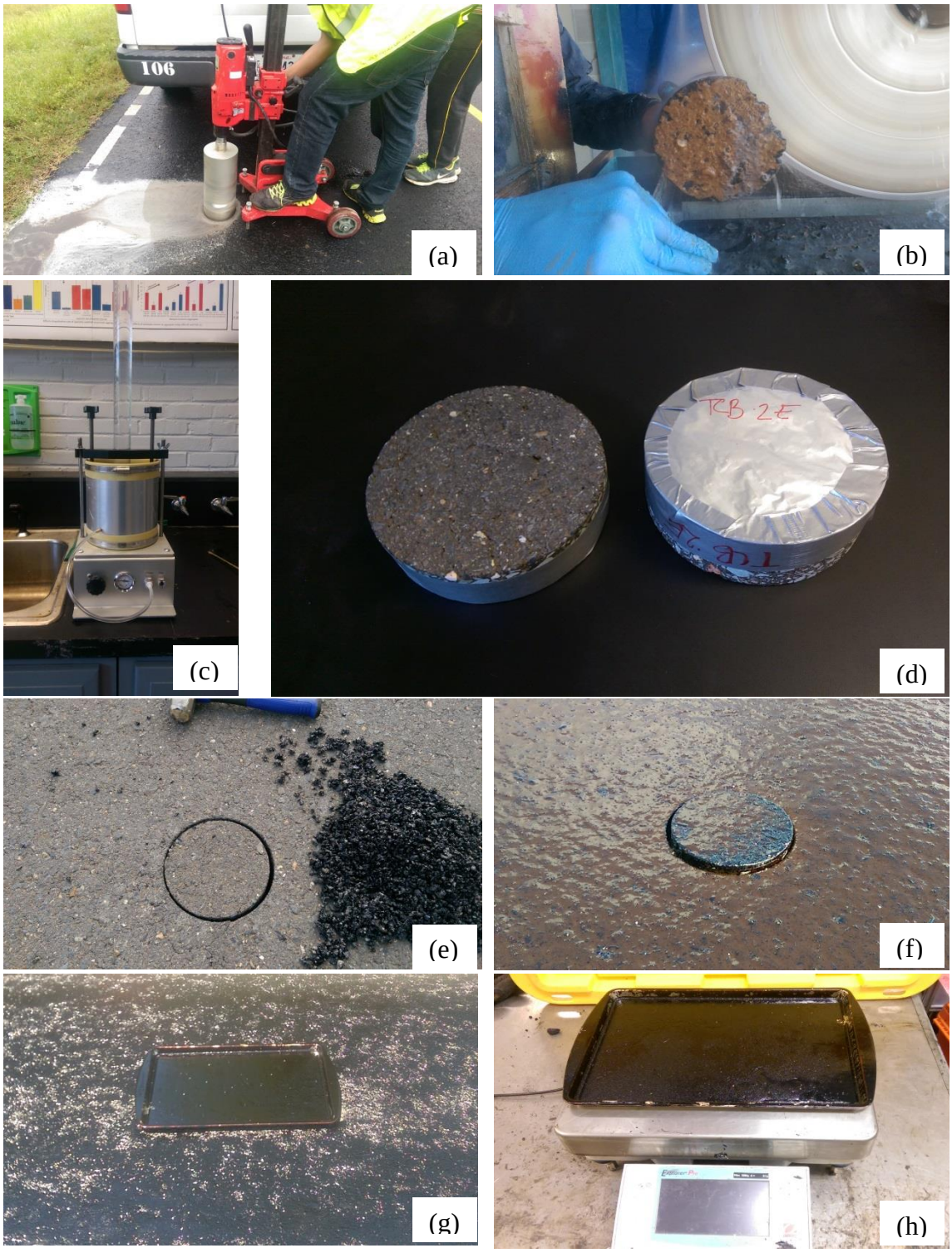

Figure 7-2 Hydraulic conductivity test on field core and field residue collection. (a) Core drilling, (b) Sawing off the core bottom, (c) Hydraulic conductivity test, (d) Covering of the bottom (e) Return of the core right before fog sealing, (f) Application of fog seal, (g) collection of the emulsion, (h) measurement of the field residue content.

7.2.2 Measurement of Friction Parameters

The micro-texture of the surface was measured by the British pendulum tester per ASTM E 303. Macro-texture depth was evaluated by the volumetric technique per ASTM E 965. The friction parameters for the CSS-1H emulsion is reported in this paper. As mentioned earlier, three application rates were applied on each road. Three different spots located 10 feet apart from each other had been selected and marked for each application rate. The British pendulum number (BPN) and Mean texture depth (MTD) results from these three spots were averaged to get the value for one section with an application rate. British pendulum tester and volumetric sand patch test were done on the same spot both before and after the fog seal application. Loose sand was swept away before running these two tests, which increased the repeatability of the test results. After fog seal application, the readings were taken within the first 48 hours, 7 days later, one month and three months later. The friction readings were also taken one day before the fog seal application. BPN (after temperature adjustment) and MTD were converted to the international friction index parameter per ASTM E 1960.

7.3 Results and Discussions

7.3.1 Summary of Fog Seal Construction Observations

Temperature, wind, and humidity affect the breaking time of emulsion. Warm weather and relatively lower humidity are necessary for better curing. Table 7-2 summarizes the description of the weather, road condition, and drying time for all the roads. It was observed that high ambient and pavement temperature reduces the curing time of the emulsion. On Preston road, the ambient and surface temperatures were 81°F and 96.2°F, respectively, and the fog seal cured in less than 2.5 hours, the fastest among

all other roads. The lowest pavement temperature was observed in Tacoma Blvd_64 road and it required the longest time to cure, approximately 3.5 hours. In flat surfaces, emulsion started to break (coalescing to solid asphalt) within 30 minutes but the tackiness of the surface was present for a while. Except in deep puddles and shaded regions, a complete curing (complete removal of the water) was observed to be less than 2.5 hours. In places with deep puddles where it was not breaking after 2 hours, the excess emulsion was removed off from the road using a hand broom. This process added some more time to fully cure the emulsion in those small places and is reflected in the traffic opening time in Table 7-2. It was also observed that the shaded places have approximately 10-15°F lower surface temperature than the un-shaded place and it took approximately 30-60 more minutes to completely cure. Among the three application rates, 0.4 gal/yd2 took more time to fully cure than the 0.2 gal/yd2 in all four roads.

Table 7-2 Summary of field observation during fog seal application (CSS-1H).

Road ID	Application Rate (Gal/yd^2)	Ambient Temp. (°F)	Surface Temp. (°F)	Humidity (%)	Average Wind Speed (MPH)	Curing Time (HH:MM)	Traffic Opened (HH:MM)	Remarks
Munnerlyn Chapel	0.2	68	77.3	39	6	2:40	3:30	No Shaded Places
	0.3					3:00		
	0.4					3:30		Negligible Puddles
Tacoma Blvd_PG 64	0.2	66.5	75.2	45	2	2:10	3:45	Few Shaded Places
	0.3					2:30		
	0.4					3:30		Few Puddles
Tacoma Blvd_PG 70	0.2	75	86.2	35	2	2:00	3:00	No shaded Places
	0.3					2:30		
	0.4					2:30		Few Puddles
Preston	0.2	81	96.2	19	9	1:20	3:00	Few Shaded Places
	0.3					1:20		
	0.4					2:20		Lots of Deep Puddles

7.3.2 Hydraulic Conductivity Reduction

Table 7-3 shows the hydraulic conductivity for CSS-1H Emulsion on Different Cores. According to Table 7-3, it can be observed that 8 out of 16 comparisons showed an increase in hydraulic conductivity after fog seal application. A gross average of the reduction in hydraulic conductivity shows that overall hydraulic conductivity increased after fog seal application, which is theoretically contradictory. However, a closer look at corresponding air voids of the specimen will provide a better understanding of the scenario. It is observed that even if the specimens were collected within close vicinity to each other the air voids varied significantly. The air voids have an exponential effect on hydraulic conductivity, whereas the sealing effect of the fog seal is not as significant. A

minute change in air voids is enough to produce a large variation in hydraulic conductivity and completely hide the improvement due to fog seal. This phenomenon is clear in the last four specimens of Table 7-3, where all four air voids of fog seal treated cores are higher than the untreated cores, and all four specimens showed an increase in hydraulic conductivity. For the second specimen (PR 0.2_2) of the table, two specimens had similar air voids but the value of k still increased. The only solution to reduce this sort of variability and decisively conclude about the sealing potential of the fog seal is to test the same specimen before and after the fog seal application.

Table 7-3 hydraulic conductivity for css-1h emulsion on different cores (the hydraulic conductivity was tested before and after the fog sealing on the different cores).

Road ID	Specimen _ID	Application Rate (After Dilution of Emulsion at 30E:70W) (gal/yd^2)	Air Voids (not fog sealed specimens) (%)	Air Voids (Fog sealed specimens) (%)	Hydraulic Conductivity (K) cm/s X 10^{-5}		% Reduction of K
					Before Fog Seal	After Fog Seal	
Preston – WB[1]	PR 0.2_1	0.2	4.8	4.8	5.4	4.0	26.0
	PR 0.2_2	0.2	4.9	4.9	4.8	5.5	-14.9
	PR 0.4_1	0.4	5.8	4.4	28.6	0.5	98.4
	PR 0.4_2	0.4	5.9	5.0	23.4	1.4	94.1
Munnerlyn Chapel – EB[2]	MC 0.2_1	0.2	7.6	5.8	44.7	426.0	-854.0
	MC 0.2_2	0.2	7.0	7.1	27.4	285.1	-940.5
	MC 0.4_1	0.4	9.0	9.3	408.0	96.8	76.3
	MC 0.4_2	0.4	10.7	10.8	832.1	55.9	93.3
Tacoma Blvd_PG 70 –EB[2]	TCB 0.2_1	0.2	4.7	4.8	0.9	1.2	-34.7
	TCB 0.2_2	0.2	5.2	5.2	3.4	1.5	55.1
	TCB 0.4_1	0.4	7.2	3.3	12.4	0.9	92.5
	TCB 0.4_2	0.4	6.6	3.8	17.9	5.9	67.0
Tacoma Blvd_PG 64 – EB[2]	TCE 0.2_1	0.2	4.3	5.4	2.5	7.7	-206.8
	TCE 0.2_2	0.2	4.1	9.2	1.1	45.7	-4103.2
	TCE 0.4_1	0.4	5.3	6.9	13.8	67.2	-386.5
	TCE 0.4_2	0.4	5.7	6.8	46.1	54.1	-17.4

[1]East Bound Lane, [2] West Bound Lane

In response to this problem, the researcher modified the specimen collection process from the road during the second phase of the permeability study. During this phase, core specimens were collected from the road and then tested for hydraulic conductivity. They were then returned to the road right before fog sealing and brought to the lab again after the fog sealing to re-evaluate the hydraulic conductivity. This allowed the researcher to test the same specimen for hydraulic conductivity before and after the fog seal application. Table 7-4 shows the reduction in hydraulic conductivity (K) for 24 core specimens tested in the study, which contains four different roads, three different application rates of the emulsion, two specimens for each rate, and a wide range of air voids (4.1-10.7%). When observing the reduction in hydraulic conductivity from Table 7-4, it is clear that fog seal has the potential to seal the voids and reduce the permeability of the pavement. Out of the 24 specimens tested in this phase, only two specimens showed an increase in K. The 5th specimen from Preston road, which showed an increase in the K value was run over by traffic by accident at the time of fog seal application, probably damaging the specimen. No specific practical reason was found for the two specimens that showed an increase in permeability. The reduction in hydraulic conductivity varied widely, from 0.7 to 77.7%. Although the fog seal application rate was controlled by the emulsion distributor truck, the actual residue content rate that was sprayed on top of the specimen surface was measured by collecting emulsion on top of a flat tray (Figure 7-2 g). For the Tacoma Blvd (64 and 70) sections, the residue content rate on the surface was very close to the expected value. The distributor truck over-sprayed at 0.1 gal/yd2 application rate on Munnerlyn Chapel road and two other application rates on this road were slightly higher but can be considered pretty accurate for practical purposes. For

Preston road, the residue content rate could not be determined because the trays were run over by traffic by mistake as mentioned earlier.

Table 7-4 Hydraulic conductivity for e-fog on same cores (the hydraulic conductivity was tested before and after the fog sealing on the same cores).

Road ID	Application Rate (gal/yd^2) (Diluted by the Manufacturer)	Measured field Residue Content (mg/cm^2)	Specimen Height (cm)	Air Voids (%)	Hydraulic Conductivity (K) cm/s X 10^{-5}		% Reduction in K
					Before Fog Seal	After Fog Seal	
Preston – EB[1]	0.1	NA	4.03	4.8	5.4	3.4	36.5
	0.1		4.57	4.9	4.8	4.2	12.5
	0.16		7.00	5.4	13.2	7.2	45.4
	0.16		5.81	5.8	17.2	7.6	56.0
	0.22		4.38	5.8	28.6	NA	NA
	0.22		4.64	5.9	23.4	23.3	0.7
Munnerlyn Chapel – WB[2]	0.1	36.6	5.23	7.6	44.7	31.6	29.3
	0.1		4.93	7.0	27.4	29.3	-7.1
	0.16	34.7	6.55	7.9	165.7	86.1	48.0
	0.16		7.42	7.3	62.2	55.9	10.1
	0.22	41.8	7.61	9.0	408.0	208.2	49.0
	0.22		6.21	10.7	832.1	224.9	73.0
Tacoma Blvd_PG 70 –WB[2]	0.1	22.1	4.40	4.7	0.9	1.1	-19.4
	0.1		3.99	5.2	3.4	1.8	46.0
	0.16	32.4	3.98	7.0	29.1	19.5	33.2
	0.16		3.70	5.8	30.4	19.1	37.1
	0.22	39.5	3.16	7.2	12.4	2.8	77.7
	0.22		2.87	6.6	17.9	5.5	69.3
Tacoma Blvd_PG 64 – WB[2]	0.1	20.6	4.25	4.3	2.5	2.3	8.8
	0.1		3.96	4.1	1.1	0.3	71.8
	0.16	28.4	3.46	5.2	31.5	22.6	28.3
	0.16		3.31	4.2	12.8	6.4	49.8
	0.22	39.5	3.77	5.3	13.8	13.2	4.2
	0.22		3.54	5.7	46.1	35.7	22.6

[1]West Bound Lane, [2]East Bound Lane

7.3.3 Effect of Application Rate on Hydraulic Conductivity

Figure 7-3 (a) shows the average reduction in hydraulic conductivity for three different fog seal application rates and four different pavements. It is clear from Figure 7-3(a) that not all roads showed an increase in the reduction in hydraulic conductivity with the increase of application rate. Munnerlyn chapel and Tacoma Blvd_70 section showed a 108% and 452% increase in the reduction in hydraulic conductivity from 0.10 gal/yd2 to 0.22 gal/yd2. This significant increase in the reduction in hydraulic conductivity was not observed in two other roads. Figure 7-3(b) shows the average reduction in hydraulic conductivity for the different application rates. Slightly better sealing is observed with the increase of application rate. Reduction in hydraulic conductivity increased by 12.7% and 23% for 0.16 gal/yd2 and 0.22 gal/yd2, respectively, from the minimum 0.1 gal/yd2 rate. Although, doubling the material application rate did not help in better sealing as expected if the standard deviations of the results are considered. Also, the wide range of value shown for 0.22 gal/yd2 made it more difficult to strictly conclude that higher application rate aids better sealing.

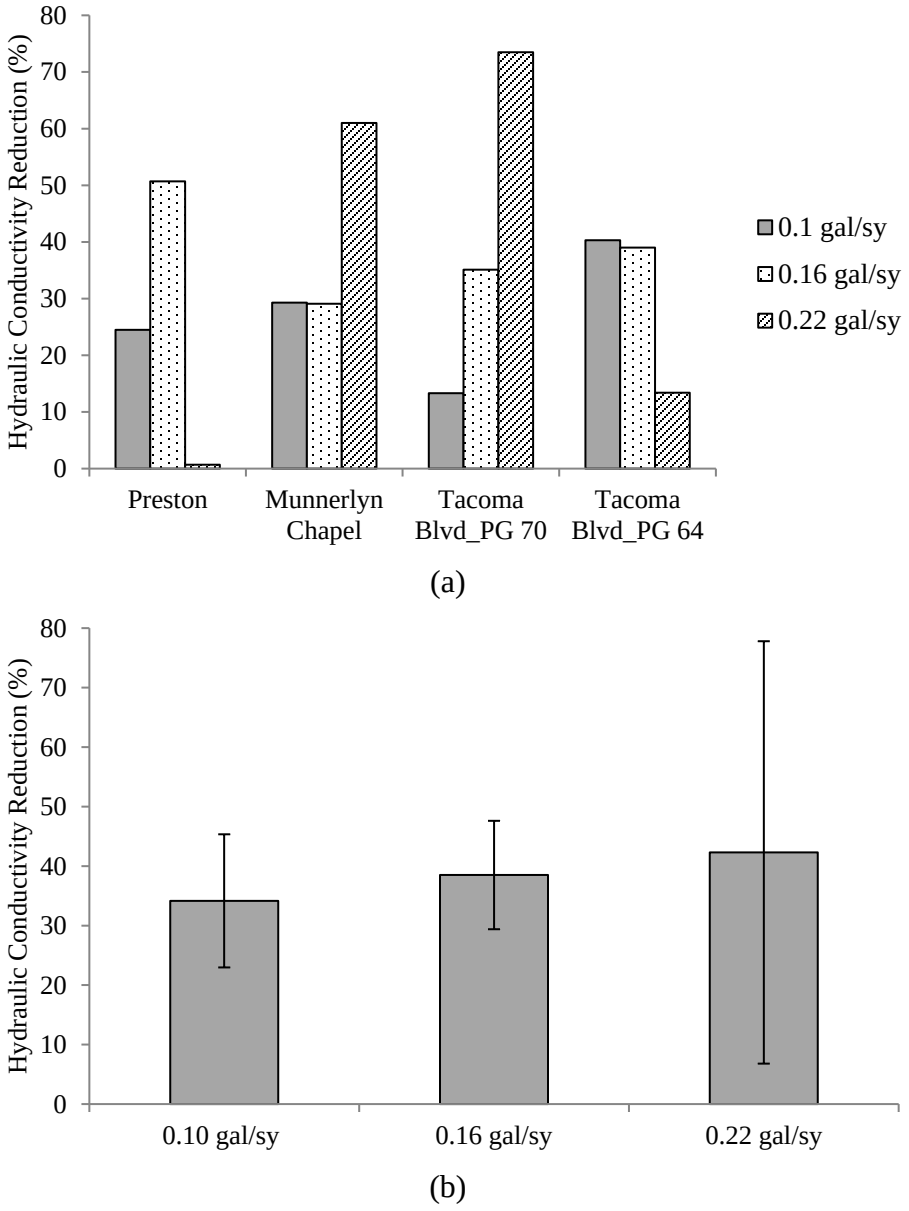

Figure 7-3 Average reductions in hydraulic conductivity performed on the same cores, a) with different roads b) with different application rates.

The relationship between hydraulic conductivity and air void content was found to follow a simple power function for both before and after fog seal application. For specimens before fog sealing the function is $K = 6 \times 10^{-4}$ (Air voids) $^{5.7767}$, with an R^2 of 0.74. For specimens after fog sealing the function is $K = 1 \times 10^{-3}$ (Air voids) $^{5.2455}$, with an R^2 of 0.61. Table 7-5 shows the summary of the R^2 for the relationship of % reduction

in hydraulic conductivity with air voids. It was assumed that air voids might influence the level of reduction achieved by the fog seal. Higher interconnected air voids increase the permeability of the mix and as a result, fog seal can easily penetrate through the specimen. It can clog or seal more interconnected voids, thus reducing the final permeability. If this statement is true, then % reduction in k vs air voids plot will have a high R^2 value with a positive slope. However, from Table 7-5, it can be observed that, other than Munnerlyn Chapel road, there was no strong correlation with reduction in K and air voids. R^2 values were also very low for the specimens of different roads but a particular application rate. This means that reduction in permeability does not depend on initial permeability and the sealing capacity (measured by the reduction of K) of fog seal will not vary for high or low air void surface.

Table 7-5 Correlation coefficient (R^2) between percent reduction in hydraulic conductivity and air voids.

Road ID	Application rate			R^2 considering different application rates but not a particular road
	0.1 (gal/yd^2)	0.16 (gal/yd^2)	0.22 (gal/yd^2)	
Preston	-	-	-	0.0
Munnerlyn Chapel	-	-	-	0.81
Tacoma Blvd_PG 70	-	-	-	0.18
Tacoma Blvd_PG 64	-	-	-	0.35
R^2 considering different roads but at a particular application rate	0.03	0.12	0.43	0.10

7.3.4 Results of Friction after Fog Seal Application

Micro-texture of the pavement surface was evaluated by using the British pendulum tester and the volumetric sand patch test was used to evaluate the Mean Texture Depth (MTD), which represents the macro-texture of the pavement surface. British Pendulum Number (BPN) and MTD values were then converted to international friction index parameter F60, which is an estimated coefficient of friction at 60 km/h.

Figure 7-4 shows the value of F60 of the pavement before and after the fog seal application for all four roads with the change of time and application rate. Figure 7-4 confirms that irrespective of road type and application rate, fog seal causes a sudden drop in the friction value (F60). The highest drop in friction was observed in the Tacoma Blvd_64 section (Figure 7-4 b) for a 0.4 gal/yd2 application rate, which is 39.38%. If the average of the three rates is considered, the same section also showed the highest drop in friction of 38%. It can be observed from Figure 7-4 that for most pavement and application rate combinations, the fog sealed surface does not return to the original level of friction even after three months of service. Therefore, fog seal should be used with caution if the existing pavement already has low surface friction, as it may cause a significant loss of friction for a considerable amount of time. Preston Road (Figure 7-4 d) showed a slight upward trend of gaining friction after the fog seal application at all three rates. In Preston road, for 0.2 and 0.4 gal/yd2, the initially lost F60 was recovered 22.4% and 26.6%, respectively, in 3 months. These two values are the highest among all other combinations. Interestingly, of the four roads, Preston road showed both the highest gain in friction within three months, as well as the highest AADT (annual average daily traffic). Therefore, one can presume that higher traffic causes more abrasive action between tire and fog seal surface. This action gradually removes the thin coating of the emulsion from the top of the aggregate, helping the pavement to return to its original level of friction.

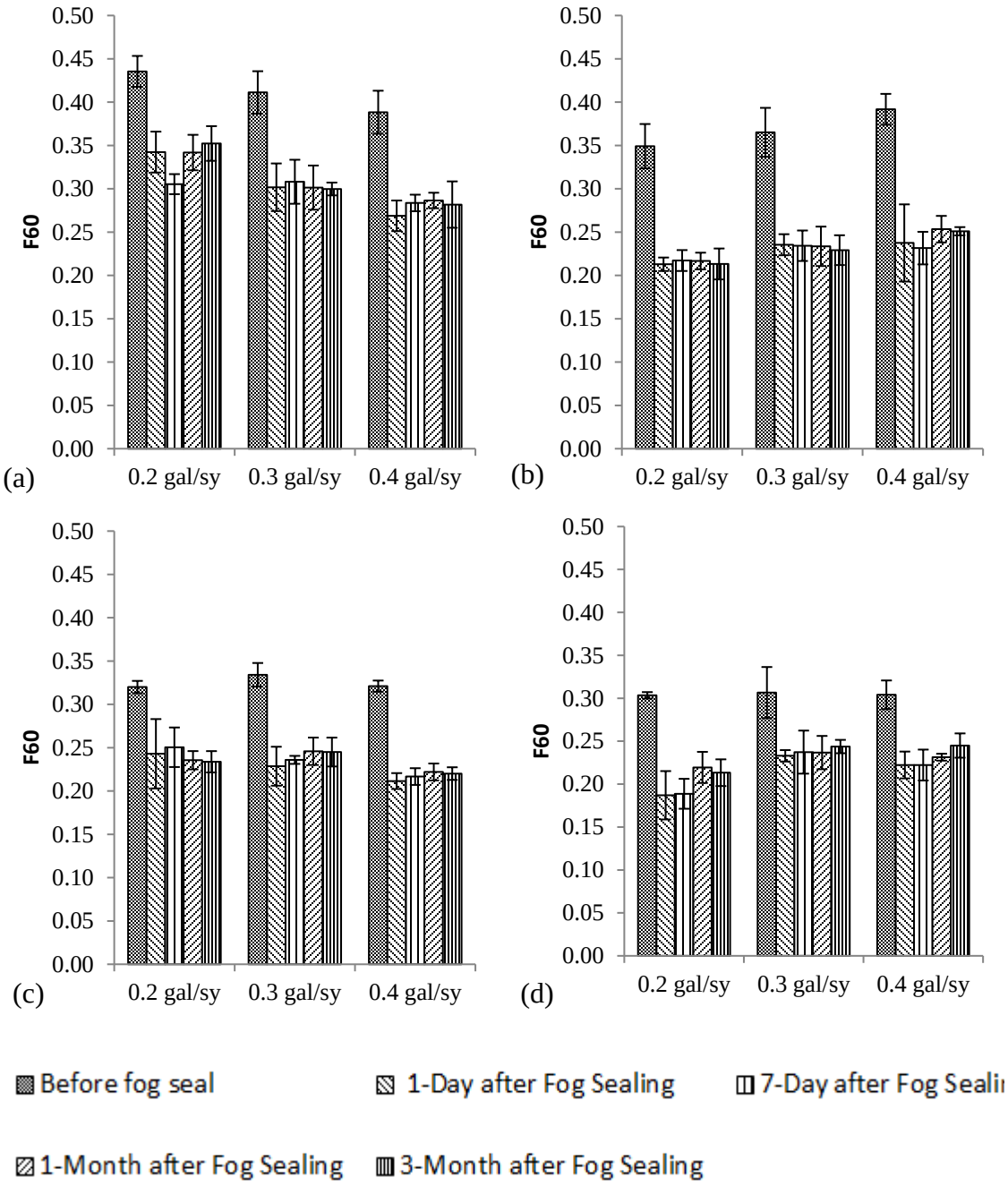

Figure 7-4 F60 values for all roads with time and application rate. a) Munnerlyn chapel road, b) Tacoma Blvd_PG 64, c) Tacoma Blvd_PG 70, d) Preston Road.

7.3.5 Effect of Application Rate on Friction Index

Figure 7-5 shows the initial average reduction of friction parameters (MTD, BPN, and F60) for different application rates. It can be observed from Figure 7-5 that the mean

texture depth evaluated by the volumetric sand patch method reduces approximately 12.5% after the fog seal application. Based on the data presented here, it is clear that MTD does not show any sensitivity within the practical range of the application rate used in the study. Reduction of the mean texture depth with the increase of application rate may be observed for a few pavement and application rate combinations, but considering all four surfaces, MTD is insensitive to the application rate. The reason behind this phenomenon may be that any minimum practical rate of fog seal that can cover the whole surface is enough to seal the macro pores of the surface, causing a large difference in macro-texture after the fog seal treatment. However, further increasing the rate will not be able to seal any new pores. Rather, it will add a super fine thickness on top of the sealed pores, which will not create any significant change in the volumetric sand patch method. Fog seal tends to reduce the BPN, which is a function of micro-texture of the road, more than the macro-texture depth (MTD). Figure 7-5 shows that the average reduction in British pendulum number representing the micro-texture of the surface is approximately 30%, which is higher than the reduction of MTD. BPN also showed a slight sensitivity to the fog seal application rate. 0.4 gal/yd2 application rate showed a 9% more reduction in BPN value than 0.2 gal/yd2. Similar trends and nearly similar values are obtained for international friction parameter F60, which is expected because micro-texture has a higher effect on the friction of a pavement. On average, a 20 to 40% reduction of international friction parameter F60 is expected from fog seal application irrespective of any practical application rate and road surface.

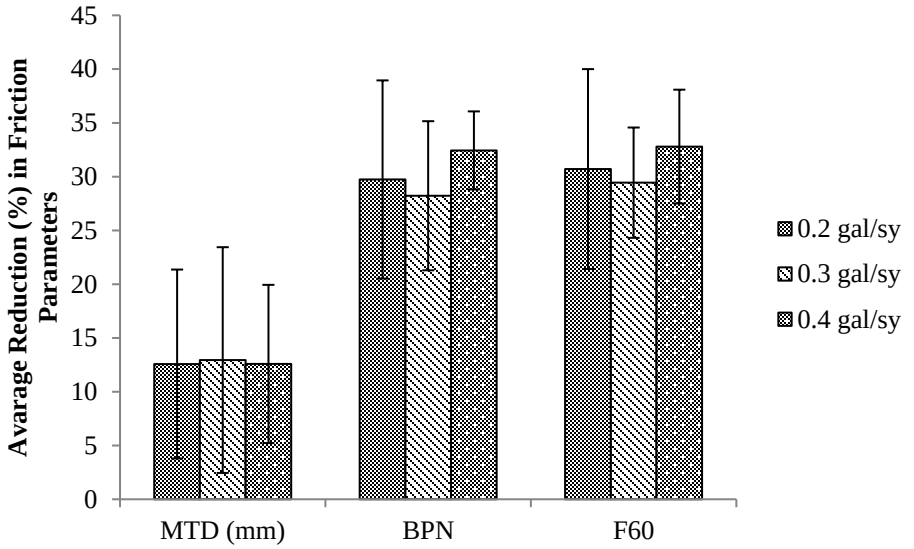

Figure 7-5 Initial average reductions (%) of friction parameters for different application rates.

7.3.6 Precautions for Field Application

Application of fog seals before the pavement condition get worse, would cost less than reconstruction and rehabilitation treatment [7.10]. Fog seal improves the aggregate retention and increases the service life of the pavement by increasing the pavement's impermeability to air and water by sealing the small cracks [7.11]. Permeability was found to be related with moisture induced damage of the pavement [7.12]. Low air voids reduce the higher aging rate of the pavement mix [7.5]. Rejuvenating fog seals can soften the hardened asphalt due to aging and can restore the desired mechanical properties of the pavement surface [7.3]. In spite of all those benefits mentioned above fog seal is often not recommended for medium and high-volume road because of its lengthy period of traffic opening time. Main trade off for fog seal use is the significant drop in skid resistance and consequently the safety issue. This study quantified the change in hydraulic conductivity and the skid resistance because of application of fog seal. The reduction in hydraulic conductivity might not be significant enough to convince the decision maker to compromise the safety because of the reduction in skid resistance. A life cycle cost analysis of pavement and accident data analysis because of fog seal

application need to be performed. An engineer must assess a complete cost-benefit balance before application of fog seal in the field.

7.4 Conclusions

This paper presents information about fog seal performance and effectiveness using a reduction in hydraulic conductivity and international friction index parameter F60 as an indicator for low volume roads. Based on the results presented in the study, the following conclusions can be made.

- Reduction in hydraulic conductivity is a good measure of the sealing potential of the Fog seal. However, to decisively conclude about the sealing potential, the same specimen needs to be tested before and after the fog seal application. A small change in air voids is enough to produce a large variation in hydraulic conductivity and completely hide the improvement due to fog seal.
- The same core was tested before and after fog sealing to exactly quantify the effect of fog seal on permeability. It was observed that fog seal has significant potential to reduce the hydraulic conductivity. Considering all four pavements and application rates of 0.1-0.22 gal/yd^2, the average reduction in hydraulic conductivity was 38.5%, varying from 0.7 to 0.77%.
- Reduction in hydraulic conductivity shows slight sensitivity to the application rate, but it does not depend on the initial hydraulic conductivity or air voids. This means the sealing capacity of the fog seal will not vary for high or low air void surface.

- It was observed that high ambient and pavement temperature reduces the curing time of the emulsion. If the ambient temperature is more than 65°F, fog seal is expected to be fully cured within 2.5 to 3.5 hours for a 0.2-0.4 gal/yd^2 application rate. Too many shaded areas and puddles may add 30-60 minutes more on final curing time.
- Irrespective of road type and application rate, fog seal causes a sudden drop in the International Friction index parameter F_{60} by 20 to 40%. Fog seal changes both micro and macro-texture of the road, but it affects micro-texture more than the macro-texture.
- A fog sealed surface does not return to its original level of friction, even after three months of service for most pavement and application rate combinations. Therefore, fog seal should be used with caution if the existing pavement already has low surface friction.

CHAPTER 8

CONCLUSIONS AND RECOMMENDATIONS

Findings from each study are presented at the end of the corresponding chapter. The overall conclusions and recommendations for future work are mentioned in this chapter.

8.1 Conclusions

The general conclusions are as follows:

- When asphalt mixture is subjected to aging in the mixing plant or in the field during the service life, only asphalt binders undergo the chemical changes and consequently ages. To determine the aging effect, both binder and mix are tested separately. Generally, in the laboratory, binders are aged through different special oxidative aging ovens before rheological testing, and asphalt mixes are aged in standard ovens before mechanical testing to identify the effect of aging. It is important to make sure that the standard binder aging procedure is simulating the mix aging. In this study, mix aging is simulated in the laboratory by oven aging and the binder aging is performed using traditional rolling thin film oven. A correlation is established between these two aging methods and an equation is proposed which can be used to determine the duration and temperature for RTFO oven aging to get the exact aging effect from mix oven aging. The aging effect is

defined by the stiffness of the binder which changes linearly with time and temperature in both the binder and mix aging methods. Mix oven aging shows more sensitivity to temperature than that of binder aging.

- The identification of the aging effect by spectroscopic analysis is quicker and convenient to perform than the rheological as well as mechanical characterization. Fourier transformed infrared (FT-IR) spectroscopy was used in this study to comprehend and compare the chemical changes that occur through the aging process. Carbonyl index can successfully quantify binder and mix aging, but the sulfoxide index is not adequate to conclusively determine the aging of asphalt although both the indices are affected by aging.
- A quick extraction process is developed in this study which can produce enough binder from the mix for testing in FT-IRS. The process is very simple, time-saving, and easily implementable in the field.
- Reclaimed Asphalt Pavement (RAP) is added in asphalt mixture for economic and environmental interest, however, quantification of the aging state of these RAP and determination of the quantity of RAP in the fresh mix is necessary for quality control purpose. By applying the quick extraction process and the carbonyl index concept, FT-IR spectroscopy can precisely detect the presence of an aged binder in the mix within a very short time and can quantify the amount of RAP present in the fresh mix. So, the handheld FT-IR is a potential candidate to be used as a quality control tool in the field.
- Highly aged binder in RAP makes the mix stiffer and escalates the cracking. To accommodate a higher amount of RAP in hot mix asphalt use of rejuvenators is

the most suitable strategy. A rejuvenated mix must be tested for its cracking resistance before being applied in the field. In this study, four types of cracking tests were performed on asphalt mix made with two completely different categories of rejuvenators: petroleum-based and bio-based oil. Both the rejuvenators can effectively restore the cracking potential of the mix although for high RAP content the cracking potential cannot be restored to the level of control mix. Petroleum-based rejuvenators performed better than the bio-based rejuvenator in all the cracking tests.

- Less bio-based rejuvenator is required to lower the RAP binder grade to the desired level. But it is more susceptible to long-term aging.
- A sound understanding of the cracking mechanism is necessary to design a cracking resistant mix. Various testing configurations, such as the indirect tension (IDT) test, the single-edge notch beam (SEB) test, the disk-shaped compact tension (DCT) test, and the semi-circular bending (SCB) test, are used to measure the cracking resistance of asphalt mix. To analyze the crack that propagates through asphalt binder or mastic, the cohesive zone material (CZM) model approach is suitable for asphalt mix and can be implemented in finite element methods. In this study critical energy release rate (*Jc*) which can be determined by ASTM D 8044 test is calculated by utilizing a finite element model of SCB specimen incorporating the CZM model to simulate the fracture. The CZM properties of fine aggregate mastic were determined in the laboratory by a double cantilever beam test. This study affirms that failure criteria in the SCB test at intermediate temperature can be modeled successfully using the CZM model.

- An antioxidant is an additive to asphalt binder that can slow down the aging. In this study, three different kinds of lignin were investigated to enhance asphalt binder's rheological properties. All three types of lignin improved the high-temperature performance grade, and black liquor lignin and lignin produced from rice hulls improved the long-term aging index of the binder. Up to 6% asphalt binder is replaced by the black liquor lignin and the resultant mix showed better cracking resistance and an improved flexibility index compared to the control mix.
- Rejuvenating agents can be used during the mixing process (discussed earlier) or can be directly applied on pavement surface as a fog seal. Apart from its rejuvenating effect, there arises two important issues due to the application of fog seal: reduction of hydraulic conductivity and reduction in frictional resistance. In this study, eleven roads in northern Louisiana were chosen for fog seal application. Reduction in hydraulic conductivity is a good measure of the sealing potential of the Fog seal. It is concluded that fog seal has significant potential to reduce the hydraulic conductivity. Reduction in hydraulic conductivity shows slight sensitivity to the application rate, but it does not depend on the initial hydraulic conductivity or air voids. Irrespective of road type and application rate, fog seal causes a sudden drop in the International Friction index parameter. A Fog sealed surface does not return to its original level of friction, even after three months of service for most pavement and application rate combinations. Therefore, fog seal should be used with caution if the existing pavement already has low surface friction.

8.2 Suggestions for Future Work

Some recommendations and suggestions for future study are as follows:

- Mix and binder aging performed in a controlled environment exhibits good correlations. Because of a wide variety of factors, RTFO aging cannot be directly correlated with plant aging. Future studies can be performed by comparing the laboratory binder aging with the mix aging from different mixing plants by varying the mixing as well as storage time and temperature for different binder grades. Based on that database, the RTFO aging test protocol can be adjusted depending on the actual field condition.
- The attenuated total reflectance (ATR) feature of FT-IR spectroscopy is used in this study to implement FT-IR in the field for quality control purposes. This method requires binder extraction. In the future, the diffused reflectance (DR) feature should be investigated to eliminate the extraction process and to make it much quicker. Also, an aging scale can be introduced based on laboratory and field aging of asphalt mix and RAP can be classified according to that scale. Rigorous chemo-metric analysis should be performed to capture the effects of other functional groups (if any) to quantify asphalt aging.
- Cohesive Zone Material (CZM) model is utilized for fracture analysis through a semi-circular bend test. In the future, the time-dependent visco-elastic effect of binder and the material heterogeneity of the mix can be included in the model to simulate the crack. Instead of a 2-D model, a 3-D model can be created and different other types of tests (disk shape compact tension, single-edge notch

beam, indirect tension test, overlay test) should be simulated to verify the applicability of CZM model to all the cracking tests of asphalt mix.

REFERENCES

1.1. https://www.asphaltpavement.org/index.php?option=com_content&view=article&id=14&Itemid=33

1.2. https://www.infrastructurereportcard.org/state-item/louisiana/

1.3. http://asphaltmagazine.com/understanding-asphalt-pavement-distresses-five-distresses-explained/

1.4. Zhou, F., Newcomb, D., Gurganus, C., Banihashemrad, S., Sakhaeifar, M., Park, E.S. and Lytton, R., 2016. Field Validation of Laboratory Tests to Assess Cracking Resistance of Asphalt Mixtures: An Experimental Design.

2.1. R. Bonaquist, Mix Design Practices for Warm Mix Asphalt, NCHRP Report 691, Transportation Research Board, Washington, D.C. 2011.

2.2. A. Copeland, N. Gibson, M. Corrigan, A Cross-Cutting Comparison between Hot Mix Asphalt and Warm Mix Asphalt, 2nd International WMA Conference, St. Louis, MO, 2011.

2.3. R. Abbas, M. Nazzal, S. Kaya, S. Akinbowale, B. Subedi, M. S. Arefin, L. Abu Qtaish, Effect of Aging on Foamed Warm Mix Asphalt Produced by Water Injection. J. Mat. in Civil Eng. (2016) https://doi.org/10.1061/(ASCE)MT.1943-5533.0001617

2.4. W. Ali, A. R. Abbas, M. Nazzal, D. Powers, Laboratory Evaluation of Foamed Warm Mix Asphalt, Inter. J. Pave. Res. Tech. (2012), https://doi.org/10.6135/ijprt.org.tw/2012.5(2).93

2.5. M. R. M. Hasan, S. W. Goh, Z. You, Comparative study on the properties of WMA mixture using foamed admixture and free water system, Const. Build. Mat. (2013) https://doi.org/10.1016/j.conbuildmat.2013.06.028

2.6. H. Malladi, D. Ayyala, A. A. Tayebali, N. P. Khosla, Laboratory evaluation of warm-mix asphalt mixtures for moisture and rutting susceptibility, J. Mat. Civil Eng. (2014) https://doi.org/10.1061/(ASCE)MT.1943-5533.0001121, 04014162.

2.7. N. Bower, H. Wen, K. Willoughby, J. Weston, J. DeVol, Evaluation of the performance of warm mix asphalt in Washington state, Inter. J. Pave. Eng. (2014) https://doi.org/10.1080/10298436.2014.993199

2.8. J. A. D'Angelo, E. E. Harm, J. C. Bartoszek, G. L. Baumgardner, M. R. Corrigan, J. E. Cowsert, T. P. Harman, M. Jamshidi, H. W. Jones, H.W., D. E. Newcomb, B. D. Prowell, Warm-mix asphalt: European practice, FHWA-PL-08-007, Federal Highway Administration, Washington, D.C. 2008.

2.9. J. Zhang, E. R. Brown, P. S. Kandhal, R. West, An overview of fundamental and simulative performance tests for Hot Mix Asphalt, J. ASTM Inter. (2005) https://doi.org/10.1520/JAI12254

2.10. S. Arafat, N. M. Wasiuddin, Evaluation of a Full-Scale Wheel Load Tester to Determine the Rutting and Moisture Susceptibility of Asphalt Mix in Laboratory, International Conference on Transportation and Development (2018) https://doi.org/10.1061/9780784481554.032.

2.11. W. D. Fernández-Gómez, H. R. Quintana, F. R. Lizcano, A review of asphalt and asphalt mixture aging, Ing. Investig. Ingenieria e investigacion, 33(1) (2013) 5-12.

2.12. R. B. McGennis, R. M. Anderson, T. W. Kennedy, M. Solaimanian, Background of Superpave asphalt mixture design and analysis, FHWA-SA-95-003, Federal Highway Administration, Washington, D.C. 1995.

2.13. A. Shalaby, Modelling short-term aging of asphalt binders using the rolling thin film oven test, Can. J. Civil. Eng. (2002) https://doi.org/10.1139/l01-086.

2.14. A. Hofko, A. C. Falchetto, J. Grenfell, L. Huber, X. Lu, L. Porot, L. D. Poulikakos, Z. You, Effect of short-term ageing temperature on bitumen properties, Road. Mat. Pave. Des. (2017) https://doi.org/10.1080/14680629.2017.1304268

2.15. M. Alavi, X. Lau, D. Jones, J. Harvey, Modification of the Rolling Thin Film Oven (RTFO) Test for Realistic Short-term Aging of Asphalt Rubber Binders, 52nd Petersen Asphalt Research Conference, Laramie, WY, 2015.

2.16. J. Jia, X. Zhang, Modification of the rolling thin film oven test for modified asphalt. In Proceedings of the 24th Southern African Transport Conference (SATC), 2005.

2.17. A. E. Martin, E. Arambula, F. Yin, L. G. Cucalon, A. Chowdhury, R. Lytton, J. Epps, C. Estakhri, E. S. Park, Evaluation of the moisture susceptibility of WMA technologies, NCHRP Report 763, Transportation Research Board, Washington D.C. 2014.

2.18. S. J. Lee, S. N. Amirkhanian, K. Shatanawi, K. W. Kim, Short-term aging characterization of asphalt binders using gel permeation chromatography and selected Superpave binder tests, Const. Build. Mat. (2008) https://doi.org/10.1016/j.conbuildmat.2007.08.005.

2.19. Louisiana Department of Transportation and Development (LADOTD), 2006. Louisiana standard specifications for roads and bridges.

2.20. T. Gandhi, Effects of warm asphalt additives on asphalt binder and mixture properties, Doctoral dissertation, Clemson University, 2008.

3.1. Kaseer, F., A. E. Martin, and E. Arámbula-Mercado 2019. "Use of recycling agents in asphalt mixtures with high recycled materials contents in the United States: A literature review." Constr. Build. Mater., 211, https://doi.org/10.1016/j.conbuildmat.2019.03.286

3.2. Liu, M., M. A. Ferry, R. R. Davison, C. J. Glover, and J. A. Bullin. 1998. "Oxygen Uptake as Correlated to Carbonyl Growth in Aged Asphalts and Asphalt Corbett Fractions." Ind. Eng. Chem. Res., 37(12), https://doi.org/10.1021/ie980450o

3.3. Glover, C. J., A. E. Martin, A. Chowdhury, R. Han, N. Prapaitrakul, X. Jin, and J. Lawrence. 2009. Evaluation of binder aging and its influence in aging of hot mix asphalt concrete: literature review and experimental design (No. FHWA/TX-08/0-6009-1). Texas Transportation Institute.

3.4. Fernández-Gómez, W. D., H. Rondón Quintana, H., and F. Reyes Lizcano 2013. "A review of asphalt and asphalt mixture aging: Una revision". Ingenieria e investigacion, 33(1), 5-12.

3.5. Derrick, M. R., D. Stulik, and J. M. Landry. 2000. Infrared spectroscopy in conservation science. Getty Publications.

3.6. Huang, S. C., and W. Grimes. 2010." Influence of aging temperature on rheological and chemical properties of asphalt binders." Transp. Res. Rec., 2179(1), https://doi.org/10.3141/2179-05

3.7. Kaveh, F., and S. A. Hesp. 2011. "Spectroscopic analysis of pressure aging vessel protocols for the accelerated laboratory aging of asphalt cements." In Proc., 1st Conf. of Transp. Res. Group of India, Bangalore, India

3.8. Qin, Q., J. F. Schabron, R. B. Boysen, and M. J. Farrar. 2014." Field aging effect on chemistry and rheology of asphalt binders and rheological predictions for field aging." Fuel, 121, https://doi.org/10.1016/j.fuel.2013.12.040

3.9. Liang, Y., R. Wu, J. T. Harvey, D. Jones, and M. Z. Alavi. 2019. “Investigation into the Oxidative Aging of Asphalt Binders.” Transp. Res. Rec., https://doi.org/10.1177/0361198119843096

3.10. Hofko, B., M. Z. Alavi, H. Grothe, D. Jones, D., and J. Harvey. 2017. “Repeatability and sensitivity of FTIR ATR spectral analysis methods for bituminous binders.” Mater. Struct. 50(3), https://doi.org/10.1617/s11527-017-1059-x

3.11. Hofko, B., L. Porot, A. F. Cannone, L. Poulikakos, L. Huber, X. Lu, and H. Grothe. 2018. “FTIR spectral analysis of bituminous binders: reproducibility and impact of ageing temperature”. Mater. Struct., 51(2), https://doi.org/10.1617/s11527-018-1170-7

3.12. Jing, R., A. Varveri, X. Liu, T. Scarpas, and S. Erkens. 2018. “Chemo-mechanics of Ageing on Bituminous Materials.” In 97th Annual Meeting of the Transp. Res. Board, Washington, DC.

3.13. Noor, L., N. M. Wasiuddin, N. M. 2018. “Effects of Extraction Solvent, Fine Particles, and Reclaimed Asphalt Pavement Aggregate in Aging Determination of Asphalt Binder by ATR-FTIRS.” In Int. Conf. on Transp. Dev. 2018: Airfield and Highway Pavements. https://doi.org/10.1061/9780784481554.031

3.14. Chen, C., F. Yin, P. Turner, R. C. West, and N. Tran. 2018. “Selecting a Laboratory Loose Mix Aging Protocol for the NCAT Top-Down Cracking Experiment.” Transp. Res. Rec., 2672(28), https://doi.org/10.1177/0361198118790639

3.15. Yut, I., A. Bernier, and A. Zofka. 2015. “Field applications of portable infrared spectroscopy to asphalt products.” Introduction to Unmanned Aircraft Systems, 127.

4.1. Copeland, A., 2011. Reclaimed asphalt pavement in asphalt mixtures: State of the practice (No. FHWA-HRT-11-021). United States. Federal Highway Administration. Office of Research, Development, and Technology.

4.2. McDaniel, R.S., Soleymani, H., Anderson, R.M., Turner, P. and Peterson, R., 2000. Recommended use of reclaimed asphalt pavement in the Superpave mix design method. NCHRP Web document, 30.

4.3. West, R.C., Willis, J.R. and Marasteanu, M.O., 2013. Improved mix design, evaluation, and materials management practices for hot mix asphalt with high reclaimed asphalt pavement content (Vol. 752). Transportation Research Board.

4.4. West, R., Michael, J., Turochy, R. and Maghsoodloo, S., 2011, January. A comparison of virgin and recycled asphalt pavements using long-term pavement

performance SPS-5 data. In Proc., Transportation research board 90th annual meeting. Washington, DC: Transportation Research Board, Paper.

4.5. Li, X., M. O. Marasteanu, R. C. Williams, and T. R. Clyne, "Effect of RAP (Proportion and Type) and Binder Grade on the Properties of Asphalt Mixtures." Transportation Research Record 2051, pp. 90–97, Transportation Research Board of the National Academies, Washington, D.C. (2008).

4.6. Mogawer, W., Bennert, T., Daniel, J.S., Bonaquist, R., Austerman, A. and Booshehrian, A., 2012. Performance characteristics of plant produced high RAP mixtures. Road Materials and Pavement Design, 13(sup1), pp.183-208.

4.7. Ali, H. and Mohammadafzali, M., 2015. Long-term aging of recycled binders (No. BDV29 Two 977-01). Florida. Dept. of Transportation. Research Center.

4.8. Behnia, B., Ahmed, S., Dave, E.V. and Buttlar, W.G., 2010. Fracture Characterization of Asphalt Mixtures with Reclaimed Asphalt. International Journal of Pavement Research & Technology, 3(2).

4.9. Al-Qadi, I.L., Aurangzeb, Q., Carpenter, S.H., Pine, W.J. and Trepanier, J., 2012. Impact of high RAP contents on structural and performance properties of asphalt mixtures.

4.10. Shu, X., Huang, B. and Vukosavljevic, D., 2008. Laboratory evaluation of fatigue characteristics of recycled asphalt mixture. Construction and Building Materials, 22(7), pp.1323-1330.

4.11. McDaniel, R.S., Shah, A. and Huber, G., 2012. Investigation of low-and high-temperature properties of plant-produced RAP mixtures (No. FHWA-HRT-11-058). United States. Federal Highway Administration. Office of Pavement Technology.

4.12. Tran, N.H., Taylor, A. and Willis, R., 2012. Effect of rejuvenator on performance properties of HMA mixtures with high RAP and RAS contents. NCAT Report, pp.12-05.

4.13. Zadshir, M., Hosseinnezhad, S. and Fini, E.H., 2019. Deagglomeration of oxidized asphaltenes as a measure of true rejuvenation for severely aged asphalt binder. Construction and Building Materials, 209, pp.416-424.

4.14. Yu, X., Zaumanis, M., Dos Santos, S. and Poulikakos, L.D., 2014. Rheological, microscopic, and chemical characterization of the rejuvenating effect on asphalt binders. Fuel, 135, pp.162-171.

4.15. NCAT (2014) “NCAT Researchers Explore Multiple Uses of Rejuvenators.” Asphalt Technology News, Vol. 26, No. 1 (Spring), http://www.ncat.us/info-pubs/newsletters/spring-2014/rejuvenators.html

4.16. Pavement Technology, Inc., weblink: https://www.pavetechinc.com/bio-based-rejuvenators-a-review-of-functionality/

4.17. Zaumanis, M. and Mallick, R.B., 2015. Review of very high-content reclaimed asphalt use in plant-produced pavements: state of the art. International Journal of Pavement Engineering, 16(1), pp.39-55.

4.18. X. Yu, M. Zaumanis, S. Santos, L.D. Poulikakos, Rheological, microscopic, and chemical characterization of the rejuvenating effect on asphalt binders, Fuel 135 (2014) 162–171.

4.19. Mogawer, W.S., Booshehrian, A., Vahidi, S. and Austerman, A.J., 2013. Evaluating the effect of rejuvenators on the degree of blending and performance of high RAP, RAS, and RAP/RAS mixtures. Road Materials and Pavement Design, 14(sup2), pp.193-213.

4.20. Lee, C., R. Terrel, and J. Mahoney. “Test for Efficiency of Mixing of Recycled Asphalt Paving Mixtures,” Transportation Research Record 911, TRB, Washington, DC, 1983, pp. 51-60.

4.21. Zaumanis, M., Mallick, R. and Frank, R., 2013. Evaluation of Rejuvenator's Effectiveness with Conventional Mix Testing for 100% Reclaimed Asphalt Pavement Mixtures. Transportation Research Record: Journal of the Transportation Research Board, (2370), pp.17-25.

4.22. Zaumanis, M., Mallick, R.B., Poulikakos, L. and Frank, R., 2014. Influence of six rejuvenators on the performance properties of Reclaimed Asphalt Pavement (RAP) binder and 100% recycled asphalt mixtures. Construction and Building Materials, 71, pp.538-550.

4.23. Saha, R., Melaku, R.S., Karki, B., Berg, A. and Gedafa, D.S., 2020. Effect of Bio-Oils on Binder and Mix Properties with High RAP Binder Content. Journal of Materials in Civil Engineering, 32(3), p.04020007.

4.24. Hajj, E., Souliman, M., Alavi, M. and Loría Salazar, L., 2013. Influence of hydrogreen bioasphalt on viscoelastic properties of reclaimed asphalt mixtures. Transportation Research Record: Journal of the Transportation Research Board, (2371), pp.13-22.

4.25. Tran, N.H., Taylor, A. and Willis, R., 2012. Effect of rejuvenator on performance properties of HMA mixtures with high RAP and RAS contents. NCAT Report, pp.12-05.

4.26. Turner, P., Taylor, A. and Tran, P.N., 2015. Laboratory evaluation of SYLVAROADTM RP 1000 rejuvenator. NCAT Rep. 15, 3.

4.27. Tran, N., Taylor, A., Turner, P., Holmes, C. and Porot, L., 2017. Effect of rejuvenator on performance characteristics of high RAP mixture. Road Materials and Pavement Design, 18(sup1), pp.183-208.

4.28. Kaseer, F., Yin, F., Arámbula-Mercado, E. and Epps Martin, A., 2017. Stiffness characterization of asphalt mixtures with high recycled material content and recycling agents. Transportation Research Record, 2633(1), pp.58-68.

4.29. Yin, F., Kaseer, F., Arámbula-Mercado, E. and Epps Martin, A., 2017. Characterising the long-term rejuvenating effectiveness of recycling agents on asphalt blends and mixtures with high RAP and RAS contents. Road Materials and Pavement Design, 18(sup4), pp.273-292.

4.30. Ahmed, R.B., Hossain, K., and Aurilio, M., 2020. Rheological Characterization of Rejuvenated Asphalt Binders. 99th annual meeting of the Transportation Research Board, Washington D.C.

4.31. Hajj, E.Y., Sebaaly, P.E. and Shrestha, R., 2009. Laboratory evaluation of mixes containing recycled asphalt pavement (RAP). Road Materials and Pavement Design, 10(3), pp.495-517.

4.32. Mogawer, W.S., Austerman, A.J., Kluttz, R. and Puchalski, S., 2016. Using polymer modification and rejuvenators to improve the performance of high reclaimed asphalt pavement mixtures. Transportation Research Record, 2575(1), pp.10-18.

4.33. Kaseer, F., Martin, A.E. and Arámbula-Mercado, E., 2019. Use of recycling agents in asphalt mixtures with high recycled materials contents in the United States: A literature review. Construction and Building Materials, 211, pp.974-987.

4.34. Noor, L., Wasiuddin, N.M., Mohammad, L.N. and Salomon, D., 2019, November. Use of Fourier Transform Infrared (FT-IR) Spectroscopy to Determine the Type and Quantity of Rejuvenator Used in Asphalt Binder. In International Congress and Exhibition" Sustainable Civil Infrastructures" (pp. 70-84). Springer, Cham.

4.35. Chen, C., Yin, F., Turner, P., West, R.C. and Tran, N., 2018. Selecting a laboratory loose mix aging protocol for the NCAT top-down cracking experiment. Transportation Research Record, 2672(28), pp.359-371.

4.36. Louisiana. Department of Transportation and Development. issuing body, 2016. Louisiana Standard Specifications for Roads and Bridges: 2016 Edition. Louisiana Department of Transportation and Development.

4.37. Al-Qadi, I.L., Elseifi, M. and Carpenter, S.H., 2007. Reclaimed asphalt pavement—a literature review.

4.38. Christensen, D.W. and Anderson, D.A., 1992. Interpretation of dynamic mechanical test data for paving grade asphalt cements (with discussion). Journal of the Association of Asphalt Paving Technologists, 61.

4.39. Taylor, A.J., 2018. Cracking Group Experiment – Laboratory Results, NCAT Test Track Conference, Auburn University.

4.40. Karki, P. and Zhou, F., 2016. Effect of rejuvenators on rheological, chemical, and aging properties of asphalt binders containing recycled binders. Transportation Research Record, 2574(1), pp.74-82.

4.41. Arámbula-Mercado, E., Kaseer, F., Martin, A.E., Yin, F. and Cucalon, L.G., 2018. Evaluation of recycling agent dosage selection and incorporation methods for asphalt mixtures with high RAP and RAS contents. Construction and Building Materials, 158, pp.432-442.

4.42. Tarbox, S. and Daniel, J.S., 2012. Effects of long-term oven aging on reclaimed asphalt pavement mixtures. Transportation research record, 2294(1), pp.1-15.

4.43. Arafat, S. and Wasiuddin, N.M., 2019. A comparative study between the effectiveness of a softer grade binder and a rejuvenating agent in hot mix asphalt with reclaimed asphalt pavement. In Airfield and Highway Pavements 2019: Innovation and Sustainability in Highway and Airfield Pavement Technology (pp. 77-87). Reston, VA: American Society of Civil Engineers.

4.44. Saha, G. and Biligiri, K.P., 2016. Fracture properties of asphalt mixtures using semi-circular bending test: a state-of-the-art review and future research. Construction and Building Materials, 105, pp.103-112.

5.1. Xu, X.P. and Needleman, A., 1994. Numerical simulations of fast crack growth in brittle solids. Journal of the Mechanics and Physics of Solids, 42(9), pp.1397-1434.

5.2. Bazant, Z.P. and Planas, J., 1997. Fracture and size effect in concrete and other quasibrittle materials (Vol. 16). CRC press.

5.3. Song, S.H., Paulino, G.H. and Buttlar, W.G., 2006. Simulation of crack propagation in asphalt concrete using an intrinsic cohesive zone model. Journal of Engineering Mechanics, 132(11), pp.1215-1223.

5.4. Aragao, F.T.S. and Kim, Y.R., 2011. Characterization of fracture properties of asphalt mixtures based on cohesive zone modeling and digital image correlation

technique (No. 11-1229).

5.5. Li, X. and Marasteanu, M.O., 2005. Cohesive modeling of fracture in asphalt mixtures at low temperatures. International Journal of Fracture, 136(1-4), pp.285-308.Kim, Y.R., 2011. Cohesive zone model to predict fracture in bituminous materials and asphaltic pavements: state-of-the-art review. International Journal of Pavement Engineering, 12(4), pp.343-356.

5.6. Pirmohammad, S., Khoramishad, H. and Ayatollahi, M.R., 2016. Effects of asphalt concrete characteristics on cohesive zone model parameters of hot mix asphalt mixtures. Canadian Journal of Civil Engineering, 43(3), pp.226-232.

5.7. Kim, H., Wagoner, M.P. and Buttlar, W.G., 2008. Simulation of fracture behavior in asphalt concrete using a heterogeneous cohesive zone discrete element model. Journal of materials in civil engineering, 20(8), pp.552-563.

5.8. Dave, E.V. and Buttlar, W.G., 2010. Low temperature cracking prediction with consideration of temperature dependent bulk and fracture properties. Road materials and pavement design, 11(sup1), pp.33-59.

5.9. Soares, J.B., Colares de Freitas, F.A. and Allen, D.H., 2003. Crack modeling of asphaltic mixtures considering heterogeneity of the material. Transportation Research Record, 1832, pp.113-120.

5.10. Dave, E.V. and Behnia, B., 2018. Cohesive zone fracture modelling of asphalt pavements with applications to design of high-performance asphalt overlays. International Journal of Pavement Engineering, 19(3), pp.319-337.

5.11. Harvey, J.A.F. and Cebon, D., 2005. Fracture tests on bitumen films. Journal of materials in civil engineering, 17(1), pp.99-106.

5.12. Rajan, S., Sutton, M.A., Fuerte, R. and Kidane, A., 2018. Traction-separation relationship for polymer-modified bitumen under Mode I loading: Double cantilever beam experiment with stereo digital image correlation. Engineering Fracture Mechanics, 187, pp.404-421.

5.13. Kim, Y.R., 2011. Cohesive zone model to predict fracture in bituminous materials and asphaltic pavements: state-of-the-art review. International Journal of Pavement Engineering, 12(4), pp.343-356.

5.14. Dugdale, D.S., 1960. Yielding of steel sheets containing slits. Journal of the Mechanics and Physics of Solids, 8(2), pp.100-104.

5.15. Barenblatt, G.I., 1962. The mathematical theory of equilibrium cracks in brittle fracture. Advances in applied mechanics, 7(1), pp.55-129.

5.16. Alfano, G. and Crisfield, M., 2001. Finite element interface models for the delamination analysis of laminated composites: mechanical and computational issues. International journal for numerical methods in engineering, 50(7), pp.1701-1736.

5.17. Gowrishankar, S., Mei, H., Liechti, K.M. and Huang, R., 2012. A comparison of direct and iterative methods for determining traction-separation relations. International journal of fracture, 177(2), pp.109-128.

5.18. Högberg, J.L., Sørensen, B.F. and Stigh, U., 2007. Constitutive behaviour of mixed mode loaded adhesive layer. International Journal of Solids and Structures, 44(25-26), pp.8335-8354.

5.19. Dastjerdi, A.K., Tan, E. and Barthelat, F., 2013. Direct measurement of the cohesive law of adhesives using a rigid double cantilever beam technique. Experimental Mechanics, 53(9), pp.1763-1772.

5.20. https://www.dot.state.mn.us/materials/manuals/laboratory/1854.pdf. Last visited: June 21, 2020

6.1. Thives, L.P., Ghisi, E., 2017. Asphalt mixtures emission and energy consumption: A review. Renewable & Sustainable Energy Reviews 72, 473-484.

6.2. Zhu, J., Birgisson, B., Kringos, N., 2014. Review article: Polymer modification of bitumen: Advances and challenges. European Polymer Journal 54, 18-38.

6.3. Singh, S., Verma, J.P., de Araujo Pereira, A.P., Sivakumar, N., 2018. book review: Production of biofuels and chemicals from lignin. Journal of Cleaner Production 203, 966-967.

6.4. Mabrouk, A., Jalel, L., Maria González, A., Xabier, E., 2018. Economic analysis of a biorefinery process for catechol production from lignin. Journal of Cleaner Production 198, 133-142.

6.5. Kauldhar, B.S., Yadav, S.K., 2018. Turning waste to wealth: A direct process for recovery of nano-silica and lignin from paddy straw agro-waste. Journal of Cleaner Production 194, 158-166.

6.6. Terrel, R.L., Rimsritong, S., 1979. Wood lignins used as extenders for asphalt in bituminous pavements. Association of Asphalt Paving Technologists 48, 111-134.

6.7. Cavalli, M.C., Zaumanis, M., Mazza, E., Partl, M.N., Poulikakos, L.D., 2018. Effect of ageing on the mechanical and chemical properties of binder from RAP treated with bio-based rejuvenators. Composites Part B: Engineering 141, 174-181.

6.8. Zaumanis, M., Mallick, R.B., Poulikakos, L., Frank, R., 2014. Influence of six rejuvenators on the performance properties of Reclaimed Asphalt Pavement (RAP) binder and 100% recycled asphalt mixtures. Construction and Building Materials 71, 538-550.

6.9. Williams, R.C., McCready, N.S., 2008. The Utilization of Agriculturally Derived Lignin as an Antioxidant in Asphalt Binder. InTrans Project Reports Paper 14.

6.10. Xie, S., Li, Q., Karki, P., Zhou, F., Yuan, J.S., 2017. Lignin as Renewable and Superior Asphalt Binder Modifier. ACS Sustainable Chem. Eng. 5, 2817−2823.

6.11. Xu, G., Wang, H., Zhu, H., 2017. Rheological properties and anti-aging performance of asphalt binder modified with wood lignin. Construction and Building Materials 151, 801-808.

6.12. Robertson, R.E., Bishara, S.W., Mahoney, D., 2006. Lignin as Antioxidant: Limited Study on Asphalts Frequently Used on Kansas Roads, Transportation Research Board 85th Annual Meeting. Transportation Research Board, Washington, DC, United States.

6.13. Hobson, C., 2017. Evaluation of lignin as an antioxidant in asphalt binders and bituminous mixtures: technical summary. Kansas Department of Transportation.

6.14. Vliet, D.v., Slaghek, T., Giezen, C., Haaksman, I., 2016. Lignin as a green alternative for bitumen, 6th Eurasphalt & Eurobitume Congress. Prague, Czech Republic.

6.15. Sundstrom, D.W., Kiel, H.E., Daubenspeck, T.H., 1983. Use of Byproduct Lignins as Extenders in Asphalt. Industrial and Engineering Chemistry Product Research and Development 22(3), 496-500.

6.16. Batista, K.B., Padilha, R.P.L., Castro, T.O., Pasa, V.M.D., Lins, V.F.C., Silva, C.F.S.C., Leite, L.F.M., Araújo, M.F.A.S., 2018. High-temperature, low-temperature and weathering aging performance of lignin modified asphalt binders. Industrial Crops and Products 111, 107-116.

6.17. Sánchez-González, Á., Martín-Martínez, F.J., Dobado, J., 2017. The role of weak interactions in lignin polymerization. Journal of molecular modeling 23(3), 80.

6.18. Boeriu, C.G., Fiţigău, F.I., Gosselink, R.J.A., Frissen, A.E., Stoutjesdijk, J., Peter, F., 2014. Fractionation of five technical lignins by selective extraction in green solvents and characterisation of isolated fractions. Industrial Crops & Products 62, 481-490.

6.19. Lim, J.S., Manan, Z.A., Alwi, S.R.W., Hashim, H., 2012. A review on utilisation of biomass from rice industry as a source of renewable energy. Renewable &

Sustainable Energy Reviews 16(5), 3084-3094.

6.20. Wang, W.X., Martin, J.C., Zhang, N., Ma, C., Han, A.J., Sun, L.Y., 2011. Harvesting silica nanoparticles from rice husks. J. Nanopart. Res. 13(12), 6981-6990.

6.21. Ouyang, Y.S., 2001. Mesomechanical characterization of in situ rice grain hulls. Transactions of the Asae 44(2), 357-367.

6.22. Francisco, M., van den Bruinhorst, A., Kroon, M.C., 2012. New natural and renewable low transition temperature mixtures (LTTMs): screening as solvents for lignocellulosic biomass processing. Green Chemistry 14(8), 2153-2157.

6.23. Durand, E., Lecomte, J., Villeneuve, P., 2013. Deep eutectic solvents: Synthesis, application, and focus on lipase-catalyzed reactions. European Journal of Lipid Science and Technology 101(12).

6.24. Gorke, J., Srienc, F., Kazlauskas, R., 2010. Toward Advanced Ionic Liquids. Polar, Enzyme-friendly Solvents for Biocatalysis. Biotechnol. Bioprocess Eng. 15(1), 40-53.

6.25. Lamers, P., Roni, M.S., Tumuluru, J.S., Jacobson, J.J., Cafferty, K.G., Hansen, J.K., Kenney, K., Teymouri, F., Bals, B., 2015. Techno-economic analysis of decentralized biomass processing depots. Bioresource Technology 194, 205-213.

6.26. D'Angelo, J., 2007. Effect of polymer-asphalt binder compatibility and cross-link density of non-recoverable compliance in the MSCR test method, Southeastern Asphalt User/Producer Group Conference. San Antonio, TX.

6.27. Islam, R.M., William King, J., Wasiuddin, N.M., 2015. Correlating Long-Term Chip Seals Performance and Rheological Properties of Aged Asphalt Binders. Journal of Materials in Civil Engineering 28(5).

6.28. Tejado, A., Peña, C., Labidi, J., Echeverria, J.M., Mondragon, I., 2007. Physico-chemical characterization of lignins from different sources for use in phenol–formaldehyde resin synthesis. Bioresource Technology 98, 1655-1663.

6.29. da Costa Lopes, A.M., João, K.G., Bogel-Łukasik, E., Roseiro, L.B., Bogel-Łukasik, R., 2013. Pretreatment and Fractionation of Wheat Straw Using Various Ionic Liquids. Journal of Agricultural and Food Chemistry 61(33), 7874-7882.

6.30. Shi, J.T., Li, J., 2012. Metabolites and chemical group changes in the wood-forming tissue of pinus koraiensis under inclined conditions. BioResources 7(3), 3463-3475.

6.31. Arámbula Mercado, E., Park, E.S., Epps Martin, A., Spiegelman, C., Glover, C.J., 2005. Factors affecting binder properties between production and construction. Journal of Materials in Civil Engineering 17(1), 89-98.

6.32. Karlsson, R., Isacsson, U., 2003. Investigations on bitumen rejuvenator diffusion and structural stability. pp. 463-501.

7.1. Ali, H., and M. Mohammadafzali. Asphalt Surface Treatment Practice in Southeastern United States. Final Report 515. Southeast Transportation Consortium, Baton Rouge, LA, 2014.

7.2. Im, J. H., and Y. R. Kim. Methods for Fog Seal Field Test with Polymer-Modified Emulsions. In Transportation Research Record: Journal of The Transportation Research Board, No. 2361, Transportation Research Board of The National Academies, Washington, D.C., 2013, pp. 88-97.

7.3. King, G. N., and H. King. Spray-Applied Surface Seal: Fog and Rejuvenator Seals. Presented at 87th Annual Meeting of the Transportation Research Board, Washington, D.C., 2008.

7.4. Booth, E.H.S., R. Gaughan, and G. Holleran. Some Uses of Bitumen Emulsions in SA and NSW. In Proceedings, Australian Road Research Board, March 1988, pp. 387-401.

7.5. Prapaitrakul, N., T. J. Freeman, and C. J. Glover. Assessing the Ability of Fog Seals to Seal Pavements, to Rejuvenate In Situ Binder, and to Retard Binder Oxidation. FHWA/TX-06/0-5091-3. Texas A&M University, Texas Transportation Institute, College Station, Texas, 2007.

7.6. Kim, S., J. A. Musselman, and G. A. Sholar. Evaluation of Fog Seal Preservation Technique on US 17 and US 27. State Materials Office, Florida Department of Transportation, Gainesville, FL, 2014.

7.7. Qureshi, N. A., N. H. Tran, and D. Watson. Effect of Using Fog Seals without Sanding on Surface Friction and Durability of OGFC. Presented at 91st Annual Meeting of the Transportation Research Board, Washington, D.C., 2012.

7.8. Fog Seal Guidelines. California Department of Transportation (CADOT), Caltrans Division of Maintenance, Sacramento, CA, 2003.

7.9. Li, S., S. Noureldin, Y. Jiang, and Y. Sun. Evaluation of pavement surface friction treatments. Publication FHWA/IN/JTRP- 2012/04. Joint Transportation Research Program, Indiana Department of Transportation and Purdue University, West Lafayette, Indiana, 2012. DOI: 10.5703/1288284314663

7.10. Liu, L., Hossain, M. and Miller, R.W., 2010. Costs and benefits of thin surface treatments on bituminous pavements in Kansas. Transportation research record, 2150(1), pp.47-54

7.11. Wood, T.J., Janisch, D.W. and Gaillard, F.S., 2006. *Minnesota seal coat handbook 2006* (No. MN/RC-2006-34).

7.12. Tarefder, R.A. and Ahmad, M., 2013. On the durability of asphalt pavements due to excessive permeability. In Int. J. Pavements Conf. (pp. 182-192).